
Politecnico di Torino

ScuDo
Scuola di Dottorato ~ Doctoral School
WHAT YOU ARE, TAKES YOU FAR

Doctoral Dissertation
Doctoral Program in Environmental Engineering ($38^{th}$cycle)

# Space-time estimation of flood quantiles

By

**Luigi Cafiero**

******

**Supervisor(s):**
Prof. Alberto Viglione, Supervisor
Prof. Günter Blöschl, Co-Supervisor
Prof. Francesco Laio, Co-Supervisor

**Doctoral Examination Committee:**
Dr. Stacey A. Archfield, U.S. Geological Survey
Prof. Francesco Marra, University of Padova

Politecnico di Torino
2026

This publication is part of the project **PNRR-NGEU** which has received funding from the **MUR – DM 351/202**.

# Declaration

I hereby declare that, the contents and organization of this dissertation constitute my own original work and does not compromise in any way the rights of third parties, including those relating to the security of personal data.

Luigi Cafiero
2026

* This dissertation is presented in partial fulfillment of the requirements for **Ph.D. degree** in the Graduate School of Politecnico di Torino (ScuDo).

# Acknowledgements

First and foremost, I want to thank my supervisor, Alberto Viglione. He gave me the space to grow as a researcher and that included the space to make mistakes. Not every supervisor does that, and it made all the difference. I am genuinely grateful for the independence he encouraged and the trust he placed in me throughout these years.

To my family: thank you for always being there. You supported me without ever needing to fully understand what I was doing, and that kind of support, unconditional and steady, is something I never took for granted.

And to my colleagues, who are after three years simply my closest friends. We grew up together. You were there to host me when I needed it, to make plans with, and to dream out loud with. I could not have asked for better people to share these years with.

# Abstract

Flood frequency analysis is a cornerstone of hydrological design and flood risk management, yet it remains challenged by pronounced spatial heterogeneity and increasing temporal non-stationarity, mainly driven by climate and land use change. Traditional approaches commonly assume that observations are independent, identically distributed, and stationary over time. These assumptions may prove inadequate to represent evolving flood-generating processes and to support robust decision-making under future hydroclimatic conditions. This doctoral thesis addresses these challenges by making advances towards the development of a spatio-temporal framework for flood frequency estimation, explicitly accounting for uncertainty, also applicable to ungauged or poorly gauged basins.

First, from a spatial perspective, the thesis advances regional flood frequency analysis by introducing a multi-model framework that integrates flood quantile estimates and associated uncertainties from three distinct regional models calibrated on a shared, harmonized dataset. Applied to the Po River basin, this approach yields more robust and stable design flood estimates than the individual regional models. These results provide the basis for a systematic revision of design floods across the Po River basin, supporting an update of flood hazard assessments for hydraulic planning and risk management.

Second, from a temporal perspective, the thesis develops an operational methodology to incorporate precipitation extremes variation into flood frequency analysis. Intensity–Duration–Frequency (IDF) curves and Flood Frequency Curves (FFC) are related through quantile-quantile relationships, whose slopes represent the elasticity of floods to precipitation extremes. Assuming that the percentage variations of precipitation and flood quantiles are linked by the quantile-quantile relationship, modified FFCs accounting for the projected changes in precipitation extremes are obtained. Extensive sensitivity analyses and numerical experiments are conducted to

delineate the domain of applicability of the approach. Results show that the method performs robustly for large return periods and in catchments where flood changes are primarily controlled by precipitation extremes, while its reliability decreases where runoff generation processes play a dominant role. Applications to more than 200 catchments in the Po River basin, using CMIP5-CORDEX projections under the RCP8.5 scenario (2071–2100), reveal strong spatial heterogeneity in flood response and a nonlinear amplification of rare flood extremes.

Third, the thesis introduces a Bayesian event-based flood frequency model that explicitly represents storm characteristics, antecedent soil moisture conditions, and temperature-driven processes. This framework enables consistent propagation of uncertainty from climate forcing to flood quantiles and allows attribution of projected flood changes to individual physical mechanisms. Applications to Austrian catchments show that changes in precipitation intensity are the dominant driver of projected flood increases, while also representing the largest source of uncertainty due to climate model spread. Processes related to temperature and soil moisture exert a secondary but more systematic influence, modulating flood response across seasons and return periods with comparatively lower uncertainty. By disentangling the contributions of uncertainty sources, the analysis demonstrates that flood quantile projection uncertainty is driven mainly by (i) parameter-response uncertainty, arising from model parameter uncertainties propagation under future climate conditions, and (ii) climate-forcing uncertainty, reflecting differences among ensemble members of the climate model projections.

Taken together, these results demonstrate that flood frequency curves should be interpreted as dynamic representations of evolving hydrological systems. The thesis highlights the complementarity of the proposed approaches—the combination of different regional models, the method of elasticity for incorporating precipitation change into flood frequency analysis, and the derived distribution approach for the attribution of flood changes to different mechanisms—and provides a flexible toolbox for flood estimation under climate change. The proposed frameworks contribute to a more transferable and robust assessment of flood hazards, supporting adaptation strategies and hydraulic design in a changing climate.

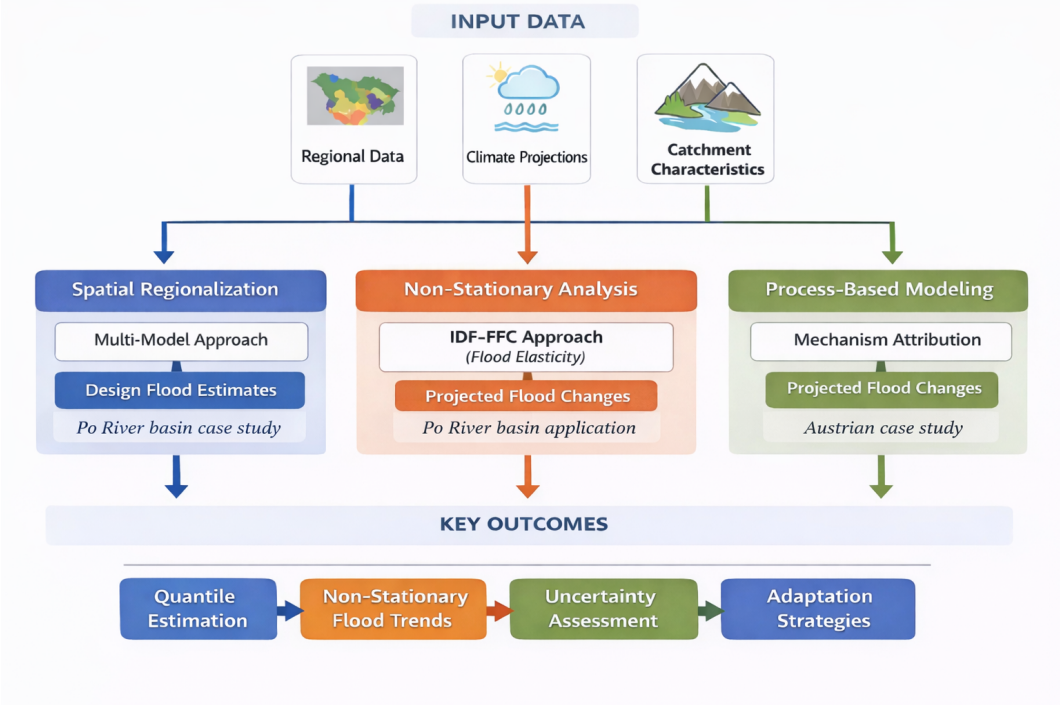


Fig. 1 Schematic view of the thesis outcomes.

# Contents

# Chapter 1

# Introduction

## 1.1 General Context

### 1.1.1 The role of rivers for human society

Rivers have always played a fundamental role in the development of human civilization. Since the earliest settlements, human societies have relied on rivers for drinking water, food production, transportation, energy generation, and trade. Major civilizations, from the Nile and Mesopotamia to the Indus and the Danube, have flourished along riverbanks, where the combination of fertile floodplains and navigable waterways provided the foundations for agriculture, commerce, and cultural exchange (Leopold, 1994; Montgomery, 2007; Petts and Calow, 1996).

Beyond their direct benefits, rivers are central to maintaining ecological integrity. They regulate sediment transport, sustain wetlands and biodiversity, and connect terrestrial and coastal ecosystems. The natural variability of river regimes through floods and droughts has historically shaped not only landscapes but also human adaptation strategies. However, in the Anthropocene era, this relationship has become increasingly complex and reciprocal. Human activities have a profound impact on river systems, influencing their hydrology, morphology, and ecological functions through dam construction, channelization, urbanization, land-use change, and water abstraction.

As noted by Sivapalan et al. (2012), the interaction between human and natural systems forms a coupled socio-hydrological framework, in which human decisions and river dynamics evolve together. For instance, the construction of flood protection infrastructure alters floodplain connectivity and sediment dynamics, while at the same time shaping societal perceptions of risk and safety. Conversely, changes in river behavior, such as flood frequency or sediment transport, feed back into human decision-making, influencing future management, policy, and settlement patterns.

Throughout history, floods have been both destructive forces and catalysts for societal evolution. The history of Vienna exemplifies this dual role. Located on the banks of the Danube River, the city has been repeatedly affected by severe floods, notably those of 1501, 1830, 1899, and 1954 (Habersack et al., 2016). Each catastrophic event triggered new regulatory or engineering responses, reflecting the evolving relationship between society, infrastructure, and natural processes. The 19$^{\text{th}}$-century *Danube Regulation Project* transformed Vienna's river corridor, creating a new, straighter riverbed and artificial levees to mitigate flood risk (Hauer et al., 2019). Later, in the 1970s–1980s, the construction of the *Donauinsel* (Danube Island) added an innovative flood-control and recreational structure, an artificial island acting as a flood relief channel. This project marked a shift from rigid hydraulic control to integrated river basin management, anticipating modern approaches that balance safety, ecology, and recreation. Figure 1.1 illustrates a flood event of the Danube in Vienna that occurred in 2009, highlighting the controlled inundation of designated floodplain areas along the Neue Donau and the Donauinsel, and exemplifying the functioning of the city's integrated flood management system under high-flow conditions.

Despite centuries of progress in river engineering and management, floods remain among the most frequent and devastating natural hazards worldwide. According to the World Meteorological Organization, floods account for over 40% of natural disaster impacts globally (WMO, 2021). The consequences extend beyond immediate human casualties: they include long-term economic losses, damage to infrastructure, disruption of services, and psychological and cultural impacts (Gupta et al., 2021). Between 1980 and 2020, flood-related damages in Europe alone exceeded €500 billion, and the frequency of large flood events has shown an increasing tendency in several regions (Blöschl et al., 2019b; Hall et al., 2014).

Fig. 1.1 Flood event of the Danube River in Vienna on 25 June 2009. The photograph illustrates the inundation of the floodplain areas along the Neue Donau and the Donauinsel, with partially submerged riparian vegetation indicating elevated water levels during the flood. The image was taken from the Floridsdorfer Brücke and documents the spatial extent of flooding within the engineered Danube corridor.

This persistent vulnerability calls for a sustainable floodplain management as requested by EU Floods Directive (2007/60/EC) as well as a comprehensive understanding of flood-generating mechanisms and their variability in space and time. Reliable flood frequency estimation underpins this understanding.

### 1.1.2 Flood generation mechanisms

Floods are the outcome of complex interactions between atmospheric forcing, catchment characteristics, and runoff generation processes. They arise when the combination of precipitation, snowmelt, and antecedent moisture conditions exceeds the capacity of the landscape and river network to store and convey water. Understanding the mechanisms that generate floods is essential for interpreting spatial and temporal patterns of flood frequency and magnitude, as well as for predicting how these may evolve under changing climatic and land-use conditions (Blöschl et al., 2023).

From a meteorological perspective, floods are triggered by extreme precipitation events, which can result from a variety of atmospheric conditions. At one end of the spectrum are convective storms, caused by a strong updraft of warm, moist air usually produced by strong radiation. These storms typically cover small spatial scales, last few hours, and can reach very high intensities. At the other end are large-scale synoptic systems, such as frontal depressions or atmospheric rivers, which produce widespread and persistent, but less intense rainfall.

Flood frequency reflects the combined influence of rainfall variability at multiple temporal scales and its interaction with landscape dynamics, including soil moisture, vegetation, and snow processes. For example, even under similar rainfall totals, catchments with wetter antecedent conditions are more likely to generate high runoff than those that are dry or highly permeable. Flood processes often exhibit a strong seasonality as a result of the interplay between atmospheric processes and catchment state. For example, in the European Alps, rainfall extremes often occur in autumn, yet annual flood peaks typically arise in late spring or early summer, when snowmelt coincides with moderate rainfall events. This apparent mismatch between precipitation and flood seasonality underscores the mediating role of catchment processes in translating atmospheric forcing into discharge responses (Blöschl et al., 2023; Parajka et al., 2010).

Floods also vary on inter-annual to decadal time scales as a result of large-scale climate oscillations. Phenomena such as El Niño–Southern Oscillation (ENSO), the North Atlantic Oscillation (NAO), or the Atlantic Multidecadal Oscillation (AMO) influence regional precipitation patterns, storm tracks, and temperature regimes, thereby altering flood hazard over time (Kundzewicz, 2012). These modes of variability may reinforce or counteract the effects of long-term climate trends, contributing to the complex temporal dynamics of flood risk.

At the catchment scale, runoff generation controls how rainfall is transformed into infiltration, storage, and surface flow. This transformation reflects the interplay between soil properties, land cover, rainfall characteristics, and antecedent moisture conditions. The latter introduces a form of hydrological "memory", whereby previous wetness states influence the catchment response to subsequent rainfall events (Marchi et al., 2010). Under very large rainfall amounts, however, antecedent soil moisture becomes less influential, as precipitation volume and event characteristics such as intensity and duration increasingly dominate runoff production (Blöschl et al., 2023). Runoff responses may therefore vary both spatially within a catchment during a single event and temporally across different events, with abrupt changes in runoff behaviour possible once critical rainfall thresholds are exceeded (Gioia et al., 2008). In this regard, Merz and Blöschl (2003) introduced a process-oriented classification of floods at the catchment scale, demonstrating that flood-generating mechanisms display systematic variability across space, seasons, and event magnitudes, with implications for the interpretation of flood statistics.

The diversity of flood-generating mechanisms has direct implications for the statistical description of flood frequency. When flood peaks at a given site arise from distinct physical processes, the observed record is effectively a mixture of populations, each with its own probability distribution and tail behaviour. This process heterogeneity can produce non-standard features in flood frequency curves, including step changes and heavy tails, that single parametric distributions may not capture (Rogger et al., 2012b). The problem is compounded under non-stationary conditions: if the relative frequency of flood-generating mechanisms shifts over time (Tarasova et al., 2023), the mixture itself changes, and the statistical properties of the flood record evolve in ways that reflect process change rather than simple trends in a fixed distribution.

Overall, floods emerge from the dynamic coupling between climate forcing and catchment response. The frequency and magnitude of flood events cannot be attributed solely to precipitation statistics, but must be understood in the context of how landscape characteristics, soil moisture dynamics, and long-term climate variability modulate the transformation of rainfall into runoff. This integrated view forms the basis for modern approaches to flood estimation and risk management.

### 1.1.3 Flood frequency estimation

Throughout history, one of the main ways societies have adapted to flooding is by interpreting its severity through how frequently floods occur, by framing floods in probabilistic rather than purely descriptive terms. From an engineering point of view, assessing the likelihood of extreme events is essential for the design of flood protection measures and for evaluating their economic efficiency within cost–benefit frameworks. Accordingly, hydrology aims to quantify the relationship between flood magnitude, commonly defined as the peak discharge measured at a specific point along a river, and flood frequency. This relationship underpins the estimation of design floods and provides the basis for probabilistic approaches to flood risk assessment (Blöschl et al., 2023).

Flood frequency analysis provides a statistical framework for quantifying the likelihood and magnitude of flood events based on observed hydrological records. A central concept in this framework is the *return period* (also known as the *recurrence interval*), which represents the average time interval between occurrences of a flood of a specified magnitude or greater. This definition rests on the assumption that the statistical properties of the flood process remain constant over time (stationarity), so that past observations can be used to characterize future flood probabilities. Under this assumption, the return period $T$ is the inverse of the annual exceedance probability $p$. For instance, a 100-year flood (i.e., $T = 100$) corresponds to an annual exceedance probability of $p = 0.01$, meaning that in any given year, there is a 1% chance that a flood of equal or greater magnitude will occur (Coles, 2001; Stedinger, 1993).

Associated with the return period is the concept of the *flood quantile*, defined as the discharge $q_T$ corresponding to a given return period $T$. The estimation of flood quantiles relies on fitting a probability distribution to extreme flow data, typically annual

maximum discharges or peak-over-threshold values. Commonly used distributions in hydrology include the Generalized Extreme Value (GEV) and the Log-Pearson Type III distributions (Coles, 2001; Hosking and Wallis, 1997). The estimated quantile $q_T$ provides the design discharge used in the planning and safety assessment of hydraulic structures such as dams, bridges, levees, and drainage systems. Figure 1.2 (a) shows an example of a flood frequency curve of a generic catchment, and the relevance of the choice of the theoretical distribution. In particular, the differences among alternative models become negligible for moderate return periods, whereas they grow rapidly for large return periods. This behavior highlights that the key element distinguishing the distributions is the way the upper tail is represented. Distributions characterized by heavier right tails assign a higher probability to extreme floods and therefore lead to substantially larger design discharges for large return periods (as in the GEV distribution in the example). Conversely, models with light or bounded tails implicitly limit the magnitude of rare events, resulting in less conservative estimates (as in the Log-Pearson Type III distribution in the example). Here, the 3-parameter lognormal distribution represents an intermediate case in terms of tail behaviour and associated design discharges. Thus, the selection of the theoretical distribution mainly affects the extrapolation beyond the range of observed data, rather than the fit to frequent events (see Hu et al. (2020) for a sensitivity analysis of flood frequency to various sample sizes, statistical models, and parameter estimation methods).

Figure 1.2 (b) further emphasizes that the flood frequency curve should not be regarded as static or stationary. Even when the most suitable distribution is assumed, the 3-parameter lognormal in the example, the curve may evolve over time as flood-generating mechanisms and their interactions change, leading to flood-rich periods or flood-poor periods. This temporal variability challenges the traditional assumption of stationarity underlying classical flood frequency analysis and motivates approaches that explicitly account for changes in catchment response over time.

Flood quantile estimation plays a dual role: it provides essential input for engineering design and supports risk-based decision-making in flood insurance, land-use regulation, and climate adaptation strategies. However, these estimates are affected by substantial uncertainty, particularly for large return periods. One major source of uncertainty arises from the representation of the upper tail of the flood distribution, which controls the extrapolation beyond the range of observed data and directly influences the estimation of design discharges. Additionally, the number of available observations (annual maximum discharges) strongly affects the reliability of quan-

tile estimates: small sample sizes increase uncertainty and limit the confidence in extrapolations for rare floods.

In addition, classical frequency analysis relies on the assumption that hydrological time series are stationary, meaning that their statistical properties (mean, variance, and higher-order moments) remain constant over time. Increasing evidence suggests that this assumption is often violated under the combined effects of climate change and land-use modifications (Katz, 2013; Madsen et al., 2014b). As a result, contemporary research has increasingly focused on developing modeling frameworks that explicitly account for temporal variability and non-stationary processes, with the aim of providing more robust and physically consistent flood quantile estimates. In this context, Chapter 2 addresses uncertainty associated with quantile estimation, while Chapter 3 and 4 focus on the issue of non-stationarity in flood frequency curves and design discharges.

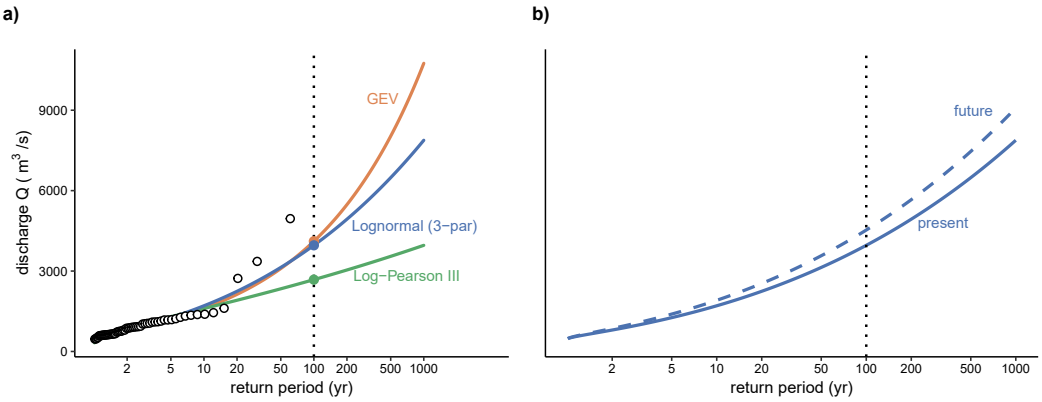


Fig. 1.2 (a) Example of flood frequency estimation. Empty circles represent observation of annual maxima, with an associated empirical return period. The curves represent the theoretical distributions fitted to the observations. The choice of the distribution is a key aspect for the estimation of the design discharges (full circles). (b) Example of the variation in time of the flood frequency curve obtained with the assumption that the 3-parameter lognormal distribution is the most suitable one for the explanatory catchment.

## 1.2 Space-time analysis

Classical flood frequency analysis (FFA) typically follows an *at-site* approach, in which annual maximum discharge (or peak-over-threshold) series are fitted with theoretical probability distributions. The fitted distribution is then used to estimate design

discharges associated with prescribed return periods. This method assumes that observations are independent, identically distributed, and stationary in time. Such assumptions are convenient but often unrealistic, as hydrological processes are influenced by climate variability, catchment heterogeneity, and human interventions (e.g., land-use changes, dam operations). Moreover, the reliability of purely local analyses is constrained by the limited length and quality of observed discharge records. Therefore, this work addresses two key challenges in hydrology: the estimation of design floods at ungauged or poorly gauged locations, where direct discharge observations are unavailable or insufficient, and the issue of non-stationarity, particularly that induced by climate change.

### 1.2.1 Spatial perspective: regional models

Classical flood frequency analysis (FFA) based on the *at-site* approach has intrinsic limitations. Although observed flood records provide essential insights into the statistical behavior of river discharge, relying solely on measured annual maxima is rarely sufficient for comprehensive flood estimation. Streamflow records are often short, discontinuous, or of uncertain quality, and thus may not fully capture the range of possible hydrological extremes. This limitation becomes particularly critical when extrapolating probability distributions beyond the observed data to estimate rare design floods, where the uncertainty grows rapidly. Moreover, in most locations worldwide, direct discharge measurements are simply unavailable, making at-site frequency analysis impossible. As a result, hydrologists have developed alternative approaches that exploit information from other sources. Among these, rainfall–runoff modeling, regionalization techniques, and process-based reasoning emerge to predict flood characteristics in ungauged or poorly gauged basins.

The seminal work of Dalrymple (1960) introduced the *Regional Flood Frequency Analysis* (RFFA), providing a robust framework for pooling flood data from hydrologically homogeneous regions, and promoting a comparative hydrology approach. The key assumption is that catchments within a region share a common frequency distribution that differs only by a scaling factor, typically the mean annual flood. This assumption enables the estimation of flood quantiles at ungauged sites by transferring information from gauged catchments within the same region. The delineation of homogeneous regions is a key aspect when dealing with regional flood frequency analysis. As a general rule, catchments can be considered similar when they respond

to climatic variability in comparable ways. Figure 1.3 shows an example of this concept for Austria, where catchments are grouped into distinct hydrological regions characterized by similar runoff behaviour (Merz and Blöschl, 2009a). These similarities are often the result of similar trajectories of co-evolution of climate, soils, vegetation, and landscape (Blöschl et al., 2023). The underlying assumption is that similar catchments in terms of climate and catchment characteristics have a similar hydrological behaviour. In real applications, this hypothesis is usually tested in gauged catchments.

With respect to flood frequency, the similarity between catchments can be inferred from their flood frequency curves, as similarities in curve shape serve as proxies for similarity in flood-generating processes. A common assumption is that neighboring catchments tend to behave similarly, since rainfall–runoff controls often vary smoothly in space. Spatial proximity thus represents the most basic and widely used criterion for defining similarity. Merz and Blöschl (2004) indeed showed that spatial proximity was among the strongest predictors of flood behavior compared with other catchment descriptors in Austria. Beyond spatial proximity, other approaches to defining similarity include runoff, climate, and catchment characteristics. When investigating flood similarity, scaling flood frequency curves by the mean annual flood is particularly convenient, as it allows comparisons that are independent of catchment size. In such cases, the coefficient of variation ($CV$) of flood peaks, reflecting the steepness of the dimensionless or scaled flood frequency (growth curve), is commonly used as a similarity measure.

Regarding climate similarity, catchments can be compared in terms of extreme rainfall. Climate similarity can be assessed through indicators of extreme rainfall. Intensity–duration–frequency (IDF) curves, which describe the cumulative distributions of extreme rainfall over specified durations, provide a useful alternative to other similarity metrics. Additional climatic descriptors include the seasonality of extreme rainfall and the mean annual precipitation (Madsen et al., 1997; Petrow et al., 2007). Finally, catchment similarity is often evaluated in terms of physical and land-use characteristics such as catchment area, degree of urbanization, drainage density, and topographic elevation (Eaton et al., 2002; Viglione et al., 2010a,b).

Based on hydrological similarities, basins can be grouped into homogeneous regions, allowing the assumption that extreme events not observed at a particular site may have occurred elsewhere within the same region. By pooling data from these

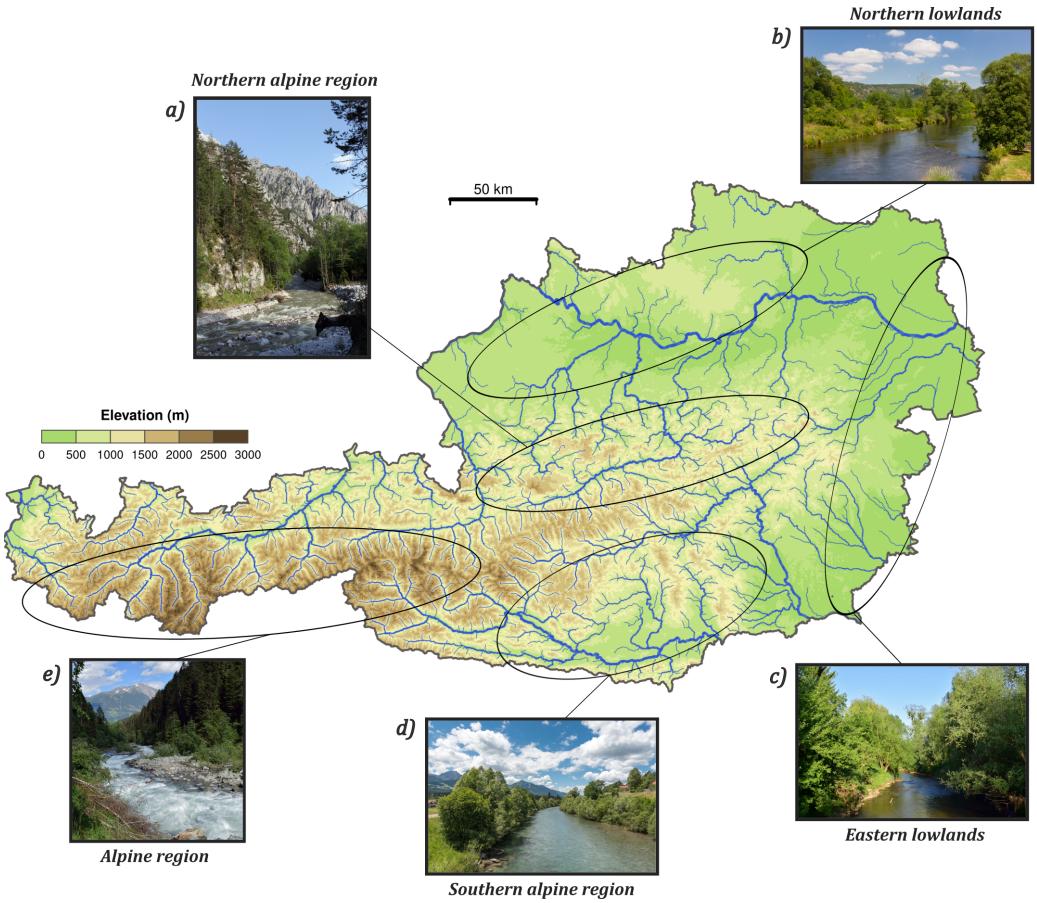


Fig. 1.3 Similarities of catchments and hydrological regions in Austria. The map illustrates the main hydrological regions of Austria, identified based on similarities in runoff behavior following the classification proposed by Merz and Blöschl (2009a). These regions reflect consistent combinations of climatic, physiographic, and hydrological controls on catchment response. Representative examples of river reaches are shown for each region: (a) Enns at Johnsbach (northern alpine region), (b) Kamp at Buchberg (northern lowlands), (c) Raab at Feldbach (eastern lowlands), (d) Gail at Watschig in the southern alpine region, and (e) Isel in Virgen (alpine region). Together, the map and photographs illustrate how catchments sharing similar runoff characteristics can be grouped into distinct hydrological regions.

hydrologically similar catchments, a more representative regional sample can be obtained. This approach enables the estimation of flood frequency at ungauged sites and improves predictions in basins with short or incomplete flood records. When estimating floods with return periods exceeding 100 years, even records spanning several decades may provide insufficient information for reliable extrapolation. Indeed, simple Monte Carlo experiments demonstrate that estimation uncertainty remains substantial even with a 100-year record, highlighting the fundamental challenge of inferring rare event probabilities from finite samples

Once a homogeneous region composed of catchments similar to the target ungauged basin has been identified, the corresponding flood peak data can be analyzed and transferred to the ungauged site. One of the most widely used regional approaches is the index flood approach (Dalrymple, 1960; Hosking and Wallis, 1997), which estimates the $T$-year flood as the product of a scale factor, the index flood, typically represented by the mean or median annual flood, and a growth factor describing the relationship between dimensionless flood magnitude and return period. The index flood is often estimated through regression equations, although more sophisticated methods based on geostatistics or process-based reasoning have also been developed. Farquharson et al. (1992) observed that arid catchments tend to exhibit steeper growth curves than humid ones, due to their greater variability and skewness, indicating a higher propensity for outliers. In this framework, the index flood is site-dependent, whereas the growth curve is assumed to be common to all catchments within a homogeneous region. Another widely adopted method is regression-based modeling. In these approaches, similarity is defined implicitly through functional relationships between flood characteristics and catchment or climatic descriptors, implying a continuous spatial variability of flood frequency parameters. These methods assume a relationship between the parameters of the flood frequency distribution and the physical or climatic characteristics of the catchment (Griffis and Stedinger, 2007; Thomas et al., 1970). Generalized Least Squares (GLS) regressions are commonly employed (Tasker and Stedinger, 1989), although maximum-likelihood and Bayesian formulations have also been proposed (Micevski and Kuczera, 2009). These approaches reveal correlations between flood characteristics and basin descriptors, yet correlation alone does not imply causality; therefore, such relationships must always be interpreted within a hydrological framework. Subsequent developments include geostatistical techniques that explicitly account for the spatial correlation of flood characteristics along river networks as the topological kriging (Top-Kriging)

method (Archfield et al., 2013; Skøien et al., 2006). In practice, regional models are often applied not only to ungauged basins but also to those with short records. In such cases, local observations are used to estimate the index flood, while regional information provides the corresponding growth curve (Hebson, 1987; Laio et al., 2011).

An alternative to the previously described statistical methods for regional flood frequency analysis is represented by process-based approaches (e.g., Wright et al., 2020). In these methods, regional or local rainfall information is used as input to rainfall-runoff models that convert precipitation into streamflow. The complexity of these models can vary widely, ranging from very simple conceptual formulations to highly detailed distributed representations. Such methods offer several advantages but also present notable challenges. A first advantage is that, in many regions, rainfall records are typically longer and denser than streamflow observations, leading to more reliable rainfall frequency estimates. A second advantage is that rainfall-runoff models explicitly represent the dominant hydrological processes, including local effects such as storage or hydraulic structures, whereas regional flood frequency analysis transfers only statistical information about annual maximum floods. When estimating floods associated with large return periods, process-based approaches may also provide more realistic estimates, as extreme floods can arise from processes that differ substantially from those captured in limited observed flood records. On the other hand, process-based methods require specification of numerous parameters for the rainfall-runoff model, which is particularly challenging in ungauged basins. These parameters are usually calibrated in gauged catchments and subsequently regionalized to ungauged ones, introducing additional sources of uncertainty, especially when complex model structures are employed. Furthermore, model calibration for flood estimation demands data that include extreme events, not only ordinary floods, which are often scarce or unavailable. The classic and simplest example of process-based methods is the *rational* method, first introduced by Mulvaney (1850) and still widely used around the world. It is an event-based approach that employs a so-called *design storm* as input, derived from the intensity–duration–frequency (IDF) curves for the catchment of interest. The basic concept underlying the rational formula is that the flood peak of a given return period $T$ depends on the annual maximum rainfall intensity with the same return period $T$ and a duration equal to the catchment response time, the catchment area, and a conversion factor that transforms rainfall into runoff (the apparent runoff coefficient). Despite its simplicity, this method

remains popular among practitioners, particularly for small ungauged basins. IDF curves are typically estimated from available rainfall data, while conversion factors are derived for gauged catchments as a function of the return period and then averaged regionally for use in ungauged basins. The dependency of the conversion factor on the return period arises from the influence of event magnitude on rainfall–runoff transformation processes, as discussed previously. While the *rational* method is a clear illustration of both the principles and limitations of process-based approaches, more physically realistic and advanced rainfall–runoff models can also be employed. Among these, *derived distribution* methods (e.g., Eagleson, 1972) represent a family of event-based approaches in which rainfall events are either synthetically designed or based on observed event populations, from which the mapping between rainfall and flood frequencies is inferred. In the design-storm approach, floods are simulated for discrete design events defined by the joint probability of rainfall intensity and duration. A deterministic rainfall–runoff model then transforms these inputs into flood peaks through runoff generation and routing components. A probabilistic framework combines the two, enabling prediction of floods associated with specified return periods. A major challenge, however, lies in the fact that model parameters may vary with event magnitude, and the relationship between the return periods of rainfall inputs and flood peaks depends on storm duration, intensity, antecedent wetness, and other hydrological processes. For example, Viglione and Bloschl (2009) and Viglione et al. (2009) found that both rainfall duration and, especially, the runoff coefficient play a fundamental role in linking rainfall and flood return periods. In arid climates, the flood return period can even be hundreds of times larger than that of the corresponding precipitation event. To overcome the challenge of assigning return periods to individual events, the *entire population approach* can be adopted (Sivapalan et al., 2005). In this framework, all rainfall events are considered, and their associated floods are simulated to derive an empirical relationship between rainfall and flood frequencies. In general, when applying derived distribution approaches, the main difficulty lies in quantifying the joint probabilities of the various controls on the flood frequency curve, such as rainfall duration, temporal patterns, multiple storm events, soil moisture, and routing characteristics. A conceptually distinct approach is represented by *stochastic storm transposition* (SST). Unlike derived distribution methods, which rely on synthetic or parametrically described rainfall inputs, SST exploits the spatial variability of observed storms: a storm recorded anywhere within a meteorologically homogeneous region is assumed to

have had an equal probability of occurring over any other location within that region. This probabilistic rationale, formalized by Foufoula-Georgiou (1989), effectively enlarges the sample of extreme rainfall events available for frequency analysis beyond what local records alone would allow, while preserving the observed spatial and temporal structure of real storms. Building on this concept, Franchini et al. (1996) coupled SST with a rainfall–runoff model and a stochastic representation of antecedent soil moisture conditions to derive flood frequency curves directly, extending the transposition framework from rainfall to flood frequency estimation. Finally, *continuous rainfall–runoff models* (e.g., Falter et al., 2015; Grimaldi et al., 2013), which simulate hydrological processes in a time-continuous manner, can also be employed for flood frequency analysis. In these approaches, rainfall is generated using a stochastic model, and the resulting hydrographs are analyzed to extract flood peaks. The main challenge here remains the accurate representation of flood events with increasing return periods, which requires accounting for changes in runoff generation mechanisms under extreme conditions.

Regional flood estimation methods thus exploit spatial information to overcome the limitations of short or missing records, allowing knowledge transfer across catchments. Yet, while spatial approaches assume that flood-generating processes remain consistent in time, this assumption may no longer hold under changing climatic or land-use conditions. This challenge calls for explicit consideration of temporal non-stationarities.

### 1.2.2 Temporal perspective: non-stationarity

The assumption of temporal stationarity in flood frequency estimation is increasingly challenged by climate variability and land-use change. The *EU Floods Directive (2007/60/EC)* explicitly calls for consideration of future changes in flood risks due to climatic and socio-economic factors (European Union, 2007). This marks a shift from purely reactive flood management toward proactive and adaptive planning strategies.

Europe has experienced a sequence of major floods in recent decades, including the extreme events in western Germany and neighboring countries in mid-July 2021 (Mohr et al., 2023), in central Italy in May 2023 (Cremonini et al., 2024; Valente et al., 2025), and in the Czech Republic and Austria in September 2024 (Hauer et al.,

2025; Komma et al., 2025). These events, and others, which frequently exceeded previously recorded levels, have raised growing concerns about the possible increase in flood frequency and magnitude, and about the extent to which human interventions have contributed to these changes (Hall et al., 2014).

Understanding how and why flood regimes change requires acknowledging the complex interplay of multiple drivers. According to Blöschl et al. (2007), three primary categories of processes influence flood behavior: modifications in river systems, transformations within catchments, and changes in atmospheric forcing. River engineering, including channelization, dam construction, and floodplain disconnection, can substantially alter flood wave propagation, affecting the timing, peak discharge, and overall shape of hydrographs. At the catchment scale, land-use alterations such as urbanization, deforestation, and agricultural practices modify runoff generation, infiltration capacity, and water storage, thereby reshaping flood responses. On an even broader scale, atmospheric drivers, such as variations in precipitation intensity, snowmelt processes, and evapotranspiration, are governed both by natural climate variability and by anthropogenic climate change. These processes interact across scales, producing highly heterogeneous spatial and temporal flood responses across Europe (Hall et al., 2014).

Flood regime changes may manifest as step changes in the mean at a specific point in time, typically resulting from the construction or removal of hydraulic structures along the river; as gradual changes or trends in the mean, often associated with land-use transformations; or as progressive changes in both the mean and variability of floods, generally driven by climatic variability. Bertola et al. (2019) analyzed the impacts of these different types of changes in Upper Austria, finding that atmospheric drivers, particularly short-duration extreme precipitation, tend to exert a stronger influence on changes in flood frequency than catchment or river-scale interventions. Two main strategies exist for investigating flood regime changes (Hall et al., 2014). The first is the *data-based approach*, which relies on long, homogeneous hydrological series to identify statistical changes without explicitly referring to the underlying physical mechanisms. Within this framework, non-parametric tests such as the Mann–Kendall or Pettitt tests are commonly used to detect monotonic trends or step changes in the mean flood magnitude (Villarini et al., 2011). Parametric alternatives include Poisson regression models combined with Chi-squared tests to assess changes in flood occurrence rates (Mangini et al., 2018). These methods typically test null hypotheses of stationarity in the mean, trend, or variability of flood

peaks, distinguishing between abrupt regime shifts (often related to engineering interventions), gradual changes (linked to land-use transformations), and slow trends or changes in variability (associated with climatic influences). The second, *process-based approach* (e.g., Barbhuiya et al., 2023), builds on cause-effect relationships to represent the chain of processes from climate over catchment to the river network. Beyond flood magnitude, the analysis of flood seasonality provides additional insight into the underlying processes of change. Shifts in the timing of annual flood peaks, for example, can indicate changes in dominant flood-generating mechanisms. For example, a transition from snowmelt-driven to rainfall-driven floods or changes in the relative importance of convective and synoptic events (Parajka et al., 2010). Such diagnostics, when integrated with trend analyses, help to distinguish between natural variability and structural modifications of the flood regime.

The relationship between precipitation and flood is not straightforward. Westra et al. (2014) found that short-duration rainfall extremes have intensified across much of Europe, while flood magnitude trends remain spatially heterogeneous, suggesting the concurrent influence of multiple controlling factors. In addition to precipitation, the other main factor modulating the rainfall–flood relationship is the antecedent catchment condition. Soil moisture and storage state determine how rainfall is partitioned between infiltration and direct runoff, and thus strongly influence the flood response (Merz and Blöschl, 2003). Numerous studies have shown that antecedent wetness plays a dominant role in shaping flood volume, particularly for smaller and more frequent floods, while for large, rare floods, precipitation intensity tends to prevail (Bennett et al., 2018; Ho et al., 2023; Wasko et al., 2021). This dual control implies that both precipitation and antecedent conditions must be jointly considered to understand and predict flood regime changes. Antecedent catchment conditions are reflected in the event runoff coefficient, which represents the share of precipitation directly contributing to the runoff. A general decrease in runoff coefficients is expected with increasing temperatures, meaning that possible rainfall increases may be offset by drier soils. Moreover, Wasko et al. (2021) found that an increase in variability of runoff coefficients is expected across most locations, resulting in increased variability in floods. Runoff coefficient also varies at the event scale according to different precipitation characteristics. Merz and Blöschl (2003) found that runoff coefficients tend to increase with rainfall depth for long-rain floods, while they exhibit a larger scatter for flash floods. Snow storage and snowmelt also play a crucial role in modulating flood response, particularly in

temperate and cold regions. In snowmelt-dominated or mixed rain–snow regimes, flood generation is strongly influenced by the timing and energy available for melt, which constrains the upper tail of the flood frequency curve (Merz and Blöschl, 2003, 2008a). Observed reductions in snow cover extent and earlier melt peaks across the Northern Hemisphere (Estilow et al., 2015; Madsen et al., 2014a) indicate that warming temperatures are already altering snow-driven flood regimes. The hydrological effects of these changes depend on regional flood seasonality and the mixing of flood-generating processes. For instance, snowmelt changes mainly affect small spring floods in southern Alpine catchments, but can influence the entire flood frequency curve in northern Europe (Kemter et al., 2020; Merz and Blöschl, 2003).

Global analyses indicate that changes in flood magnitude and frequency are not uniform across climates and regions. Using a non-stationary modeling approach, Slater et al. (2021) provided a global picture of flood trends, showing that 20-year and 50-year floods have generally increased in temperate zones but decreased in arid, tropical, polar, and cold regions, while 100-year floods show mixed trends.

In the United States, flood changes exhibit a complex and fragmented pattern. Analyses of central US stream gauges by Hirsch and Archfield (2015) reveal that while the frequency of floods has increased, the magnitude of events has remained largely unchanged, with peaks-over-threshold (POT) records highlighting these trends more clearly than annual maxima series. Broader studies across the country reveal substantial spatial variability: some groups of gauges experience minimal change, others show increases or decreases in frequency, and yet others record increases across all flood properties (peak magnitude, frequency, duration, and volume), with limited geographic cohesion and little correlation with large-scale climate indices. These findings reveal a complex, fragmented pattern of flood change across the United States (Archfield et al., 2016). Focusing on the largest floods, analyses of 473 near-natural US streams show generally stable occurrence patterns over the last five decades, with few significant annual or seasonal trends (Collins et al., 2022).

Regarding Europe, recent data-driven studies have provided new insight into these evolving patterns. Blöschl et al. (2019b) demonstrated that floods have not changed uniformly but exhibit distinct regional tendencies. In northwestern Europe, increasing autumn and winter precipitation has led to a general intensification of floods, while in southern regions, declining rainfall combined with increasing evaporation has caused a reduction in flood magnitudes, particularly in medium and large basins. In Eastern

Europe, the reduction in snow cover and snowmelt, linked to rising temperatures, has similarly contributed to declining flood discharges. Across the continent, observed flood trends range from increases of about 11% per decade to decreases of up to 23% per decade, reflecting a strong spatial contrast in hydro-climatic responses.

Although the spatial and temporal variability of these observations complicates the identification of a single continental-scale trend, the regional patterns identified by Blöschl et al. (2019b) are broadly consistent with climate model projections for the coming century (Kundzewicz et al., 2017; Thober et al., 2018). This convergence between observation and projection suggests that climate-driven alterations in flood regimes are already underway. The evidence underscores the urgent need to move beyond traditional, stationary flood frequency analysis and toward non-stationary, process-based frameworks that explicitly account for climatic variability and human influence on hydrological systems (Hall et al., 2014).

The spatially heterogeneous trends observed across Europe highlight the complexity of flood-generating processes. Catchments do not respond uniformly to climatic forcing, and the sign and magnitude of flood trends depend on both the size of the catchment and the flood magnitude considered. Smaller and larger floods often respond differently to the same external perturbations, reflecting the scale-dependent nature of the underlying hydrological and atmospheric mechanisms. Building on the continental analysis by Blöschl et al. (2019b), Bertola et al. (2020) and Bertola et al. (2021) examined whether trends in flood discharges also occur at larger return periods, while accounting explicitly for catchment scale. Their results reveal consistent spatial patterns but also substantial differences across scales. In northwestern Europe, flood magnitudes generally show positive trends, particularly in small catchments (up to 100 $km^2$), where the 100-year flood tends to increase more than the median flood. Conversely, in medium and large catchments, the magnitude of positive trends weakens and even turns negative in some regions, such as northwestern France. This pattern suggests that small basins, being more directly influenced by intense, short-duration rainfall, are more sensitive to the increasing frequency of convective storms and atmospheric rivers. In contrast, larger basins, which integrate longer-duration synoptic events and more diverse runoff generation processes, show more muted or compensating trends. In southern Europe, flood trends are generally negative, consistent with declining precipitation and soil moisture driven by rising temperatures and evapotranspiration. Yet, the rate of decrease differs between flood magnitudes: smaller floods (e.g. 2-year return period) show stronger negative trends than larger,

rarer floods (e.g. 100-year return period), leading to steeper flood frequency curves and greater flood variability. This asymmetry suggests that soil moisture depletion primarily suppresses moderate floods, while extreme events remain partly controlled by high-intensity rainfall, whose occurrence is less directly tied to mean moisture conditions. In Eastern Europe, both small and large floods exhibit pronounced negative trends across all catchment sizes. These declines are linked to warmer winters, earlier snowmelt, and shrinking snowpack extent, which collectively reduce the volume and delay the timing of spring floods. The magnitude of the decrease becomes larger with increasing catchment area, indicating that snowmelt processes (inherently large-scale and gradual) exert a dominant control on flood behavior in the region. Figure 1.4 explicitly links the effects of the main drivers of both small and large flood changes.

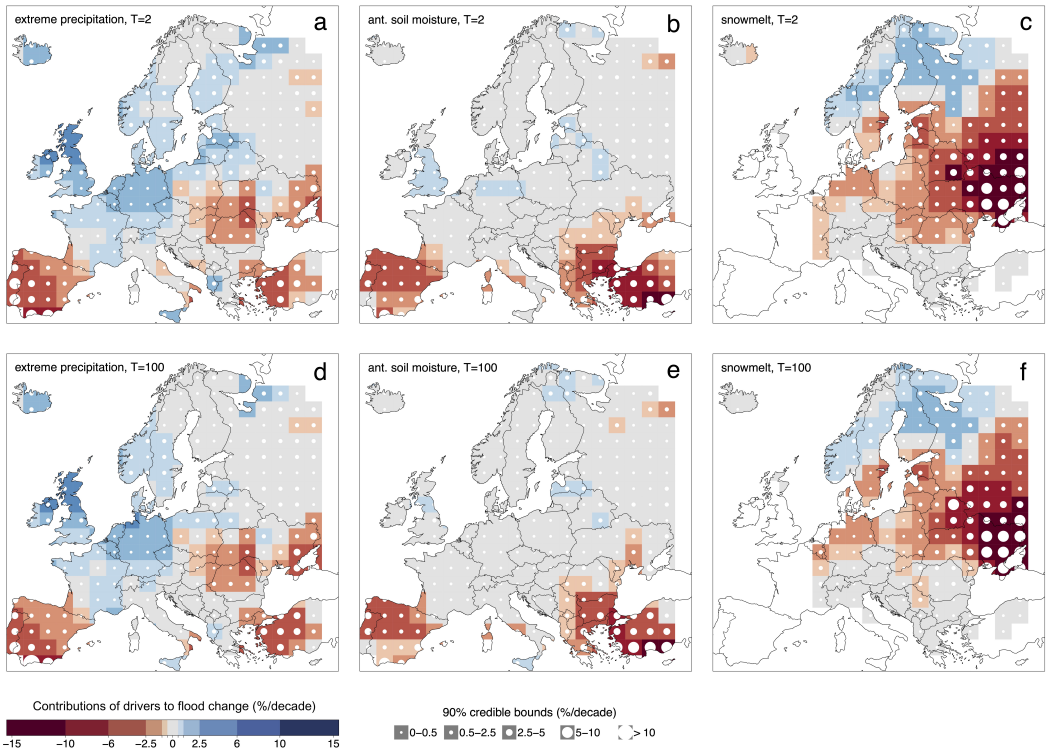


Fig. 1.4 contributions of extreme precipitation (a, d), antecedent soil moisture (b, e), and snowmelt (c, f) to changes in $q_2$ and $q_{100}$. The figures on the top row refer to ordinary floods (2-year return period), while those in the bottom row refer to rare floods (100-year return period) (Bertola et al., 2021).

A deeper understanding of flood regime changes requires moving beyond the analysis of trends in discharge magnitude and considering the underlying flood generation

processes. As highlighted by Tarasova et al. (2023), changes in the mechanisms that generate floods are key to explaining the observed spatial and temporal variability of flood behavior across Europe. In a changing climate, not only the dynamics of the atmospheric system but also the hydrological processes on the land surface are evolving. Observed shifts in flood timing and process attribution indicate that, in cold regions, floods induced by rain-on-snow are becoming more frequent at the expense of snowmelt floods, while in temperate regions, convective rainfall events increasingly dominate over synoptic-scale systems. These process-level changes directly influence both the frequency and magnitude of flood peaks. Tarasova et al. (2023) showed that shifts in these processes have contributed more to the occurrence of flood-rich and flood-poor periods than changes in extreme precipitation alone. Their results reveal pronounced regional contrasts in process dominance. In northern and Atlantic Europe, the frequency of floods generated by rainfall on wet soils has increased markedly. In these regions, wetter antecedent conditions and rising winter precipitation enhance the propensity for saturation-excess runoff, consistent with the overall increase in flood magnitude and frequency observed in northwestern Europe. Conversely, in the Mediterranean and Central-Alpine regions, the frequency of floods generated by rainfall on dry soils has increased, reflecting declining soil moisture and rising evapotranspiration. At the same time, the frequency of snow-related floods has decreased substantially across Europe, consistent with observed warming and the shrinking role of snowmelt as a flood driver. These process-based insights help explain why different regions experience contrasting flood trends and why flood magnitude trends differ between small and large floods. In the Mediterranean and Central-Alpine regions, the increasing relevance of rain on dry events, linked to drier soils and higher evaporative demand, contributes to the persistence of a flood-poor regime. However, such events exhibit heavier-tailed discharge distributions compared to other mechanisms (Merz et al., 2022), implying that while overall flood frequency may decline, the probability of singular, high-magnitude events may increase. This mechanism helps reconcile the apparent paradox of decreasing mean flood magnitudes alongside persistent or even growing risks of extreme floods (Bertola et al., 2020; Blöschl et al., 2019b). Overall, the findings of Tarasova et al. (2023) reinforce that the evolution of flood regimes cannot be fully understood without accounting for changing flood generation processes.

Considering the process-based mechanisms discussed above, the balance among precipitation, antecedent soil moisture, and snow storage and melt varies across

space, time, and flood magnitude, shaping the contrasting flood trends observed in different European hydroclimates. Recent evidence from Austria (Haslinger et al., 2025) shows marked increases in both daily and hourly heavy rainfall over the past four decades, about 8% and 15%, respectively, consistent with Clausius–Clapeyron scaling and regional temperature increases. However, the link between precipitation change and flood change is not straightforward (Figure 1.5). While daily heavy rainfall changes are consistent with flood increase in large catchments, flood increases in small catchments (25% over the last four decades) are stronger than hourly rainfall changes (Haslinger et al., 2025).

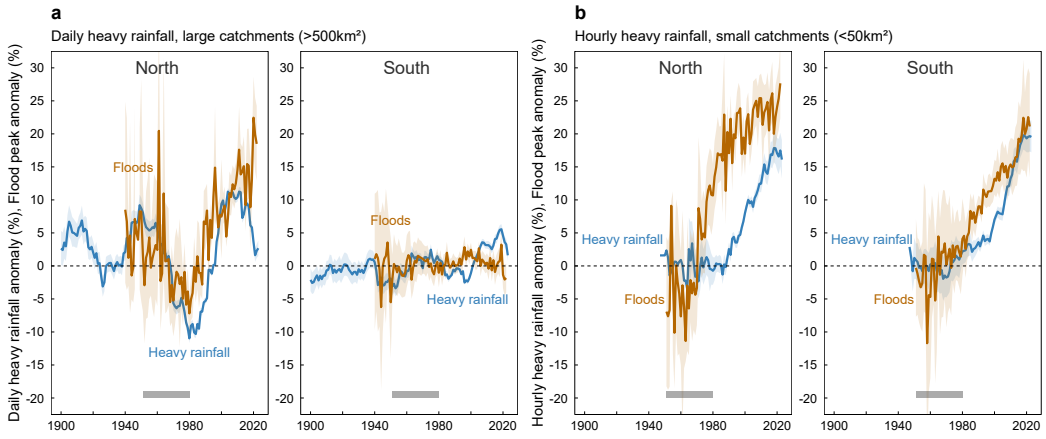


Fig. 1.5 Anomalies in daily extreme precipitation and flood peak discharges for large catchments (area > 500 km²) located north (left panels) and south (right panels) of the Alps. b, Anomalies in hourly extreme precipitation and flood peak discharges for small catchments (area < 50 km²), again separated by their position relative to the Alps. Extreme precipitation is defined by the 99th percentile, while flood peaks correspond to the mean annual maximum discharge during the warm season. The grey bars at the bottom of each panel denote the reference period. Solid curves represent the station-averaged signal, with shaded envelopes indicating the 95% confidence interval of the mean. A close correspondence emerges between daily precipitation extremes and floods in large basins, as well as between hourly precipitation extremes and floods in small basins, reflecting the role of catchment-scale water travel times in shaping flood response (Haslinger et al., 2025).

## 1.3 Existing approaches

### 1.3.1 Approaches to regional flood frequency analysis

Regionalization is a widely applied approach in hydrology for estimating design variables at ungauged sites or where data records are short relative to the recurrence interval of interest (Stedinger, 1993). A classical and extensively used technique for regional flood frequency analysis is the index-flood method (Dalrymple, 1960), whose evolution and applications have been thoroughly reviewed by Grimaldi et al. (2011a). According to this procedure, the T-year flood at a given site, $q_T$, is expressed as the product of the index flood, $q_{ind}$, which reflects the local scale of floods, and a dimensionless growth factor, representing the relationship between dimensionless flood and recurrence interval (the so-called growth curve).

The traditional implementation of the index-flood method assumes the existence of homogeneous regions, within which the statistical properties of dimensionless flood flows are invariant with location (Gabriele and Arnell, 1991). Several extensions have been proposed, such as hierarchical procedures that consider statistics of increasing order over nested regions (Gabriele and Arnell, 1991), and the region of influence (RoI) approach, which replaces fixed contiguous regions with dynamically defined pooling groups that maximize hydrological similarity with the site of interest (Burn, 1990; Castellarin et al., 2001; Zrinji and Burn, 1996). More recent advances remove the need to define explicit boundaries, instead allowing regional parameters to vary continuously with geomorphoclimatic indices (Alila, 1999; Di Baldassarre et al., 2006a,b) or using geostatistical techniques.

The index flood, $q_{ind}$, can be directly estimated as the arithmetic mean of annual maxima when sufficient at-site data are available. For ungauged sites, indirect methods are required, the most common being multiregression models linking $q_{ind}$ to catchment descriptors such as drainage area, precipitation, and channel length (Brath et al., 2001; Castellarin et al., 2007). The selection of descriptors and calibration of parameters can be performed via stepwise regression or alternative multivariate methods, including artificial neural networks, principal component analysis, or canonical correlation analysis (Chokmani and Ouarda, 2004; Ouarda et al., 2001; Shu and Burn, 2004). Statistical indirect models generally provide more accurate estimates than conceptual models for ungauged basins (Brath et al., 2001).

Once the index flood is determined, the regional dimensionless quantile, $q_T$, must be estimated. This requires the identification of a homogeneous pooling group of sites and the selection of a suitable regional frequency distribution. Hosking and Wallis (Hosking and Wallis, 1997) proposed an approach based on L-moments, summarizing the frequency regime of the pooling group through regional L-moment ratios. Numerous applications have demonstrated the reliability of this approach in different hydrological contexts (Bobee et al., 1996; Robson and Reed, 1999). Homogeneity of the pooling group is a key requirement for effective estimation of the growth factor, and can be assessed through standardized measures of intersite variability of L-moments (Stedinger and Lu, 1995; Viglione et al., 2007).

Selection of the parent distribution is also guided by regional L-moments. Candidate distributions typically include generalized logistic (GLO), generalized Pareto (GPA), lognormal (LN3), Pearson type III (PE3), and generalized extreme value (GEV) (Hosking and Wallis, 1997; Peel et al., 2001; Vogel and Fennessey, 1993). The GEV distribution, in particular, has been widely documented as suitable for representing the frequency of geophysical extremes in diverse contexts (Castellarin et al., 2001; Robson and Reed, 1999; Stedinger, 1993; Vogel and Wilson, 1996).

Validation of the regional model is essential, particularly for predictions in ungauged basins. The jack-knife resampling procedure provides a robust cross-validation framework, where each gauging station is sequentially excluded from the analysis, the regional model is recalibrated, and the quantity of interest is predicted for the excluded site. Estimates are then compared to reference values using metrics such as relative bias, mean squared error, and the Nash–Sutcliffe efficiency (Castellarin, 2007; Shao and Tu, 2012).

In recent years, machine learning (ML) techniques have emerged as a promising tool for regional flood frequency analysis (RFFA), complementing and in some cases surpassing traditional regression-based methods (Nourani and Moradkhani, 2017; Vafakhah et al., 2012; Wittenberg, 1999). Classical approaches, such as multiple linear regression and its nonlinear variants, have been widely used due to their simplicity and computational efficiency. However, they assume either linear or simple log-transformed relationships between watershed attributes and flood quantiles, which can be limiting because hydrological processes are inherently nonlinear and influenced by complex spatial and temporal variability (Vafakhah et al., 2012; Wittenberg, 1999). Machine learning models, including artificial neural

networks (ANNs) (Shu and Ouarda, 2008), decision trees (DTs) (Vafakhah et al., 2012), support vector regression (SVR) (Nourani and Moradkhani, 2017), adaptive neuro-fuzzy inference systems (ANFIS) (Vafakhah et al., 2012), genetic algorithms (GA) (Shu and Ouarda, 2008) can capture complex nonlinear relationships and interactions among multiple catchment descriptors, often improving the accuracy of flood quantile predictions.

These methods also offer practical advantages: they require relatively fewer assumptions about the underlying physical processes, can handle large and heterogeneous datasets, and provide flexibility in model design and variable selection. Examples of successful applications include ANN models applied to hundreds of gauging stations and combined ANN–canonical correlation analysis models for improving regional generalization across catchments (Afrin et al., 2025; Shu and Ouarda, 2008). Nonetheless, the use of ML in RFFA also has limitations: model performance heavily depends on the availability of high-quality and sufficiently large datasets, and the interpretability of ML models can be limited compared to traditional physically-based or statistical models. Moreover, their effectiveness in regions with sparse data remains uncertain (Aziz et al., 2014). Overall, ML-based approaches are increasingly recognized as a valuable complement to other traditional methods, particularly when nonlinearities and complex interactions dominate flood behavior (Zalnezhad et al., 2022).

### 1.3.2 Approaches to non-stationarity in flood frequency analysis

As discussed in the previous sections, understanding changes in flood regimes can be approached from two complementary perspectives: the data-based approach, and the process-based approach. Where long and reliable data series are not available, or are missing as in ungauged basins, the process-based approach is the most used prediction tool. In this regard, Barbhuiya et al. (2023) provide a review of the methods developed to deal with non-stationarity in flood frequency analysis, including some case studies. The most popular approach, which is a combination of data-based and process-based methods, is the use of time-varying parameters of the probability distribution of flood peaks, using time or hydroclimatic variables like temperature or mean annual precipitation as covariates. Generalized Additive Models are used to estimate the location, shape and scale parameters of the distribution (GAMLSS framework). For example, Šraj et al. (2016) compared stationary and non-stationary

models using the GEV distribution with parameters dependent on time and annual precipitation. They found that the best performance for 2 gauging stations in Slovenia is obtained using the annual precipitation as a covariate. Westra et al. (2013) used globally averaged near-surface temperature as a covariate for non-stationary generalized extreme value analysis, finding a statistically significant association with precipitation extremes at the global scale. A similar approach was developed by Anzolin et al. (2023) who considered climatic drivers of floods as covariates, to improve non-stationary flood frequency analysis in Brazil. They assumed a linear dependency between the location parameter of a GEV distribution and the selected covariates. Their results suggest that using local climate information (annual rainfall and annual maximum rainfall), or global climate information (El Niño Southern Oscillation) as covariates leads to better model performance when there is a significant correlation between flood and climate covariates. However, such kind of approaches may not be suitable for small-scale analyses, where local phenomena may blur large-scale atmospheric factor (Steirou et al., 2019). Moreover, short-term trends and multi-decadal shifts in some hydrological variables may be a limitation to this kind of approach (Koutsoyiannis and Montanari, 2015). To address these issues, Awasthi et al. (2022) proposed the asynchronous, semiparametric local-likelihood regression (ASLLR-MM), which relates the first two moments (mean and variance) of annual maximum floods to local climate variables. By modeling these moments locally and allowing for asynchronous effects of climate drivers, ASLLR-MM is particularly well-suited for application in specific catchments, improving flood frequency estimates under non-stationary conditions.

Building on the GAMLSS framework, regional flood frequency analysis offers a more robust approach to improve flood quantile estimation by pooling information from multiple sites according to geographical or hydrological similarity (Vogel et al., 2011). For example, Bertola et al. (2020) estimated regional flood trends using a regional Gumbel distribution, whose median and growth factor can change in time with different strengths for different catchment sizes. Their analysis revealed distinct trends across different European regions. Additionally, Bertola et al. (2021) proposed a framework for attributing these flood changes to potential drivers. In southern Europe, both antecedent soil moisture and extreme precipitation contribute to flood changes, and their relative importance depends on the return period. Cunderlik and Burn (2003) used a different approach, separating the non-stationary pooled quantile function into a time-dependent local component and a time-independent regional

component. Leclerc and Ouarda (2007) introduced a regional Flood Frequency Analysis at ungauged sites using a multiple regression model with 2 to 4 explanatory variables within the hydrologic neighborhood. Other strategies to include non-stationarity imply the usage of Bayesian approaches to incorporate expert knowledge into the modeling process (Barbhuiya et al., 2023). In particular, Guo et al. (2022) proved that non-stationary Bayesian regional flood frequency analysis coupled with linear mixed effect reduced flood estimation uncertainty when compared to stationary generalized least squares model in the Dongting Lake basin (China).

Another approach involves the use of regional climate models to evaluate hydrological responses to climate change (e.g., Fiseha et al., 2014; Mishra and Herath, 2015). Physically based hydrological models are first calibrated with observed data and then forced with bias-corrected daily outputs from the regional climate models. Although effective, this method requires meticulous calibration and complex bias correction, which can limit its practicality for broad implementation across multiple catchments. In summary, while many different approaches to address nonstationarity have been proposed in the literature, a standardized operational method for incorporating it into the calculation of Flood Frequency Curves is still lacking.

### 1.3.3 Approaches to deal with uncertainty

Uncertainty is an inherent feature of hydrological analysis, arising from data limitations, model simplifications, and the complex and evolving nature of hydrological processes. Traditionally, uncertainty has been perceived as a problem to be minimized, as it complicates decision-making and is often interpreted as undermining the reliability of flood estimates. However, an increasing body of literature argues that uncertainty can also be regarded as a resource, providing valuable information about the range of plausible outcomes and about the robustness of both models and decisions (e.g., Dittes et al., 2018; Franks et al., 2015; Meresa et al., 2021).

In the context of flood frequency estimation, explicitly acknowledging uncertainty helps to reveal the sensitivity of design values, such as the 100-year flood, to assumptions related to distribution choice, record length, and model structure. Rather than relying on a single deterministic estimate, probabilistic frameworks allow uncertainty to be represented explicitly, distinguishing between aleatory variability and epistemic uncertainty associated with limited knowledge. From this perspective, uncertainty is

not merely noise to be ignored, but a quantitative expression of the limits of current understanding and an invitation to explore alternative hypotheses.

Several methodological approaches have been developed to characterize and propagate uncertainty in flood frequency analysis. Bootstrap and resampling techniques provide a non-parametric means of quantifying sampling uncertainty by repeatedly resampling the observed data and recalculating flood quantiles. These methods are widely used to assess the variability of estimated quantiles due to finite record length, without imposing strong distributional assumptions (Chong and Choo, 2011). Similar bootstrap approaches are employed in other hydrological fields, e.g., to quantify uncertainty in water quality trend estimates (Hirsch et al., 2015).

Another approach to deal with uncertainty is the sensitivity analysis, which allows exploring how flood quantile estimates respond to variations in model parameters, input data, or methodological choices. In hydrological applications, sensitivity analysis is particularly useful for assessing the robustness of flood quantiles to decisions such as event selection criteria, threshold definition, or model configuration. Rather than identifying a single optimal setup, this approach helps delineate ranges of plausible outcomes and identify dominant sources of uncertainty (e.g., Pianosi et al., 2016; Saltelli, 2002).

A more comprehensive framework for uncertainty quantification is offered by Bayesian statistics, which originates from Bayes' theorem and assume that probability can be updated as new information becomes available. In the Bayesian perspective, model parameters and predictions are treated as random variables described by probability distributions. Bayesian flood frequency analysis combines prior information with observational data to derive posterior distributions of flood quantiles, thereby integrating multiple sources of information in a coherent probabilistic framework and naturally accounting for parameter uncertainty (e.g., Kuczera, 1999; Renard, 2011; Viglione et al., 2013).

When translated into flood risk management and protection practice, probabilistic approaches shift the focus from single design values to distributions of possible outcomes. Designing under uncertainty encourages the exploration of multiple plausible futures rather than reliance on a single "most likely" scenario (Berends et al., 2019). This perspective supports robust and adaptive planning, ensuring that flood protection measures remain effective even when future conditions deviate from

expectations. In this sense, uncertainty becomes a catalyst for better decision-making, enhancing transparency and resilience rather than representing a limitation.

## 1.4 Research Aim and Contributions

The motivation for this research stems from the recognition that many fundamental questions in hydrology remain unresolved, as highlighted by the 23 open problems identified by the international hydrological community (Blöschl et al., 2019a). Among these, the question of how flood-rich and drought-rich periods arise, whether they are changing, and why (Problem 9) is directly concerned with the variability of hydrological extremes across space and time. Addressing this question requires improved understanding and modeling of the processes governing the spatial and temporal variability of hydrological extremes, which forms a central focus of this research.

Floods, in particular, lie at the intersection of multiple sources of non-stationarity: climatic shifts, landscape alteration, and complex spatial structures in both rainfall and runoff generation. Addressing these issues requires methodological frameworks that integrate spatial dependence, temporal variability, and physical process understanding. This thesis contributes to the field of flood frequency analysis by making advances in the development of a *spatio-temporal framework* for estimating flood quantiles under non-stationary conditions. The research advances three complementary directions, each aligned with the broader scientific challenges posed by variability in time, variability in space, and the nature of hydrological extremes.

This thesis is structured into three main chapters, each derived from apparently independent research work and each developing a distinct methodology with its own specific objectives. Taken together, however, these chapters form a coherent and integrated research framework, in which the different approaches complement one another. In the first one, the key contribution lies in the update of flood quantiles in the Po River basin, achieved by integrating multiple independent regional flood frequency models, all calibrated on a common and rigorous dataset. This multi-model perspective provides a more robust and transparent framework for estimating flood quantiles at the regional scale. The second chapter develops an operative procedure to incorporate projected changes in precipitation extremes into flood frequency analysis (Cafiero et al., 2025). By exploiting quantile–quantile relationships between

precipitation extremes and flood peaks, the method translates projected changes in IDF curves into adjusted Flood Frequency Curves. This provides a practical, scalable tool to assess how shifts in extreme rainfall may propagate to future flood hazards. The third chapter introduces a Bayesian process-based framework for flood frequency analysis under non-stationary hydroclimatic conditions. The model jointly represents storms, soil moisture, and catchment response, allowing the attribution of projected flood changes to specific mechanisms, resulting in a process-consistent procedure that allows for assessing climate-sensitive flood hazards. This contributes to understanding the physical processes underlying flood frequency variations and enables linking these variations to the specific mechanisms driving flood generation.

# Chapter 2

# Characterization of flood extremes in the Po River Basin

## 2.1 Regulatory framework

Flood risk represents a major environmental, social, and economic challenge for Italy, a country characterized by complex hydrographic and geomorphological conditions. In order to address this issue within a harmonized European framework, Directive 2007/60/EC on the assessment and management of flood risks was transposed into Italian legislation through Legislative Decree No. 49/2010. This decree establishes the obligations, procedures, and governance structure for the preparation, implementation, and periodic review of Flood Risk Management Plans (PGRA), to be carried out by the Basin District Authorities in close cooperation with regional and national institutions. Public participation is identified as a mandatory and strategic component at all stages of the planning cycle. In accordance with the decree, flood risk management follows a six-year cyclical process structured around three main phases. The first phase involves a preliminary flood risk assessment, aimed at identifying areas with potentially significant flood risk by analyzing historical events, geomorphological characteristics, and the projected impacts of climate change. The second phase focuses on the preparation of flood hazard and flood risk maps, which respectively illustrate the probability and magnitude of potential inundation and the spatial distribution of exposed elements along with their potential consequences. The final phase concerns the drafting of the PGRA, which establishes flood risk

management objectives and specifies the structural and non-structural measures needed to mitigate the adverse effects of flooding on human health, the environment, cultural heritage, and economic activities.

Flood hazard maps depict the extent, water depth, and flow characteristics associated with three standardized probability scenarios (high, medium, and low probability), as required by Legislative Decree 49/2010. Correspondingly, flood risk maps provide an assessment of exposed receptors, such as population, critical infrastructure, industrial facilities, and protected areas, and classify risk into four levels (R1–R4), ranging from low to very high. The PGRA establishes risk reduction objectives that must be coherent with European and national sustainability commitments and must ensure cross-scale coordination between Basin District Authorities, Regions, and local administrations. The decree also mandates the periodic revision of all components of the risk management cycle to account for new knowledge, planning updates, and the evolving impacts of climate change. Within the national planning framework, the *Piano di Assetto Idrogeologico* (PAI) represents a fundamental tool for hydrogeological and flood risk governance. The PAI provides regulatory guidelines for land-use planning, defines acceptable levels of flood protection, typically linked to return periods of 100–200 years, and classifies areas according to degrees of restriction or protection. It serves as a complementary instrument to the PGRA by ensuring consistent protection standards for settlements, economic activities, infrastructure, and environmentally or culturally valuable areas.

In this evolving context, where updated scientific knowledge and climate change considerations are essential for effective risk management, there is a growing need for robust, data-driven analyses of hydrological extremes. Accurate characterization of flood frequency regimes represents a key component of both PGRA revisions and PAI updates, ensuring that planning decisions and protection standards reflect current and future hazard conditions. It is within this framework that the project titled *"Characterization of the Frequency Regime of Hydrological Extremes in the Po River District, also Considering Climate Change Scenarios"* was established. The project arises from a collaboration agreement between the Po River District Basin Authority (ADBPO) and five Italian universities: Politecnico di Torino (DIATI), Università di Bologna (DICAM), Politecnico di Milano (DICA), Università di Parma (UNIPR), and Università di Brescia (UNIBS). This partnership aims to develop updated methodologies for the analysis of hydrological extremes, supporting the PGRA's cyclical revision and contributing to flood risk mitigation across the entire

Po River District. By integrating updated hydro-meteorological datasets with modern analytical tools, the project seeks to provide harmonized knowledge of flood hydrology, improve the reliability of frequency estimates for extreme events, and offer quantitative support for territorial planning and flood risk mitigation strategies under both present and projected climate conditions. The project's activities cover a wide range of technical domains. One of the fundamental components is the collection, cleaning, and quality control of data, which ensures the reliability and consistency of the information used throughout the project. Another key area involves the development and validation of advanced models for analyzing the frequency of floods and rainfall events. In addition, the project focuses on the spatial extrapolation of results to poorly gauged sites through regionalization techniques, allowing for broader applicability even in areas lacking direct measurements. Finally, the project places strong emphasis on capacity-building and knowledge transfer, ensuring the long-term sustainability and practical implementation of the project's outcomes.

## 2.2 Update of flood frequency curves in the Po River basin

The objective of the project is to improve the understanding and estimation of flood frequency regimes across the Po River District. Previous planning instruments in the Po River Basin, most notably the PAI (Piano di Assetto Idrogeologico, Hydrogeological Management Plan) and the PGRA (Piano di Gestione del Rischio di Alluvioni, Flood Risk Management Plan), were largely based on studies developed between the late 1990s and early 2010s. While essential at the time, these efforts relied on datasets often truncated around 2000–2005, and on methodological standards that predate key developments in hydrology, statistics, and climate science. Since then, several critical developments have emerged. First, there has been a substantial increase in extreme weather events, with a notable rise in short-duration, intense rainfall episodes and sudden flash floods, which require more effective risk management strategies. At the same time, monitoring systems have significantly improved, offering longer and more complete time series that enhance our ability to analyze trends and understand evolving patterns. These enhanced datasets provide a more robust foundation for frequency analysis of hydrological extremes and decision-making. Lastly, progress in statistical and computational techniques has expanded the range of tools available

to model and assess flood risks with increasing accuracy and efficiency. Collectively, these developments support a more robust and flexible treatment of flood risk under evolving conditions.

Thus, the update is not only timely but necessary to ensure that planning tools accurately reflect both current and future flood risks. First, the project aims to create a harmonized and updated dataset of annual floods for all sub-basins, providing a consistent foundation for analysis across the entire region. Subsequently, the project seeks to produce updated flood frequency curves for 226 sub-basins, enabling a more precise estimation of extreme events at multiple scales. Finally, the results undergo a critical analysis and comparison with previous data used in the development of key planning instruments, providing essential insights to refine and improve the effectiveness of flood risk management strategies.

## 2.3 Hydrological dataset construction and quality control

The foundation of the analysis rests on a comprehensive hydrological dataset for the available catchments distributed throughout the Po River Basin. This dataset was assembled through a rigorous process of revision and harmonization, involving collaboration with regional environmental protection agencies (ARPA) and ADBPO. The reference dataset is the Catalogo delle Piene dei Corsi D'Acqua Italiani (Claps, 2020), which collects and systematizes historical records of annual maximum flows from the 1920s onwards. Additional stations were added via ARPA contributions taking advantage of more recent hydrometers installed in the area, particularly in the Romagna region, reaching a number of 295 stations with at least 5 measurements of annual flood. Data quality and homogeneity was then assessed. This was essential to ensure that the time series were statistically reliable for frequency analysis. To do this, a non-parametric change-point test (Pettitt Test) was applied to detect abrupt shifts in the mean of the annual maxima series. Several stations showed statistically significant changes; however, for most of these, a closer inspection of the two sub-samples identified before and after the detected change-point revealed that the difference between their means was not substantial enough to compromise the reliability and homogeneity of the series. Consequently, these records were retained

for subsequent analysis. In contrast, two stations, 'Savio at Mercato Saraceno' and 'Sarca at Malga Caret', exhibited anomalous trends and were therefore excluded from subsequent regional frequency modeling. Data were then filtered and corrected based on hydrological coherence, spatial homogeneity, and record quality. To ensure a correct application of the regional models used to estimate the flood frequency curves, particular attention was paid to removing catchments downstream of large reservoirs or with excessively large contributing areas (> 15000 $km^2$). Moreover, some time series (or individual observations) of annual peak discharges were discarded after a thorough critical review of the dataset. This review was carried out in close collaboration with the Po River Basin Authority and the regional agencies (ARPA), and also in response to initial findings from the application of the proposed regional models. Table 2.1 summarizes all the reasons why certain gauging stations were excluded from the analysis.

Table 2.1 Time series excluded from the application of regional models. Sensors marked with an asterisk indicate partial data removal. Appendix A provides the complete list of initially available stations with annual maximum series

| **Reason for exclusion** | **Removed basins** |
|---|---|
| Upstream reservoir | A034, A035, A076, A180, A214, A215, A216, A221, B022∗, B053, B072, B075, B089 |
| Duplicate Qc series | A050, A102∗, A165, B006 |
| Upstream overflows | A060, A169, A170, B028∗ |
| Non-homogeneous series | A094, B005 |
| Limited representativeness of flood behavior | A103, B033, B042, B044, B057, B059, B080, B081, B083, B086, B096 |
| Merged with downstream gauging station | A127, A129, A148 |
| Diversion or discharge structures | A144, A205, A212, A227 |
| Index flood scaling law not respected | A128∗, B004, B016∗, B043, B058, B066, B069, B098∗, B100, B103∗, B105 |
| Modulated or non-natural peak flow | A210, A217, A219, A222, A225 |

In the end, the reference dataset includes 226 river basins, whose geographic location and sample size are shown in Figure 2.1. The resulting database served as the common ground for applying and comparing different statistical models.

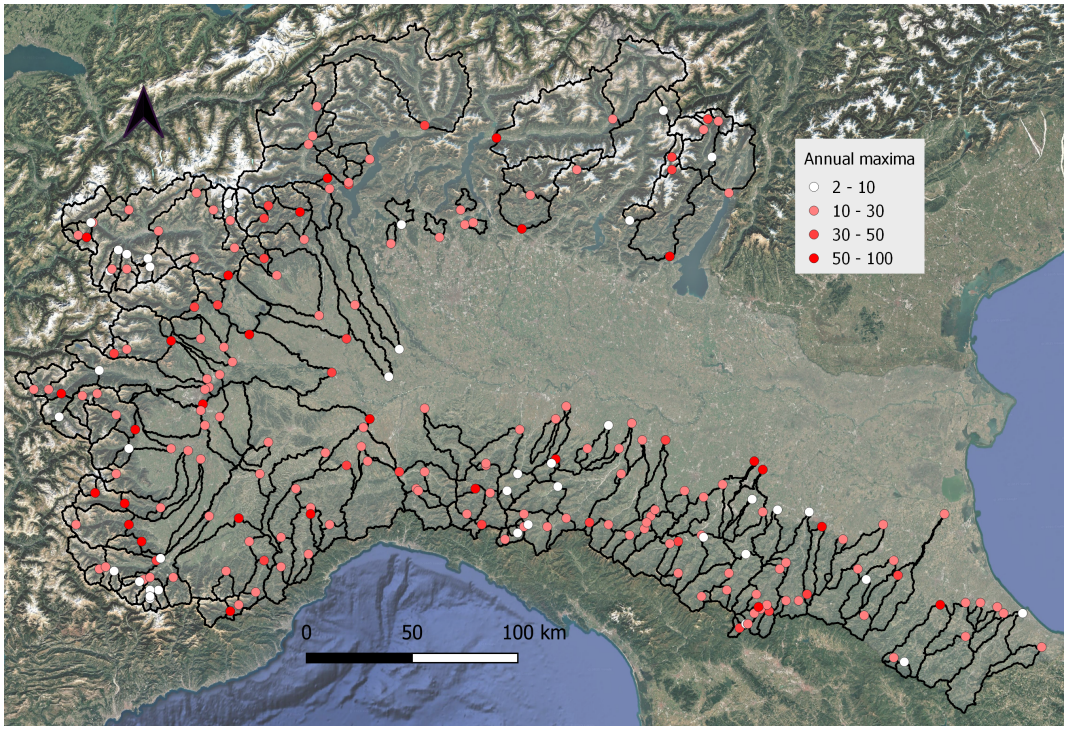


Fig. 2.1 Location of the 226 stations used in the regional analysis, together with their corresponding basin boundaries. The number of available annual flood maxima at each station is also shown.

## 2.4 Regional modeling strategies for flood frequency estimation

Before describing the regional methods, it is useful to clarify two terms that recur throughout this chapter. The *flood frequency curve* (FFC) describes the full relationship between the design discharge $q_T$ and the return period $T$, and it is therefore characterized by statistical moments (e.g., mean, coefficient of variation, and asymmetry) that define its shape. The *growth curve*, on the other hand, refers specifically to the dimensionless factor $K_T = q_T/q_{\text{ind}}$, which describes how flood quantiles scale with return period relative to the index flood $q_{\text{ind}}$. While the growth curve is a component of the flood frequency curve, it is treated separately in regional frequency analysis because it can be estimated from pooled data across hydrologically similar catchments, independently of the local index flood.

Three innovative methodologies were applied independently by the three main academic partners: Politecnico di Torino (Spatially Smooth Estimation Method (Laio et al., 2011)), Università di Bologna (Region Of Influence (Castellarin et al., 2000; Dalrymple, 1960)), and Politecnico di Milano (Updated VAPI Method (De Michele and Rosso, 2001)) each using different theoretical and computational frameworks.

### 2.4.1 Spatially Smooth Estimation Method

The Spatially Smooth Estimation Method (SSEM), developed by Laio et al. (2011) and employed by Politecnico di Torino, is a regionalization framework that enables the transfer of hydrological information from gauged to ungauged catchments. The method addresses the absence of local flow records by exploiting observations collected at multiple sites across a region, while explicitly accounting for their hydrological heterogeneity and the spatial correlation among them. In the SSEM approach, flood frequency estimation is performed through a set of generalized multiple regression models. These models relate key flood statistics to catchment descriptors such as geomorphology, climate, and land use. Specifically, the method aims to regionalize three fundamental parameters: the index flood $q_{\text{ind}}$, and the L-moment coefficients of variation and asymmetry, $L_{CV}$ and $L_{CA}$, respectively. Because these indicators summarize the magnitude and shape of the local flood-frequency distribution, their regional estimation allows the derivation of design floods even at sites without streamflow observations. The design quantile $q_T$ for a given return period $T$ is then computed as:

$$q_T = q_{\text{ind}} \cdot K(L_{CV}, L_{CA}, T) \tag{2.1}$$

where $K(\cdot)$ is an analytically derived growth factor. This formulation implies that $q_T$ can be computed at any location solely from regionalized parameters, avoiding the need for local historical series.

A key feature of the SSEM regional regressions is that they incorporate the uncertainty of site-specific flood estimates through a generalized least squares (GLS-type) structure. This formulation accounts for both the sampling variability of the L-moments, allowing the method to weight each gauged site according to the reliability of its data. As a result, the regressions yield not only regional estimates of $q_{\text{ind}}$, $L_{CV}$

and $L_{CA}$, but also their associated variances, which naturally reflect the differing accuracy of the local L-moment estimates (Laio et al., 2011).

The final regression models are the outcome of an extensive exploratory analysis. Initially, a large set of 99 geomorphological and climatic descriptors was considered. All possible combinations of these descriptors, up to a maximum of four predictors per model, were systematically tested, resulting in tens of thousands of candidate regressions for each target variable. Both additive and multiplicative (log-transformed) model structures were explored. Candidate models were screened based on statistical significance of coefficients, multicollinearity diagnostics, and goodness-of-fit metrics, and were subsequently validated through residual analysis to ensure compliance with standard regression assumptions. The resulting regression models for the entire Po River District, one for each of $q_{\text{ind}}$, $L_{CV}$, and $L_{CA}$, were obtained:

$$q_{\text{ind}} = 0.01239 \cdot A^{0.77905} \cdot k_s^{-0.16514} \cdot a^{2.09555} \cdot n^{1.3146} \tag{2.2}$$

$$L_{\text{cv}} = 0.30465 - 0.00013 \cdot MAP_{\text{mean}} - 0.12571 \cdot MAP_{\text{cv}} - 0.00541 \cdot C_2 \tag{2.3}$$

$$L_{\text{ca}} = -0.40728 - 0.2167 \cdot MAP_{\text{cv}} + 2.78896 \cdot L_{ca_{3\text{h}}} - 0.00366 \cdot C_2 \tag{2.4}$$

The list of explanatory variables used is shown in Table 2.2.

The estimation framework adopted here leads to a mixed regional–local approach. Since the SSEM regression models provide not only regional estimates of $q_{\text{ind}}$, $L_{CV}$, and $L_{CA}$ but also their associated variances, it becomes possible to compare the reliability of regional predictions with that of the corresponding at-site estimates. For gauged catchments, both the sample L-moments, whose standard deviations can be computed from the available observations, and the regional estimates, whose uncertainty follows from the GLS formulation, are simultaneously available. By directly comparing these standard deviations, one can select, for each L-moment and for each site, the estimator with the lower variance. In this way, the method yields a flexible mixed strategy in which local information is exploited whenever sufficiently reliable, while regional estimates are preferred where sampling uncertainty is high. This leads to more accurate and internally consistent flood frequency descriptors across the study region. Notably, in most cases, the flood index $q_{\text{ind}}$ exhibits a lower uncertainty when estimated directly from local observations, whereas the sample estimates of $L_{CV}$ and, in particular, $L_{CA}$ are generally affected by much larger

Table 2.2 List of explanatory variables considered in the Spatially Smooth Estimation Method for the regional regression estimations of $q_{\text{ind}}$, $L_{CV}$, and $L_{CA}$.

| Variable | Description | Type |
|---|---|---|
| A | Drainage area at the closing section | Morphological |
| a | Hourly rainfall coefficient (IDF curve) averaged over basin | Climatic |
| n | Scale invariance exponent of IDF curve (averaged) | Climatic |
| $k_s$ | Saturated permeability coefficient | Land use |
| $MAP_{mean}$ | Mean annual precipitation over basin | Climatic |
| $MAP_{cv}$ | Spatial variation coefficient of mean annual precipitation | Climatic |
| $C_2$ | Mean of the $C_2$ coefficient (Fourier series of rainfall regime) | Climatic |
| $L_{ca_{3\text{h}}}$ | $L_{CA}$ of 3-hour maximum rainfall, basin average | Climatic |

sampling variability. As a consequence, their regional counterparts tend to be more stable and display smoother spatial patterns.

In the local configuration, the uncertainty associated with the estimation of L-moments is quantified through the expressions in Equation 2.5 on the basis of Monte Carlo simulations:

$$\begin{aligned} \sigma_{q_{\text{ind}}} &= \frac{1}{\sqrt{n}} \\ \sigma_{L_{\text{CV}}} &= \frac{0.9\,L_{\text{CV}}}{\sqrt{n}} \\ \sigma_{L_{\text{CA}}} &= \frac{0.45+0.6\,|L_{\text{CA}}|}{\sqrt{n}} \end{aligned} \tag{2.5}$$

Regional estimates are instead obtained from regression models relating flood statistics to catchment descriptors. Their uncertainty does not depend on the local record length, but arises from two distinct components: (i) the intrinsic error of the regional model ($\sigma^2_{\text{model}}$) and (ii) the uncertainty associated with the estimation of the regression coefficients ($\sigma^2_{\text{reg}}$). The variance of a regional estimate $\hat{Y}$ (where $Y$ represents $q_{\text{ind}}$, $L_{\text{CV}}$, or $L_{\text{CA}}$) can be written as

$$\sigma^{2,\text{reg}}_{\hat{Y}} = \sigma^2_{\text{model}} + \sigma^2_{\text{reg}}. \tag{2.6}$$

This formulation highlights a fundamental difference between local and regional approaches: while the uncertainty of local estimates decreases with increasing data availability, the uncertainty of regional estimates is bounded below by the model error. At gauged sites, local and regional estimators can be directly compared, and the one associated with the lowest variance can be selected. Figure 2.2 compares local and regional estimates of the three L-moment parameters, highlighting those with a lower uncertainty.

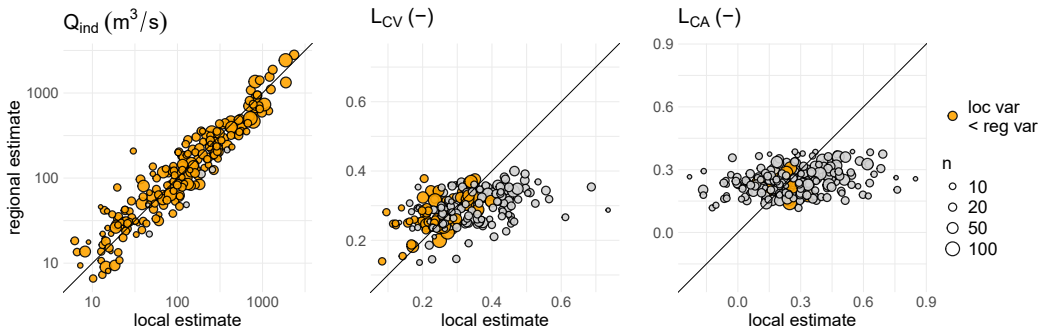


Fig. 2.2 Comparison between local and regional estimates of the L-moments $q_{\text{ind}}$, $L_{CV}$, and $L_{CA}$ derived from SSEM regressions. Each point represents a gauged catchment, with the circle size proportional to the sample length. Orange points indicate catchments where the local estimate is more reliable than the regional one (loc var $<$ reg var).

Once the regression models for $q_{\text{ind}}$, $L_{CV}$, and $L_{CA}$ are obtained, these values are used to parameterize the 3-parameter log-normal distribution (see Grimaldi et al. (2011b), Tables 2 and 4).

From this distribution, both the design quantile $q_T$ and the growth factor $K_T = q_T/q_{\text{ind}}$ can be derived for any return period $T$ at any site. The L-moments are obtained both from the regressions (regional L-moments) and at-sites using the annual maxima series (local L-moments), supporting the estimation of $q_T$ and its associated uncertainty at both gauged and ungauged sites. This framework leads to three possible configurations for estimating the flood frequency curve at a given site: a purely local estimate, a purely regional estimate, or a mixed estimate. In the first case, the lognormal distribution is parameterized using local L-moments; in the second, regional L-moments are employed; and in the third, certain L-moments are derived from local data while others come from regional information. The mixed

configuration is preferred, as it selects each L-moment (whether local or regional) based on the criterion of minimizing relative uncertainty. Figure 2.3 illustrates three estimation scenarios: a site with long records and dominant local estimation (left panel), a site with high uncertainty in local data and relying on regional estimation except for the index flood (right panel), and a site where only the L-coefficient of asymmetry is taken from the regional estimation (middle panel). Mixed estimation was the most frequent outcome, applied to 207 sites, while purely local estimation occurred in 12 sites, and purely regional in 7.

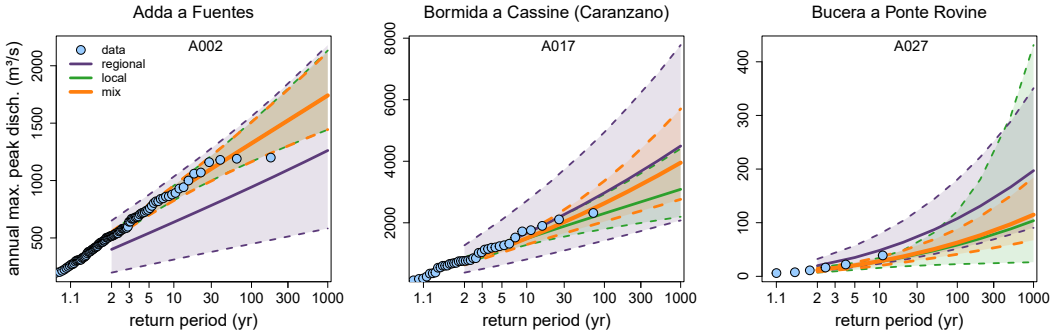


Fig. 2.3 Examples of flood frequency curves and associated 90% confidence intervals for three sites with different sample lengths. Local estimates are shown in green, regional in purple, and mixed (used in this study) in orange. In the left figure, the mixed flood frequency curve corresponds to the local one, because of the large length of the flood record. In the middle figure, the mixed model is obtained with local L-moments except for the regional L-coefficient of asymmetry $L_{CA}$. In the right figure, only the index flood $q_{\text{ind}}$ is derived from the local configuration.

### 2.4.2 Region Of Influence

This methodology groups hydrologically similar catchments, regardless of their geographic location (Castellarin et al., 2000). Regional analysis methods allow for the estimation of design flood quantiles at a target site by transferring information from gauged catchments within a hydrologically homogeneous region. Specifically, the Index-Flood method assumes that the frequency distribution of annual peak flows is identical across a homogeneous region, up to a scaling factor. In such a region, the quantile $q_T$ associated with a return period $T$ can be estimated as in Equation (2.1), where $K_T$ is the dimensionless growth factor for a given return period $T$, while $q_{\text{ind}}$ is the index flood characteristic of the site. The growth curve (i.e., $K_T$) can be estimated

from the data observed at all gauged sites within the homogeneous region. The index flood, $q_{\text{ind}}$, is typically estimated as the arithmetic mean of the annual maximum peak flow series for the site in question, provided at least 5–10 years of observations are available (Brath et al., 2001). The RoI method defines a homogeneous group of catchments using a weighted Euclidean distance based on geomorphological and climatic descriptors:

$$D_{i,j} = \left[ \sum_{m=1}^{M} w_m \left( X_{m,i} - X_{m,j} \right)^2 \right]^{1/2} \tag{2.7}$$

where $X_{m,i}$ and $X_{m,j}$ are standardized values of the $m$-th descriptor for sites $i$ and $j$, and $w_m$ is the weight for that descriptor (set to 1 here). The descriptors are derived from the dataset used for the SSEM method and reduced to four principal components via PCA, capturing over 80% of the total variance (Hotelling, 1933; Pearson, 1901). A threshold is applied to exclude dissimilar sites. For each target site, the optimal region is determined by balancing two opposing objectives: (1) maximizing the group size, and (2) maximizing homogeneity. As group size increases, homogeneity typically decreases. Internal heterogeneity is measured using the heterogeneity measure $H$ of Hosking and Wallis (1997)

$$H = \frac{V - \mu_V}{\sigma_V} \tag{2.8}$$

where $V$ is the standard deviation of the sample $L_{CV}$s, and $\mu_V$, $\sigma_V$ are the mean and standard deviation of $V$ computed from 2000 homogeneous synthetic samples using the kappa distribution. Group size is expressed in station-years, i.e., the total number of years across all flow records in the group. The target size was 400 station-years, and the heterogeneity threshold was set at $H = 2$, above which the group is considered definitely heterogeneous.

The theoretical distribution for each site was selected using the L-moment-based approach of Hosking and Wallis Hosking and Wallis (1993, 1997). Several three-parameter distributions were tested, and those with acceptable goodness-of-fit were averaged (model-averaging) to estimate the quantile. If no distribution met the criteria, a four-parameter kappa distribution was used by default.

Uncertainty in the estimated quantile for each return period was quantified through Monte Carlo resampling, by generating 1000 synthetic quantiles as the product of:

1. a dimensionless quantile from a synthetic regional sample (same size as the real group), drawn from the accepted frequency distributions;
2. a synthetic index flood drawn from a two-parameter log-normal distribution, using the log-transformed mean and standard deviation of the site observations, divided by the square root of the number of observations.

If the number of observations $N \geq 15$, the sample standard deviation was used; otherwise, the geostatistical Topkriging method was applied (Archfield et al., 2013; Skøien et al., 2006). Within the logic of the index-flood method, the 1000 iterations allow quantification of the overall uncertainty associated with the regional flood quantiles estimated through the RoI approach, by combining the uncertainty linked to the regional dimensionless distribution (term 1) with that related to the sample-based estimation of the index flood (term 2). The resulting 1000-dimensional quantiles were fitted to a three-parameter log-normal distribution to summarize the final uncertainty.

### 2.4.3 Updated VAPI Method

As part of this work, Politecnico di Milano updated the flood quantile estimates for given return periods using the North-Western VAPI Method (De Michele and Rosso, 2001). The uncertainty associated with these estimates was also assessed. This method was originally developed for rivers in North-Western Italy (the Po basin and Ligurian coastal catchments) as part of the VAPI Special Project (Flood Evaluation Project) by the CNR (National Research Center).

The North-Western VAPI Method is also based on the Index-Flood approach. The peak discharge $q_T$ associated with a given return period $T$ is computed as Equation (2.1). $K_T$ is derived using the Generalized Extreme Value (GEV) distribution applied to the normalized variable $X = Q/q_{\text{ind}}$, where $Q$ is the annual maximum peak discharge. Thus, $q_{\text{ind}}$ represents the mean of the observed annual peaks at the site. The dimensionless growth curve, representing the relationship between $K_T$ and the return period $T$, is defined by:

$$K_T = \varepsilon + \frac{\alpha}{k}\left(1 - e^{-k y_T}\right) \tag{2.9}$$

where $y_T$ is the Gumbel reduced variate, defined as:

$$y_T = -\ln\left[\ln\left(\frac{T}{T-1}\right)\right] \tag{2.10}$$

The parameters $k$, $\alpha$, and $\varepsilon$ are regional and are estimated from normalized samples using L-moments.

The homogeneous flood regions defined by De Michele and Rosso (2001) (see Figure 4.4 in their report) were retained. However, the regional parameters $k$, $\alpha$, and $\varepsilon$ were updated based on the extended dataset using the L-moment method (see Table 2.3).

Table 2.3 Homogeneous flood regions in North-Western Italy, their validity range in terms of drainage area $A$ (km$^2$), and the GEV parameters ($\alpha$, $\varepsilon$, $k$) of the normalized growth factor $X$. Region B is considered valid up to 14,000 km$^2$, although calibration relied on basins up to approximately 4,000 km$^2$. Values for Region D follow De Michele and Rosso (2001).

| **Region** | **Description** | $A$ **(km$^2$)** | **No. st.** | $n$ | $\alpha$ | $k$ |
|---|---|---|---|---|---|---|
| A | Central Alps and Pre-Alps | 40–2500 | 36 | 1040 | 0.384 | −0.103 |
| B | Western Alps and Pre-Alps | 40–4000* | 54 | 1428 | 0.370 | −0.237 |
| C | NW Apennines and Tyrrhenian basins | 10–1500 | 48 | 1167 | 0.389 | 0.652 |
| D | NE Apennines and Adriatic basins | 6–1300 | 60 | 1315 | 0.334 | −0.089 |
| aa | Alto Adige | 90–2700 | 11 | 467 | 0.292 | −0.088 |
| ZT1 | Alto Garda transition zone | 20–1100 | – | – | – | – |
| ZT2 | Maritime Alps transition zone | 50–1500 | – | – | – | – |

The uncertainty associated with flood quantile estimates is expressed via confidence intervals. For a confidence level of $100(1-\alpha/2)\%$, the confidence interval for the quantile $q_T$ is given by De Michele and Rosso (2001):

$$\left[\hat{q}_T - \zeta_{\alpha/2}\sqrt{\mathrm{Var}(\hat{q}_T)},\quad \hat{q}_T + \zeta_{\alpha/2}\sqrt{\mathrm{Var}(\hat{q}_T)}\right] \tag{2.11}$$

where $\hat{q}_T$ is the estimated quantile, $\zeta_{\alpha/2}$ is the standard normal quantile, and $\mathrm{Var}(\hat{q}_T)$ is the variance of the estimate. Assuming independence between $\hat{K}_T$ and $\hat{q}_{\mathrm{ind}}$, the variance is:

$$\mathrm{Var}(\hat{q}_T) = (\hat{q}_{\mathrm{ind}})^2 \,\mathrm{Var}(\hat{K}_T) + \left(\hat{K}_T\right)^2 \mathrm{Var}(\hat{q}_{\mathrm{ind}}) + \mathrm{Var}(\hat{q}_{\mathrm{ind}})\mathrm{Var}(\hat{K}_T) \tag{2.12}$$

where:

$$\mathrm{Var}(\hat{q}_{\mathrm{ind}}) = \frac{\mathrm{Var}(Q)}{n'} \tag{2.13}$$

with $n'$ being the number of observations at the site, and $\mathrm{Var}(Q)$ the variance of annual peak flows. The variance of the normalized quantile, $\mathrm{Var}(\hat{K}_T)$, is estimated as:

$$\mathrm{Var}(\hat{K}_T) = \frac{\alpha^2}{n} \exp\left[y_T \cdot \exp\left(-1.823k - 0.165\right)\right] \quad \text{for } k \leq 0 \tag{2.14}$$

where $y_T$ is the Gumbel reduced variate, $n$ is the normalized sample size, and $\alpha$, $k$ are the GEV parameters for the region De Michele and Rosso (2001).

### 2.4.4 Integration of historical and censored flood information

In some cases, historical records can be incorporated into flood frequency analyses to extend the temporal coverage of instrumental data. Historical flood data, often derived from archives, chronicles, or early hydrological measurements, can provide valuable insights into the occurrence and magnitude of extreme events. However, these records are frequently incomplete, imprecise, or inconsistent with systematically collected modern data. Such "censored data" may refer to events that are only partially documented (e.g., floods known to have exceeded a certain threshold but with no exact discharge value) or historical values that stand apart from the continuous instrumental series. If these data are not handled correctly, they can distort statistical analyses, bias flood frequency estimation, and lead to unreliable risk assessments. Therefore, integrating historical or censored flood information requires careful methodological choices, ensuring that the added value of long-

term perspective does not compromise the robustness of hydrological modeling and decision-making.

The integration of historical records into flood frequency analysis inevitably raises the question of stationarity. Extending the observation period increases sample size and reduces estimation uncertainty, particularly for rare events, but at the cost of potentially incorporating data generated under climatic, land-use, or hydraulic conditions that differ substantially from the present. This trade-off has no universal solution: longer series improve statistical robustness, while shorter, more recent records better reflect current catchment conditions. In the present work, the added value of extending the effective record length is considered to outweigh the uncertainty introduced by potential non-stationarities, which are acknowledged but not explicitly modeled within this framework.

In traditional flood frequency analysis, it is usually assumed that a systematic record of $n$ annual maximum flows is available (Stedinger, 1993). However, such records can often be complemented with additional information derived from significant occasional flood events, observed outside regular gauging campaigns. This integration is particularly valuable when the systematic record is short, as it strengthens the robustness of the final estimates (Bayliss and Reed, 2001). To merge systematic and non-systematic data into a single framework, Laio et al. (2011) adopted the method proposed by Wang (1990). Other methods were proposed in literature (e.g., Cohn et al., 1997), but their adoption was not pursued here for consistency with the SSEM framework. The combined sample is ordered in increasing magnitude, and probability weighted moments (PWMs) are then computed on the extended dataset. A censoring threshold, $x_0$, is introduced to represent the level above which non-systematic floods are considered reliable and worthy of inclusion. In practice, $x_0$ is usually set equal to the smallest available non-systematic observation (Bayliss and Reed, 2001). When no non-systematic information is available, the formulas reduce to the standard definitions of PWMs. From these PWMs, L-moments can be derived as linear combinations (Hosking and Wallis, 1997). Here we report the procedure adopted, inspired by Laio et al. (2011) and Wang (1990). The merged sample of total length $n_{\text{all}}$ is arranged in increasing order:

$$x_{(1)} \leq x_{(2)} \leq \ldots \leq x_{(n_{\text{all}}-l+1)} \leq \ldots \leq x_{(n_{\text{all}})}, \tag{2.15}$$

where the subscript in round brackets indicates the sorted position; the $l$ largest events, exceeding the threshold $x_0$, are considered as a censored sample. The "equivalent" length $m$ is associated to the complete record, equal to the number of years between the first and the last measurement (systematic and occasional, together).

When working with censored samples, the theoretical formula for the PWM of order $r$ of a random variable $X$ with distribution function must be split into two components (Wang, 1990):

$$\beta_r = \int_0^1 x(F)F^r\,dF = \int_0^{F_0} x(F)F^r dF + \int_{F_0}^1 x(F)F^r dF = \beta_r^{''} + \beta_r^{'}, \tag{2.16}$$

where $F_0 = F(x_0)$. The unbiased estimator of $\beta_r^{''}$ is

$$\beta_r^{''} = \frac{1}{n}\sum_{i=1}^{n_{\text{all}}} \frac{(i-1)(i-2)\cdots(i-r)}{(n-1)(n-2)\cdots(n-r)} x_{(i)}^{''}, \tag{2.17}$$

with

$$x_{(i)}^{''} = \begin{cases} x_{(i)}, & x_{(i)} < x_0 \\ 0, & x_{(i)} \geq x_0 \end{cases}.$$

Similarly, the estimator of $\beta_r^{'}$ is

$$\beta_r^{'} = \frac{1}{m}\sum_{i=m-n_{\text{all}}+1}^{m} \frac{(i-1)(i-2)\cdots(i-r)}{(m-1)(m-2)\cdots(m-r)} x_{(i)}^{'}, \tag{2.18}$$

where

$$x_{(i)}^{'} = \begin{cases} 0, & x_{(i)} < x_0 \\ x_{(i)}, & x_{(i)} \geq x_0 \end{cases}.$$

Thus $\beta_r = \beta_r^{''} + \beta_r^{'}$.

In the absence of non-systematic information, the formulas reduce to the usual definitions of PWMs. From PWMs, L-moments are obtained as linear combinations (Hosking and Wallis, 1997). The first statistic of interest is the index flood, i.e. the sample mean:

$$q_{\text{ind}} = \beta_0, \tag{2.19}$$

while the L-moment ratios are given by:

$$L_{CV} = \frac{2\beta_1 - \beta_0}{\beta_0}, \qquad L_{CA} = \frac{6\beta_2 - 6\beta_1 + \beta_0}{2\beta_1 - \beta_0}, \qquad L_{\text{kur}} = \frac{20\beta_3 - 30\beta_2 + 12\beta_1 - \beta_0}{2\beta_1 - \beta_0}. \tag{2.20}$$

Variance estimators are then introduced for $q_{\text{ind}}$, $L_{CV}$ and $L_{CA}$ to quantify uncertainty. Elamir and Seheult (2004) introduced a methodology to compute variances and covariances of sample L-moments; however, they were found to be inconsistent for short samples. For this reason, following Laio et al. (2011), the standard deviation of the index flood is defined as:

$$\sigma_{q_{\text{ind}}} = \sqrt{\frac{1}{n^2} \sum_{x_i < x_0} (x_i - q_{\text{ind}})^2 + \frac{1}{m^2} \sum_{x_i \geq x_0} (x_i - q_{\text{ind}})^2} \tag{2.21}$$

while $\sigma_{L_{CV}}$ and $\sigma_{L_{CA}}$ where calculated only on the systematic sample (see Equation 2.5).

While all three regional models were applied to the same dataset, only the Spatially Smoothed Estimation Method explicitly accounted for the inclusion of non-systematic (censored) data. This distinction is crucial and will be further emphasized in the following section.

### 2.4.5 Probabilistic integration of multiple regional flood models

Hydrological processes are inherently complex and subject to substantial variability. As such, it is challenging to obtain precise and reliable results under all conditions using a single estimation method. To address this, model combination has emerged as a promising approach for producing more robust and consistent outcomes (Okoli et al., 2018). This technique involves aggregating results from different statistical models, while explicitly accounting for the associated uncertainties. Here, the flood quantile estimates provided by the three independent methods applied in Sections 2.4.1, 2.4.2, and 2.4.3 are combined to produce a unified estimate. Each method provides, for return periods of 2, 5, 10, 20, 50, 100, 200, 500, and 1000 years, the estimated quantile and its associated confidence interval. The combination is performed using the geometric (logarithmic) pooling of the probability density

functions associated with each quantile estimate, following the approach proposed by Genest and Zidek (1986):

$$f(x) = \frac{p_1(x)^{w_1} \cdot p_2(x)^{w_2} \cdot p_3(x)^{w_3}}{\int_{-\infty}^{\infty} p_1(x)^{w_1} \cdot p_2(x)^{w_2} \cdot p_3(x)^{w_3}\, dx} \tag{2.22}$$

In this expression, $p_1(x)$ and $p_2(x)$ represent the three-parameter log-normal PDFs of the estimates provided by PoliTo (Section 2.4.1) and UniBo (Section 2.4.2), while $p_3(x)$ is the normal PDF used by PoliMi (Section 2.4.3). Equal weights $w_1 = w_2 = w_3 = \frac{1}{3}$ are assigned, ensuring no preference is given to any single method. Although the resulting combined distribution $f(x)$ cannot be expressed in closed analytical form, it can be well approximated by a three-parameter log-normal distribution, as shown by Grimaldi et al. (2011b). Figure 2.4 illustrates the full flood frequency curve obtained from the combination, while Figure 2.5 presents an example of the combined distribution for the 200-year return period.

To assess the reliability of the flood quantile distributions, probability plots are employed. The analysis is based on the assumption that, if the probabilistic model estimated for the flood quantiles is reliable, the non-exceedance probabilities of the observed annual maximum floods should be uniformly distributed. For each observed annual maximum $x_i$ (ranked in ascending order, $i = 1, \ldots, n$), the corresponding flood quantile is estimated as the empirical non-exceedance probability using the Gringorten plotting position formula:

$$F_i^{\text{emp}} = \frac{i - 0.44}{n + 0.12}. \tag{2.23}$$

For each observed $x_i$, the non-exceedance probability according to each model is obtained from the cumulative distribution function (CDF) of its PDF:

$$F_i^{\text{mod}} = \int_{-\infty}^{x_i} f(x)\, dx \tag{2.24}$$

where $f(x)$ is the combined PDF of the corresponding flood quantile obtained from geometric pooling or the PDFs of the individual models. The same procedure was also applied to each individual regional model ($p_1(x), p_2(x), p_3(x)$).

The probability plots are then constructed on the unit square by ordering the estimated non-exceedance probabilities $F_i^{\text{mod}}$ (Figures 2.6 and 2.7). Under perfect uniformity,

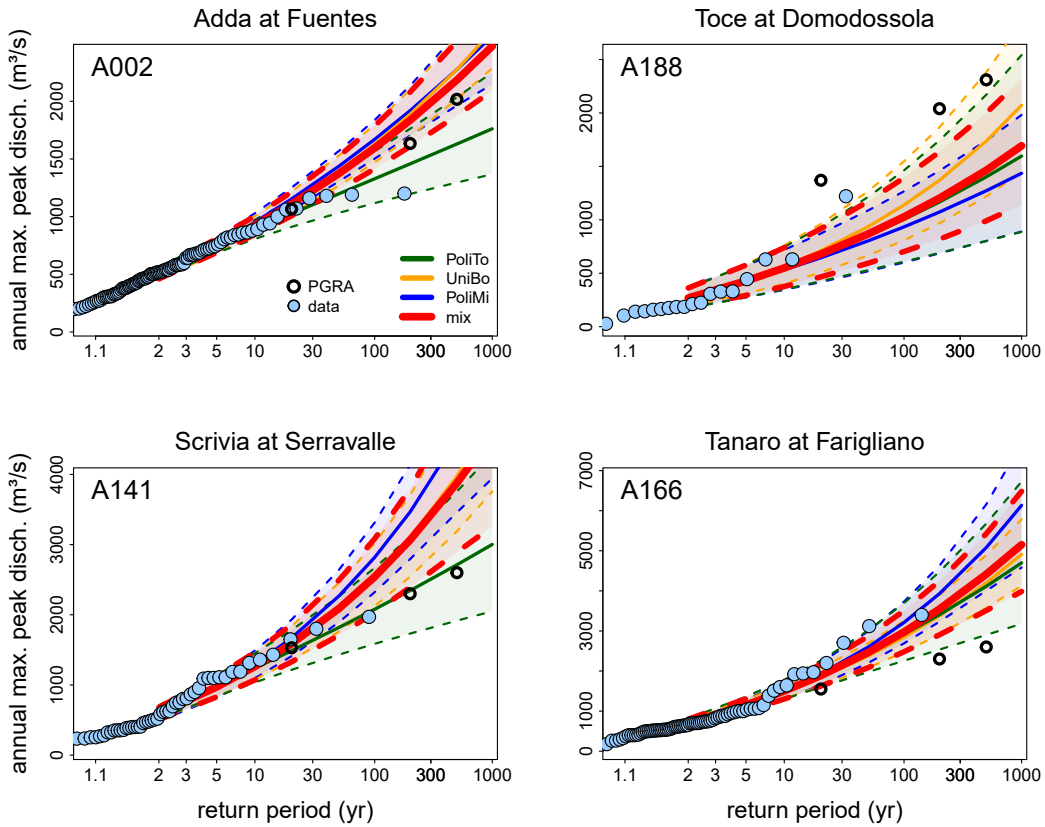


Fig. 2.4 Flood frequency curve obtained from combining the results of the three models. The design flood quantiles are also reported to facilitate the comparison between the results of this work and the current values adopted for hydrogeological and flood risk governance.

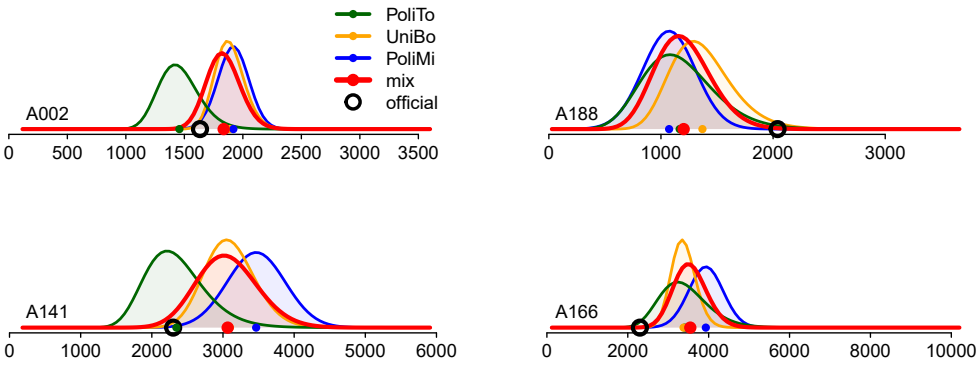


Fig. 2.5 Combined quantile distribution for a 200-year return period. The x-axis markers indicate the mean of each individual estimate.

the points should align along the bisector of the diagram. Deviations from the bisector indicate departures from uniformity and provide insight into potential deficiencies of the probabilistic model, such as systematic overprediction or underprediction of flood frequency. These plots are also useful for investigating the estimated confidence bounds. When the probability plot curve rises steeply near the lower and upper tails and flattens in the central part of the diagram, this indicates that a large number of observations fall close to the extremes of the predictive distribution, revealing an underestimation of the uncertainty and confidence bounds that are too narrow. Conversely, when the curve rises more rapidly in the central portion of the plot and is flatter near the tails, observations tend to cluster around the center of the distribution, indicating an overestimation of the uncertainty and excessively wide confidence bounds. This procedure is applied both to the combined distribution $f(x)$ and to each of the individual model distributions, allowing a comparison of the reliability and uncertainty representation across all models.

Figure 2.6 presents the probability plots for the three regional estimation methods (UniBo, PoliTo, and PoliMi) and their combined model. The plots show that the points for all models lie close to the 1:1 line across most of the probability range, indicating that the non-exceedance probabilities of the observed annual maxima tend to a uniform distribution. Minor deviations are observed at both the lower and upper ends of the distribution, which is a common feature in hydrological frequency analyses due to sampling variability, limited record lengths, and the inherent uncertainty in extreme values. Among the individual models, PoliTo shows a tendency to slightly underestimate the quantiles, which may reflect its treatment of censored data within the regional estimation procedure. The UniBo method exhibits slightly narrower lower confidence bounds, whereas PoliMi produces narrower upper bounds.

For return periods not directly estimated by the regional models (i.e., those other than 2, 5, 10, 20, 50, 100, 200, 500, and 1000 years), the corresponding distribution parameters (e.g., $\theta_1$) were obtained by linear interpolation in the logarithmic return-period domain. This procedure is necessary because the models provide estimates only for the standard quantiles. For example, the parameter $\theta_1$ for the distribution of the flood quantile with a return period of 75 years is obtained as:

$$\theta_1(T=75) = \frac{\theta_1(T=100) - \theta_1(T=50)}{\ln(100) - \ln(50)} \cdot [\ln(75) - \ln(50)] \tag{2.25}$$

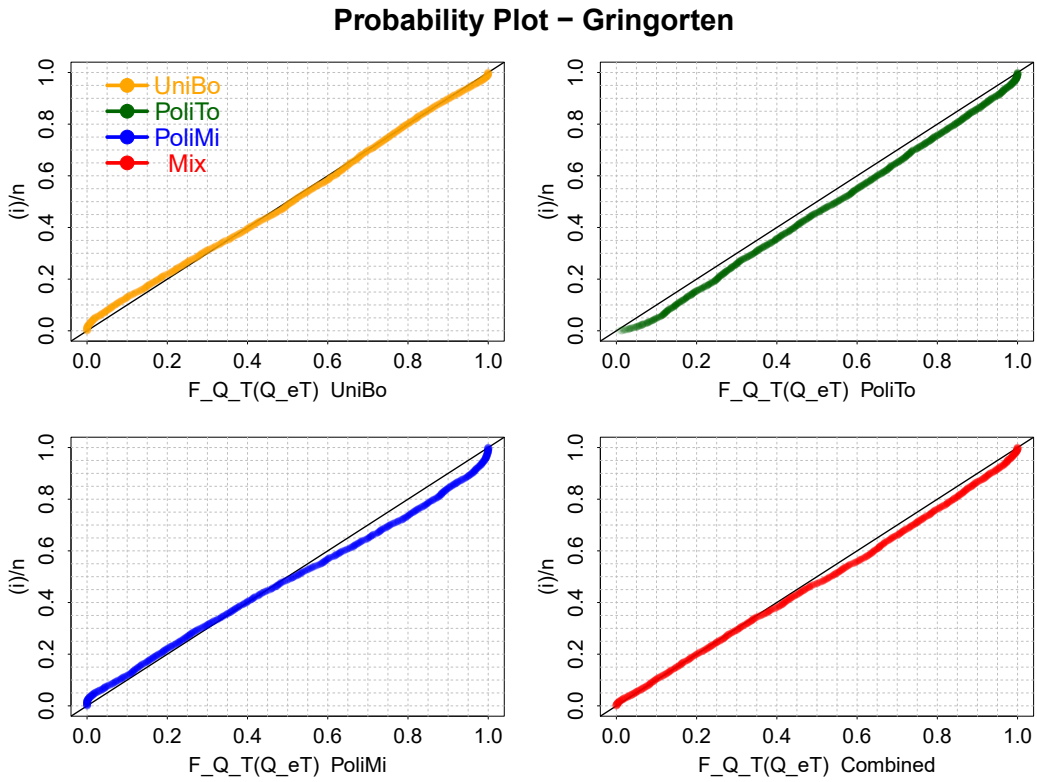


Fig. 2.6 Probability plots for all observed peak flows at gauged sites with return period exceeding 2 years (i.e., approximately 50% of the dataset). The plotting position is the Gringorten.

Because probability plots are highly sensitive to the choice of plotting position, we also adopted a method that explicitly accounts for the presence of non-systematic data, namely the Hirsch-Stedinger plotting position (Hirsch and Stedinger, 1987). Figure 2.7 reports the corresponding probability plots obtained using this alternative approach. Notably, when adopting the Hirsch-Stedinger plotting position, the PoliTo model aligns much more closely with the 1:1 diagonal. This improvement is consistent with expectations, as censored data were explicitly incorporated only in this configuration, thereby enhancing the reliability of the PoliTo regional estimates. The effects of different plotting positions on the probability plots do not introduce a relevant bias in the models with no censoring process, because only 89 out of 5576 annual maxima are non-systematic. Furthermore, under the Hirsch-Stedinger setup, the combined distribution clearly emerges as the best-performing model, showing the closest adherence to the theoretical line across the entire probability range. This finding reinforces the effectiveness of integrating multiple regional estimation meth-

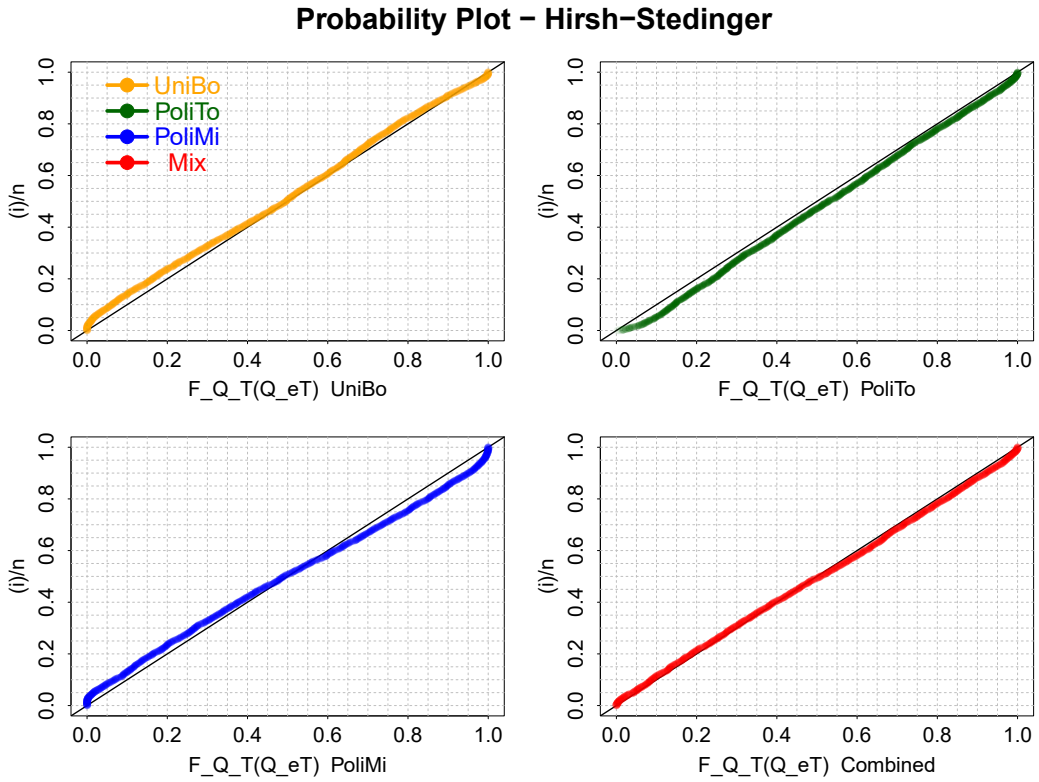


Fig. 2.7 Probability plots for all observed peak flows at gauged sites with return period exceeding 2 years (i.e., approximately 50% of the dataset). The plotting position Hirsch-Stedinger explicitly accounts for the presence of non-systematic data.

ods, each grounded in distinct statistical and hydrological assumptions, into a single, coherent model with superior overall performance and enhanced robustness in flood quantile estimation.

## 2.5 Interpretation of regional flood estimates

This section presents key findings from the updated design flood estimates across the Po River Basin. Figure 2.8 shows the locations of basins where notable anomalies were observed. Overall, no clear spatial pattern emerges, indicating that the applied methods yield generally robust results across the study area. Many anomalies can be attributed to the availability of recent discharge records, which enhance the reliability of current estimates.

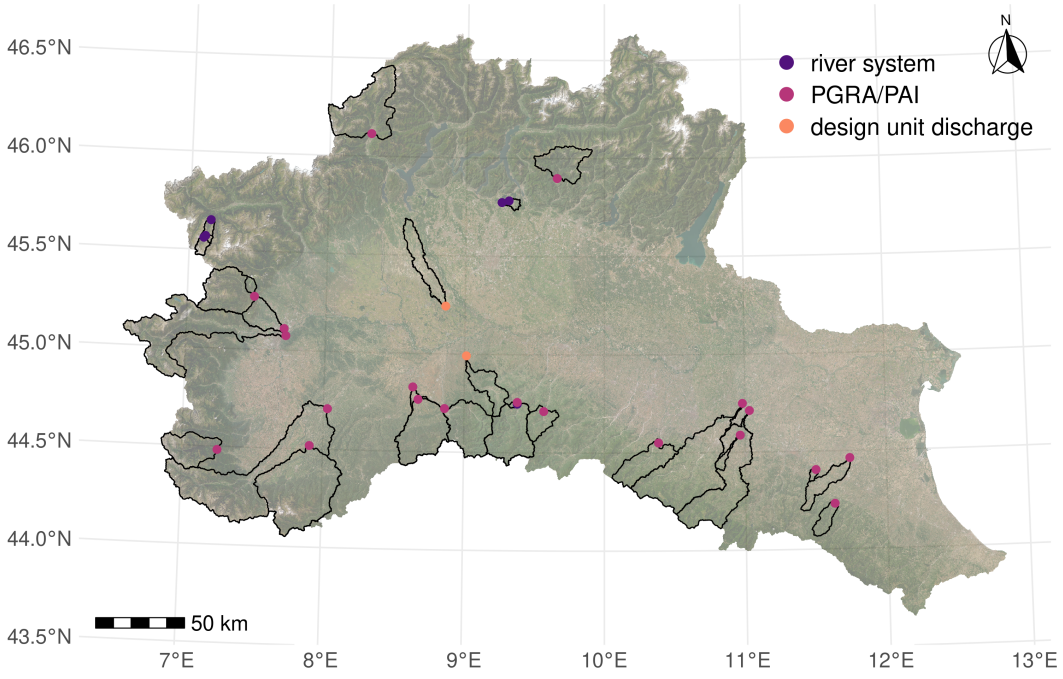


Fig. 2.8 Catchments where design flood estimates revealed significant singularities in terms of inconsistencies along the same reach, relevant differences with respect to current design flood quantiles, or abnormally low unit discharge estimates relative to neighboring basins.

The largest source of the anomalies derives from the comparison between the results of this study and the design values found in the PGRA. For example, the Tanaro River (stations A166, A167, A171) exhibits higher flood quantiles than the design floods indicated in the PGRA, particularly for long return periods. Similar patterns are observed in numerous other cases. In all instances, these differences can be attributed to longer or more recent datasets, improved scaling procedures, and hydrological processes not considered in earlier studies, which affect the estimation of extreme floods. The second source of anomalies is identified by comparing the flood frequency curves obtained in different stations belonging to the same river system. Some of these sections exhibit inconsistencies along the same reach. For instance, the upstream section of Dora di Rhemes (A054) presents unexpectedly high values compared with the downstream gauge along the same river, probably caused by short, non-aligned observation periods and a few extreme events. Figure 2.9 illustrates this in detail: the top panels show the available annual maximum discharge series for the three stations along the Dora di Rhemes. The bottom panels display the design discharge values estimated for return periods of 2, 20, 200, and 500 years, along with their 90% confidence intervals. This discrepancy can be attributed to the scarcity of data and the fact that the A054 series are much older, with one record being even non-systematic.

Finally, two stations show abnormally low unit discharge estimates relative to neighboring basins: Staffora at Voghera (A228) and Terdoppio at Gambolò (A229). These values may be influenced by hydraulic works, such as flood spillways, or atypical basin geometries, including long, narrow drainage areas.

With reference to Figure 2.5, several representative cases are further examined to better understand the differences between the individual regional models and the PGRA design values. The Adda at Fuentes and the Scrivia at Serravalle clearly illustrate the distinctive behavior of SSEM compared to the other regional approaches. At both stations, the availability of long and reliable annual maxima series means that SSEM operates in its “local” configuration, relying solely on the site data. The other regional models, however, maintain their dependence on regional growth curves regardless of record length. For the Adda at Fuentes, the PoliTo (SSEM) growth curve closely resembles a Gumbel distribution, while the other methods, including the one originally underpinning the PGRA design value, produce markedly heavier tails. A similar situation occurs for the Scrivia, although in this case the PGRA values themselves were derived assuming a Gumbel-like behavior. The combined

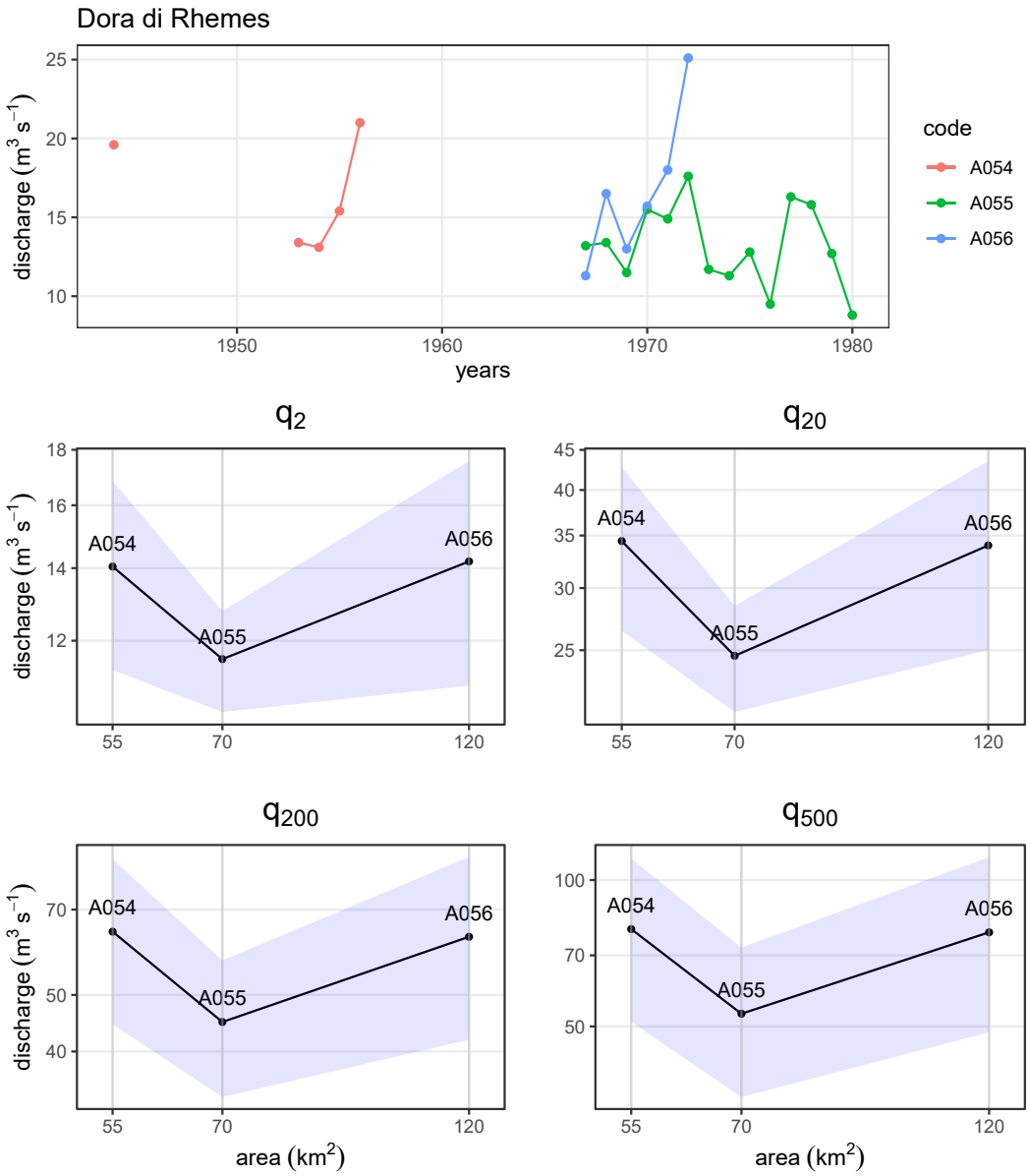


Fig. 2.9 Annual maximum discharge series and design floods for the Dora di Rhemes. Top panel: available annual maximum discharge series for the three stations along the river reach. Bottom panels: design discharge values for return periods of 2, 20, 200, and 500 years, with 90% confidence intervals. The upstream station (A054) shows higher values than the downstream stations, reflecting the scarcity and age of the data, including one non-systematic series.

regional model developed in this study instead indicates a heavier-tailed distribution, implying that design discharges for return periods exceeding 200 years should be revised upward. A comparable interpretation applies to the Tanaro at Farigliano. The PGRA estimates, originally based on a Gumbel distribution, contrast with the updated regional models, all of which suggest heavier tails and therefore higher design discharges for long return periods. This divergence is largely attributable to the occurrence of several major floods in recent decades, which provide more information on the upper tail of the distribution. A different outcome emerges for the Toce at Domodossola. Here, the combined model yields substantially lower discharges than those used in the PGRA. This discrepancy arises because the available annual maxima series is relatively recent and was not yet available when the PGRA design values were originally computed.

Overall, the integrated regional model developed in this study offers a significant advancement in flood hazard estimation for the Po River District. It provides robust flood quantile estimates even in data-scarce or hydrologically complex areas. The unified approach can serve as a foundation for future flood risk planning, civil protection strategies, and hydraulic infrastructure design. The methodology presented here offers a scalable and replicable framework for regional flood analysis applicable well beyond the Po River context. Looking ahead, further improvements could be achieved by integrating land-use dynamics and climate change projections. In Chapter 3, a practical approach to deal with the expected increase in precipitation extremes is proposed.

# Chapter 3

# How changes in future precipitation impact flood frequencies

## 3.1 Conceptual framework for linking precipitation extremes to flood frequency

The alteration of climate patterns significantly impacts the hydrology of river basins, resulting in significant implications for water resource management and infrastructure planning (Bloetscher, 2012; Dong et al., 2020). Specifically, Gobiet et al. (2014) found that the Alpine region is expected to experience an increase in the intensity of extreme precipitation events in all seasons and for most regions, leading to an increased potential for extreme flooding (Wilhelm et al., 2022). As the urgency of climate change adaptation measures becomes more evident, public administrations are recognizing the critical need to incorporate its effect on hydrological risk, in order to ensure that their infrastructures are resilient in the face of changing environmental conditions. The EU Floods Directive (2007/60/EC) states that consideration should be given to the expected impacts of climate change on flood occurrence. However, a standardized methodology for this purpose is not available at present (European Commission, 2021). It is therefore of interest to quantify the effect of climate change, and in particular of the increase of extreme precipitation, on Flood Frequency Curves (FFC). Here, a pragmatic and reliable approach for modifying flood frequency curves to accommodate the shift in precipitation extremes, as proposed by Cafiero et al. (2025), is described. The approach only requires the FFC

and the Intensity-Duration-Frequency (IDF) curves of a generic basin, as well as the expected variation of IDF curves derived from climate models. The methodology proposed by Breinl et al. (2021) is adopted, which compared IDF curves of maximum annual rainfall with FFCs while introducing the concept of elasticity as an indicator of the sensitivity of floods to changes in precipitation extremes. Quantile-quantile (q-q) relationships between FFC and IDF curves are defined, assuming that their logarithmic slope, or elasticity, can be used to transform the percentage variation of precipitation quantiles into percentage change of flood quantiles. This hypothesis, represented in Figure 3.1, is the core of the present work and is analyzed through the following three research questions, two methodological and a case-specific one:

1. Which conditions allow the usage of the proposed methodology? I.e., in which conditions does the hypothesis of using the slope of the q-q relationships for flood change projection hold?
2. Is this methodology suitable across the full distribution of floods? I.e., for all return periods?
3. What are the expected flood changes for projected precipitation changes in Northern Italy?

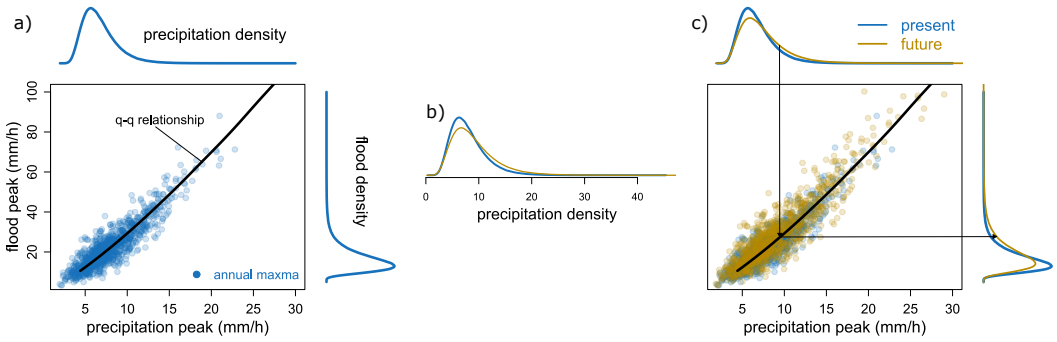


Fig. 3.1 (a) q-q relationship between the distributions of annual maxima of precipitation and flood. (b) The effect of the expected variation in precipitation extremes. (c) The consequent variation of flood extremes so that the logarithmic slope of the q-q relationship does not change.

In Chapter 2, a detailed and updated regional flood frequency analysis was developed for the Po River District, combining multiple regional approaches to obtain robust Flood Frequency Curves (FFCs). That framework provides a consistent and reliable

description of present-day flood regimes across the basin. Building on these results, a natural next step is to assess how such FFCs may evolve under projected changes in extreme precipitation. In particular, the capability to translate future precipitation changes into associated modifications of flood quantiles would provide a practical tool to support long-term flood risk planning and climate-resilient design.

The work is organized into two main parts. The first part presents the theoretical and methodological framework, focusing on the key concepts and the analytical tools employed. The second part is dedicated to the practical application of the method, illustrated through a case study developed in the Po River basin in Northern Italy.

## 3.2 Quantile–quantile relationships between precipitation and flood extremes

Consider a precipitation event hitting a catchment and generating a flood peak at the outlet. $P$ is the average liquid precipitation intensity over the catchment, and $Q$ the corresponding peak discharge at the outlet, normalized by the catchment area in order to have the same units (e.g., mm/h) for both $P$ and $Q$. The rainfall intensity $P$ is supposed to be averaged in space and time: in space, over the catchment area (or the contributing area when rainfall falls in liquid form only in a portion of the basin); in time, over the so-called critical duration, i.e. the duration maximizing the peak discharge for that given catchment. Notice that, in practice, the selection of the correct rainfall duration is not key to the application proposed here (more details on this point will be discussed in the following paragraphs). Under the mentioned definitions, the relation between $Q$ and $P$ can be formalized as

$$Q = C \cdot P \tag{3.1}$$

where $C$ is the peak runoff coefficient (non-dimensional, $0 \leq C \leq 1$). At the event scale, $C$ and $P$ are both random variables, with a potential mutual dependence since antecedent moisture conditions are often positively correlated: more intense rainfall events often come in clusters or with duration larger than the critical one for the catchment, potentially wetting the soil before the start of the peak-runoff generation phase. Let $F_Q$ be the cumulative distribution function of annual floods,

and $F_P$ the cumulative distribution function of max annual precipitation for the critical duration of the catchment, obtained independently. When accompanied by the indices 0 or 1, they refer specifically to the probability distributions in the reference period (0) or future period (1). Suppose the current-climate probability distribution of extreme rainfall, $F_{P_0}$, and peak discharge, $F_{Q_0}$, are known for the given catchment. Also suppose climate projections are available, under different scenarios, enabling one to estimate the expected future probability distribution of extreme rainfall, $F_{P_1}$, or, equivalently, the future extreme rainfall quantiles for given probability level, $q_{P_1}$, possibly expressed in variation terms with respect to the current values, $q_{P_1} = q_{P_0}(1+\delta)$, with $\delta$ being the expected future variation. Under these very common conditions, it is often asked by the stakeholders to estimate the expected future probability distribution $F_{Q_1}$ or quantiles $q_{Q_1}$ of peak discharges. An operational method for providing these estimates is presented in the following.
Temporal variations of the flood frequency curve are estimated from projected changes in the frequency curve of rainfall using the logarithmic slope of the quantile-quantile (q-q) relationship. This relationship is defined by combining the flood and rainfall frequency curves. Given a value $y$ of rainfall for the catchment's critical duration, the q-q relationship that relates $y$ to the value $z$ of the flood peak with the same non-exceedance probability is described in Equation (3.2) and considered stationary in time.

$$z = F_{Q_0}^{-1}(F_{P_0}(y)) = F_{Q_1}^{-1}(F_{P_1}(y)) \tag{3.2}$$

This assumption will be thoroughly analyzed in the following sections. The modified flood frequency curve $F_{Q_1}$ according to the variation of the frequency curve of rainfall is obtained:

$$F_{Q_1}(z) = F_{Q_0}(F_{P_0}^{-1}(F_{P_1}(y))) \tag{3.3}$$

where the lower apex '0' and '1' stand for a present and a future period respectively. Please note that the purpose here is to recreate what is generally available in operative conditions: the probability distributions of flood and precipitation are indeed obtained independently and the quantiles do not correspond to the same events.
To validate the hypothesis underlying Equations (3.2) and (3.3), a simple model based on the rational method is set up, where flood events $Q$ are the result of the

combination of two jointly distributed random variables: the maximum annual rainfall for the time of concentration of the catchment $P$ and the peak runoff coefficient $C$, as in Equation (3.1) (Mulvaney, 1850). The precipitation probability distribution $F_P$ is assumed to follow a Gumbel distribution, whereas the probability distribution of the peak runoff coefficient $F_C$ is described by a beta distribution (Gottschalk and Weingartner, 1998; Merz et al., 2006; Viglione et al., 2009). $C$ and $P$ are correlated through a Gumbel copula, so that

$$\begin{aligned} F_{C|P}(x \mid y) &= \mathbb{P}(U < u \mid V = v) = \frac{\partial}{\partial v} C_\theta(u,v) \\ &= \frac{C_\theta(u,v)}{v} \left[(-\ln u)^\theta + (-\ln v)^\theta\right]^{-1+1/\theta} (-\ln v)^{\theta-1} \end{aligned} \tag{3.4}$$

where $u = F_C(x;\alpha,\beta) = I_x(\alpha,\beta)$ is the beta distribution of $C$ with parameters $\alpha$ and $\beta$ (expressed through the regularized incomplete beta function),

$$F_P(y;\xi,\sigma) = \exp\left(-\exp\left(-\frac{y-\xi}{\sigma}\right)\right) \tag{3.5}$$

is the Gumbel distribution of $P$ with location parameter $\xi$ and scale parameter $\sigma$, and

$$C_\theta(u,v) = \exp\left[-\left((-\ln u)^\theta + (-\ln v)^\theta\right)^{1/\theta}\right] \tag{3.6}$$

is the bivariate Gumbel Copula which attributes an increasing correlation between the two random variables as the rainfall amount increases. In the equations,";" separates random variables from parameters, and "|" separates a variable to variables upon which it is conditional. The virtual world here simulated is obtained by generating one event per year for both precipitation and flood (i.e., the annual maxima of Q and P correspond to the same event). Generating more than one event per year, and therefore allowing the annual maximum P and Q not to be the same event, does not significantly change the results of the analysis (and therefore it is not shown here). This framework is in agreement with the results of Fiorentino et al. (2007), who compared cumulated rainfall and relative flood peaks using a distributed hydrological model. They found that for lower values of rainfall, flood peaks have more dispersion compared to more intense events because the initial conditions of the soil are more

variable. The choice of the copula family is not shown in the subsequent sensitivity analysis; however, similar results were obtained considering a Gaussian copula instead. The distribution of $C$ conditional on $P$ is assumed to remain unchanged under different climatic conditions, which is consistent with the assumption that the hydrologic response of the catchment does not change in time. This assumption is commonly employed in process-based methods for climate change impact assessment in hydrology.

Similarly to Viglione et al. (2009), but assuming that $C$ and $P$ are dependent, the CDF of flood, product of the two, is calculated as

$$F_Q(z;\alpha,\beta,\xi,\sigma) = \int_\Omega F_{C|P}\left(\frac{z}{y}|y;\alpha,\beta\right) \cdot f_P(y;\xi,\sigma)dy \tag{3.7}$$

where $\Omega$ indicates all possible values of $P$.

Figure 3.2 shows one hypothetical case, used as a reference case hereafter, where $\alpha_0 = 2$, $\beta_0 = 4$, $\xi_0 = 40$ mm/h, $\sigma_0 = 10$ mm/h, and the random variables $P$ and $C$ are slightly correlated ($\theta = 1.25$, which corresponds to Kendall correlation coefficient $\tau = 0.2$). In this way, the correlation between $Q$ and $P$ is similar to those found in real catchments in Austria (Blöschl et al., 2024). The frequency curves for rainfall and flood, along with the q-q relationship, are shown, including $N$=1000 pairs of simulated annual maxima of $P$ and $Q$.

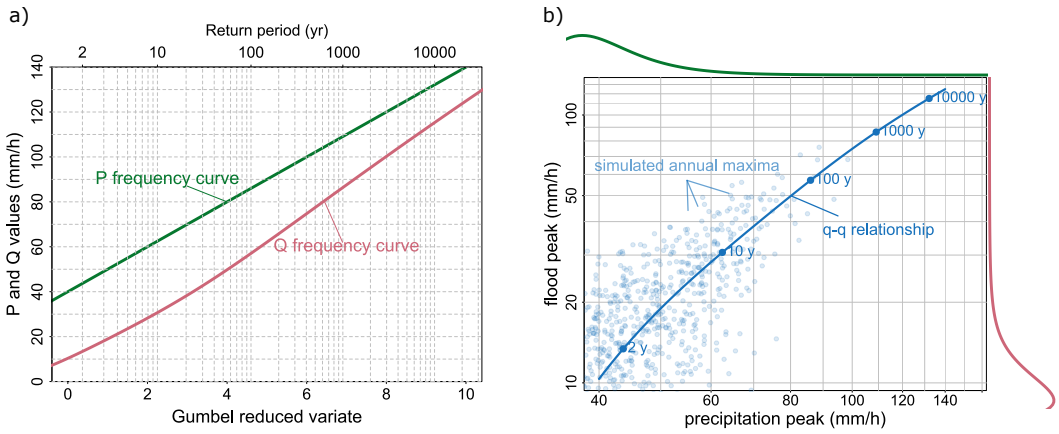


Fig. 3.2 (a) Frequency curve of flood peaks and rainfall maxima for a hypothetical catchment obtained with the model based on the rational method (Equations (3.1), (3.4), (3.5), (3.6) and (3.7)) with $\alpha_0 = 2$, $\beta_0 = 4$, $\xi_0 = 40$ mm/h, $\sigma_0 = 10$ mm/h. The random variables $P$ (rainfall) and $C$ (peak runoff coefficient) are slightly correlated ($\theta = 1.25$). (b) Quantile-quantile relationship (blue line) obtained from the frequency curves on the left with the pairs of annual maxima of rainfall and flood (dots). The curves on the top and on the right of panel (b) are proportional to the probability density functions of $P$ and $Q$ respectively. Note that the axes have been limited to emphasize the behavior of larger events.

## 3.3 Investigation on the method's main assumption

The methodology proposed in this article relies on the assumption that the logarithmic slope of the q-q relationships, or elasticity $E^{qq}$, can be used to transform the percentage variation of rainfall quantiles ($q_P$) into percentage change of flood quantiles ($q_Q$)

$$\Delta q_Q = \Delta q_P \cdot E^{qq} \tag{3.8}$$

where

$$E^{qq} = \left.\frac{dq_Q}{dq_P}\right|_{q_P} \cdot \frac{q_P}{q_Q} \tag{3.9}$$

The validity of Equation (3.3) is investigated using simulated variables according to Equations (3.4) to (3.7) when the parameters of the distributions change and considering different values of $\theta$, i.e. different correlations between the random variables $P$ and $C$. Suppose a hypothetical catchment characterized by a present

climate with rainfall distribution parameters $\xi_0 = 40$ mm/h and $\sigma_0 = 10$ mm/h, and a future climate with $\xi_1 = 44$ mm/h and $\sigma_1 = 11$ mm/h. Additionally, suppose that the hypothetical catchment has a peak runoff coefficient with parameters $\alpha_0 = 2$ and $\beta_0 = 4$ which does not change in time ($\alpha_1 = 2$ and $\beta_1 = 4$). Figure 3.3 shows the corresponding q-q relationships of the reference and future periods, as well as the shift of some of the quantiles (black lines). In other words, the hypothesis is that the elasticity of the reference q-q relationship ($E^{\mathrm{qq}}$), available in operative conditions, approximates the elasticity of the lines describing the shift of the equi-quantiles points from reference to future period ($E^{\mathrm{ref}}$). In practice, for each quantile, the shift from the reference to the future along the quantile axis is tracked. This allows to construct a continuous representation of how the distribution evolves. The logarithmic slope of this shift is calculated at each quantile to capture the rate of change in the distribution at that specific point. The resulting curve of these slopes provides a detailed, continuous view of the differences between the reference and future distributions, reflecting how the entire distribution has shifted and changed over time ($E^{\mathrm{ref}}$). In an operative context, $E^{\mathrm{ref}}$ is not available, while $E^{\mathrm{qq}}$ can be easily obtained from the frequency curves of rainfall and flood. In the described ideal numerical simulation, both the elasticities are available, and $E^{\mathrm{ref}}$ is used as a reference for $E^{\mathrm{qq}}$ to validate the methodology in Figure 3.3b. For small return periods, the elasticity is overestimated, but starting from a return period of 20-30 years, it becomes comparable. Given the imposed arbitrary variation of rainfall quantiles, future flood quantiles are obtained using the elasticities as a multiplicative factor.

$$\begin{aligned} q_{Q_1}^{\mathrm{qq}} &= q_{Q_0} \cdot (1 + \Delta q_P \cdot E^{\mathrm{qq}}) \\ q_{Q_1}^{\mathrm{ref}} &= F_Q^{-1}(p, \alpha_0, \beta_0, \xi_1, \sigma_1, \theta_0) = q_{Q_0} \cdot (1 + \Delta q_P \cdot E^{\mathrm{ref}}) \end{aligned} \tag{3.10}$$

where $q_{Q_1}^{\mathrm{qq}}$ is the future flood quantile with probability level p obtained with the q-q approach, $q_{Q_1}^{\mathrm{ref}}$ is the future flood quantile obtained with the model based on the rational method principles, $q_{Q_0}$ is the flood quantile in the reference or present period, and $\Delta q_P$ is the percentage variation of precipitation quantile. The validity of the proposed methodology is quantified through the percentage error $PE$ of future flood quantiles obtained with the q-q approach with respect to those obtained from the model.

$$PE = \frac{q_{Q_1}^{qq} - q_{Q_1}^{ref}}{q_{Q_1}^{ref}} \cdot 100 \tag{3.11}$$

Results are shown in Figure 3.4 and prove that in this specific case, the methodology is reliable starting from return periods larger than 20 years. From now on, the focus will be on the 100-year return period flood ($p = 0.99$) as a representative example of large return periods.

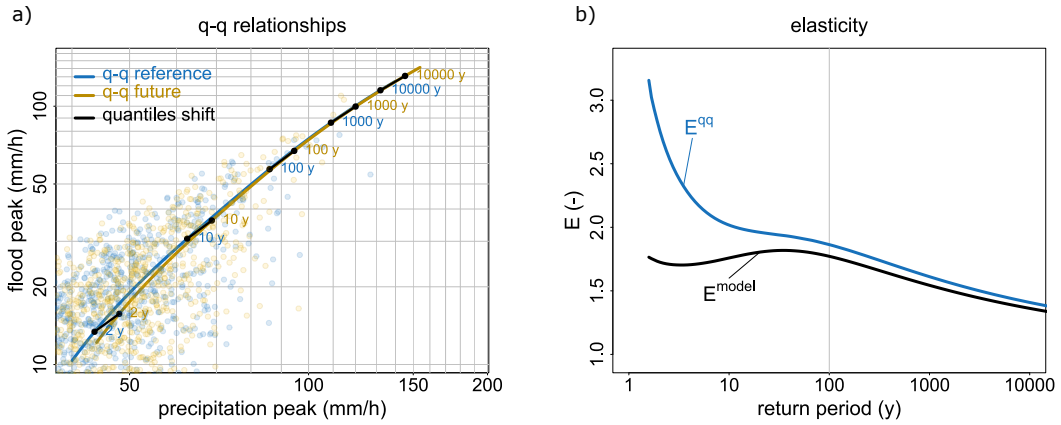


Fig. 3.3 (a) q-q relationships obtained for the reference and the future periods. The colored dots represent pairs of simulated annual maxima of precipitation and flood. The two periods differ only in terms of rainfall distribution: both the location and scale parameters are increased by 10%. The response of the catchment in terms of flood generation mechanism is kept constant and modeled through a beta distribution, which describes the peak runoff coefficient. Black lines represent some examples of the quantiles shifting from the reference to the future period. (b) Elasticity comparison between the quantiles shifting (black) lines and the q-q relationship in the reference period (blue) as a function of return periods. In this specific case, the elasticities are similar for return periods larger than 20-30 years.

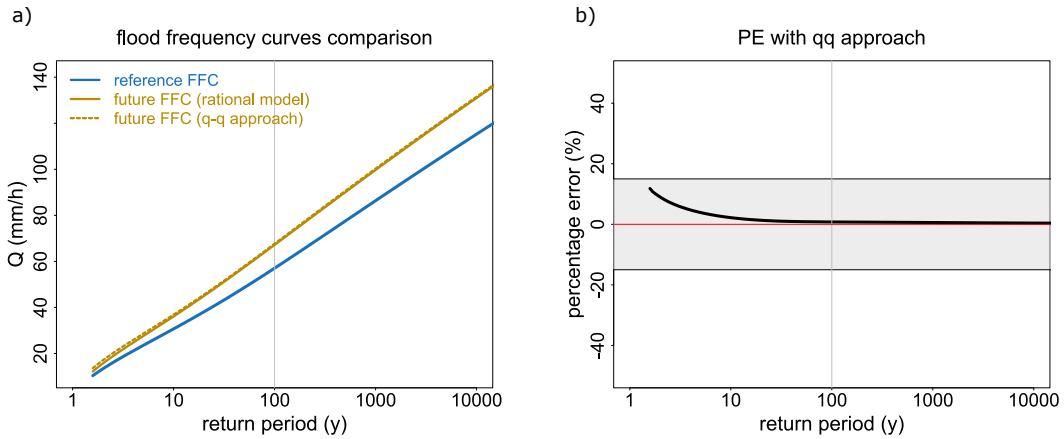


Fig. 3.4 (a) Comparison of Flood Frequency Curves obtained for the reference period (blue) and for the future period (yellow) considering the variation of rainfall distribution. Solid lines represent the FFC according to the model based on the rational method principle, while the dashed line represents the FFC according to the q-q approach. The difference tends to decrease with increasing return periods. (b) Percentage error of flood quantiles obtained for the future period using the q-q approach when compared to the flood quantiles of the future period obtained with the model based on the rational method principle. 15% error bounds are also shown. Note that the methodology is developed for large return periods (e.g. $>$ 100y).

The percentage error of the 100-year flood estimated for the future period $PE_{100}$ depends on the parameters of q-q relationships of present $(\alpha_0, \beta_0, \xi_0, \sigma_0, \theta_0)$ and future period $(\alpha_1, \beta_1, \xi_1, \sigma_1, \theta_1)$. It is therefore relevant to investigate the sensitivity of the $PE_{100}$ to these parameters to define optimal basin characteristics and rainfall variation for the applicability of the methodology. The parameters $\alpha$ and $\beta$ describe the catchment characteristics in terms of its response to rainfall events: $\alpha$ indicates the "concentration" of probability towards larger values of peak runoff coefficient, while $\beta$ indicates the "concentration" of probability towards lower values. The parameter $\theta$ describes the correlation between the annual maxima of flood and rainfall. Given the operational nature of the proposed methodology, these three parameters are considered to be stationary in time: $\alpha_0 = \alpha_1$, $\beta_0 = \beta_1$, and $\theta_0 = \theta_1$. Note that the marginal distribution of C is not stationary over time, whereas the conditional distribution of C given P is stationary. The sensitivity analysis is made on these parameters to investigate for which types of basins the q-q approach gives good results, as well as on the parameters $\xi_1$ and $\sigma_1$ describing the expected rainfall variation to investigate if the nature of rainfall variation has an impact on the validity of the hypothesis.

Nine types of catchments are identified in Figure 3.5 in terms of the type of response of the catchment and correlation between the annual maxima pair of flood and rainfall. In the first row and the last column, the different response types of the hypothetical catchments are described. In the second row of the figure, an arid (or high-infiltration) catchment is examined in terms of peak runoff coefficient distribution modeled with $\alpha_0 = 1.2$ and $\beta_0 = 10$, in the third row the parameters of the peak runoff distribution are $\alpha_0 = 2$ and $\beta_0 = 4$ resulting in an intermediate catchment, and in the last row the parameters are $\alpha_0 = 3$ and $\beta_0 = 2$ resulting in a humid (or low-infiltration) catchment. The correlation between the random variables $C$ and $P$ increases from left to right. The first column is characterized by rainfall and peak runoff coefficient fully uncorrelated (note that rainfall and flood are instead correlated). The second column is modeled with a parameter $\theta_0 = 1.25$. The third column is obtained with peak runoff coefficient and rainfall almost fully correlated. In each image, the percentage error of the estimated 100-year flood $PE_{100}$ for the future period obtained with the q-q approach for different scenarios of variation of rainfall distribution is presented. The x-axis of Figure 3.5 indicates an increase in terms of the location parameter $\xi_1$, i.e., an increase in the mean of annual maxima, while the y-axis indicates an increase in terms of the scale parameter $\sigma_1$, i.e., mainly an increase in the variance of annual maxima. The values of $\xi_0$, $\sigma_0$, $\xi_1$, and $\sigma_1$, are representative of the catchment sample available for the case study (see Section 3.4.3). The sensitivity analysis indicates that the catchment characteristics, the correlation between rainfall and peak runoff coefficient, and hence between rainfall and flood, is relevant with results that become more accurate as the correlation increases. The peak runoff coefficient distribution also influenced the methodology's accuracy: generally, the methodology yields better results for humid catchments. Finally, the nature of the rainfall distribution variation is also relevant: when the variation of precipitation extremes is in the mean (i.e., in the location parameter of the Gumbel distribution) the results are better than in the case where the variation of precipitation extremes is in their variability (i.e., in the scale parameter of the Gumbel distribution). This is particularly true for low values of correlation between flood and rainfall, and arid (or high-infiltration) basins.

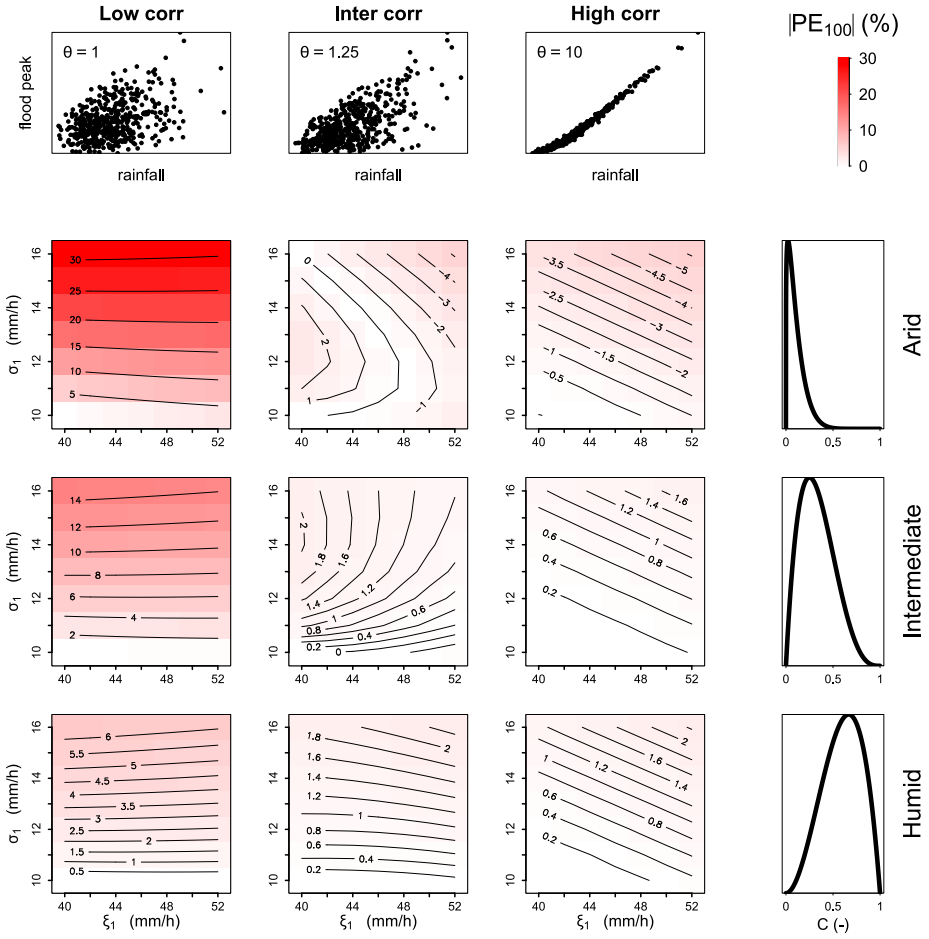


Fig. 3.5 Sensitivity analysis of the percentage error of the 100-year flood obtained for the future period using the q-q approach when compared to the 100-year flood of the future period obtained with the model based on the rational method principle (Equation (3.11)). Different types of catchments are analyzed in terms of aridity and correlation between flood and precipitation as schematized in the figures in the first row and the last column. In the second row the basins are assumed to be arid, in the third row intermediate, and in the last row they have a humid behavior. Along the different columns, the correlation between the pairs of peak runoff coefficients and precipitation annual maxima is increased. In the first column, there is no correlation; in the second column, the correlation is similar to a real case scenario, and in the third column, there is almost full correlation. The percentage errors for the 100-year flood are shown for different values of future precipitation distribution.

## 3.4 Application of the q–q framework to the Po River Basin

To illustrate its practical application, the methodology discussed above is applied to a case study set in the Po River basin in northern Italy. This area is characterized by a large alluvial plain surrounded on three sides by mountains. 227 catchments selected among those reported in Claps et al. (2024) are analyzed, with areas ranging from 10 $km^2$ to 13700 $km^2$, and mean elevation from 161 to 3123 m a.s.l. The selection was made according to the availability of at least 5 records of annual flood and areas smaller than 15000 $km^2$. These criteria depend on the application of the regional Flood Frequency Analysis described in the specific section below. Basins strongly influenced by hydraulic structures or large reservoirs were also discarded. Figure 3.6 shows the location of the outlets of the 227 basins and the corresponding catchment boundaries. Considering all the 227 stations, the station-years available are 5637. The FFCs and the IDF curves for the maximum annual precipitation, which are needed to apply the non-stationary analysis through the quantile-quantile approach, are obtained independently through the regional procedures described below. This methodology can also be applied to ungauged catchments.

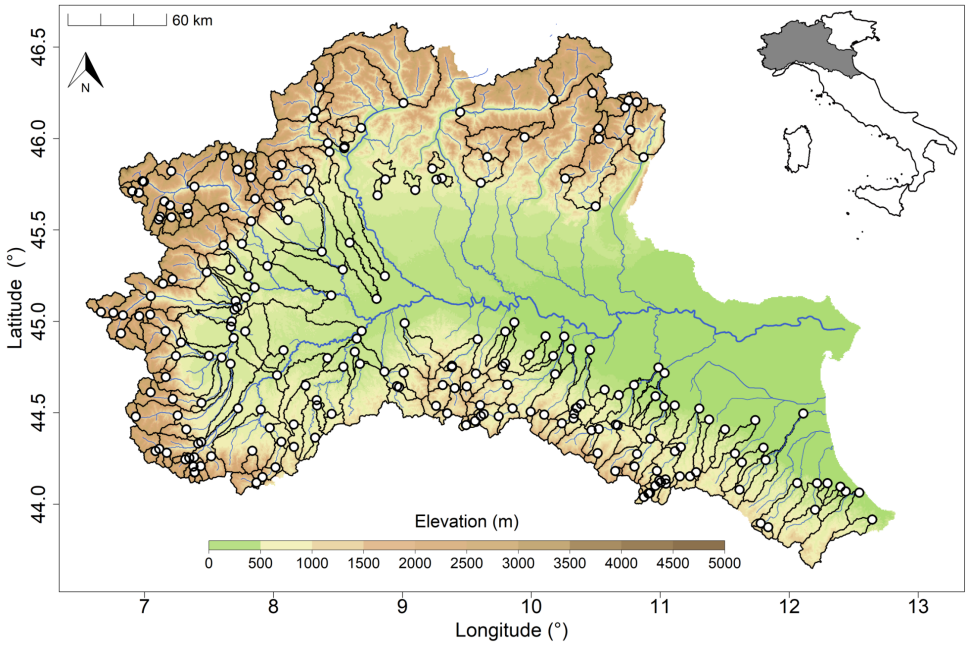


Fig. 3.6 Location of the 227 analyzed sites and identification of the basin boundaries.

### 3.4.1 Intensity Duration Frequency curves

Extreme rainfall measurements are obtained from the Improved Italian – Rainfall Extreme Dataset or $I^2 - RED$ (Mazzoglio et al., 2020), a collection of short-duration (1, 3, 6, 12 and 24 h) annual maximum rainfall depths measured by more than 5000 rain gauges from 1916 up to 2023 all over Italy. In this work, rain gauges active in the 1931-2020 period located over the Po River basin are considered. An improved version of the patched kriging (Libertino et al., 2018; Mazzoglio et al., 2022; Paola Mazzoglio and Claps, 2023), a robust gap-filling procedure for rainfall frequency analysis, was used to exploit all the available rainfall information. This methodology makes it possible to obtain an estimation of the IDF curve parameters for selected distributions (e.g., the Gumbel in this work) in gauged and ungauged locations. These curves follow the equation (3.12)

$$h_{d,T} = K_T \cdot a \cdot d^n = \left[1 - 0.5772 \cdot \sigma - \sigma \cdot \ln\left(\ln\left(\frac{T}{T-1}\right)\right)\right] \cdot a \cdot d^n \qquad (3.12)$$

where $h_{d,T}$ is the design rainfall related to duration $d$ and return period $T$ (mm); $K_T$ is the growth factor related to a return period $T$, modeled as a Gumbel distribution with mean 1 and non-dimensional scale parameter $\sigma$ (-); $a$ is the scale factor (mm/h), i.e., the expected maximum annual 1-hour precipitation; $d$ is the duration (h); and $n$ is the scaling exponent (-) that describes the rate of increase of the expected maximum annual precipitation for increasing durations. The Gumbel distribution was chosen for its two-parameter structure, which also ensures consistency with the numerical validation framework. However, being characterized by a lighter tail than heavy-tailed alternatives, it may underestimate precipitation quantiles for large return periods, potentially overestimating elasticity and, consequently, projected increases in flood quantiles. From an engineering perspective, this conservative bias is preferable to the opposite, as it avoids underestimating future flood hazard in the design of hydraulic structures. The methodology consists of three main steps: a) interpolation with a regression kriging of annual maximum rainfall depths performed year by year, separately for each duration, to obtain a rainfall data cube with a spatial extent matching the analysis areas and a number of layers equal to the number of years considered; b) calculation of the L-moments of the reconstructed series (which may originate from direct measurements or kriging interpolation), with an approach that gives greater weight to measured values; c) bias correction of both the L-moments and the reconstructed time series. The $a$ and $n$ parameters are estimated, respectively, as the intercept and the slope of the simple linear regression model applied to the logarithm of the mean rainfall extremes for 1, 3, 6, 12, and 24-hour durations. The growth factor parameter $\sigma$ is estimated with the method of L-moments as $\frac{L_{cv}}{ln(2)}$, where $L_{cv}$ is the L-coefficient of variation of the annual maxima of precipitation with duration $d$. The value of $K_T$ is assumed to be the same for all the duration of precipitation, and is estimated as the mean of the $K_T$ obtained for the 5 durations. The reader can refer to Libertino et al. (2018) for a more detailed description of the patched kriging methodology and to Paola Mazzoglio and Claps (2023) for more details on the regression model implemented to perform the year-by-year reconstruction. The entire patched kriging workflow is here run during the period 1931 – 2020 to obtain the growth factor for the Gumbel distribution for return periods of 2, 5, 10, 20, 50, 100, 200, 500, and 1000 years.

For every catchment, the time of concentration is roughly estimated from its drainage area as $t_c = 0.675 \cdot A^{0.5}$ (Ferro, 2006). This formula is one of those used in Ravazzani et al. (2019) to estimate the time of concentration of 46 basins in northern Italy and

was chosen for its simplicity (see Evangelista et al. (2023) for a review on catchment response time formulas). For the application of the q-q methodology, the evaluation of the time of concentration is a key aspect when the growth factor is different for different durations. To analyse the expected variation of the IDF curves in the future, an ensemble of 24 simulations of CORDEX models (EUR-11) of CMIP5 is used (Jacob et al., 2014; Taylor et al., 2012) with a spatial resolution of 12.5 km, temporal resolution of 1h and RCP 8.5. A control period (1981–2010) and a future period (2071–2100) are considered, calculating the percentage variation of precipitation quantiles with the same procedure previously described in Equation (3.11). Note that using percentage variation, no bias-correction procedure is needed. CORDEX models of CMIP5 were used because of the availability of a large number of different simulations over the study area (Table 3.1). The percentage variation of precipitation quantiles considered in the case study is the median of those obtained from the single simulations.

Table 3.1 List of CORDEX simulations included in the ensemble mean used to evaluate the expected variation of the Intensity-Duration-Frequency curves. The models belong to the Fifth Assessment Report (AR5) of the IPCC and have a spatial resolution of 12.5 km

| GCM name | RCM name |
|---|---|
| MPI-ESM-LR | GERICS-REMO2015 |
| MPI-ESM-LR | CLMcom-ETH-COSMO-crCLIM-v1-1 |
| MPI-ESM-LR | CNRM-ALADIN63 |
| MPI-ESM-LR | MOHC-HadREM3-GA7-05 |
| NCC-NorESM1-M | SMHI-RCA4 |
| NCC-NorESM1-M | CLMcom-ETH-COSMO-crCLIM-v1-1 |
| NCC-NorESM1-M | CNRM-ALADIN63 |
| NCC-NorESM1-M | MOHC-HadREM3-GA7-05 |
| NCC-NorESM1-M | ICTP-RegCM4-6 |
| CNRM-CERFACS-CNRM-CM5 | SMHI-RCA4 |
| CNRM-CERFACS-CNRM-CM5 | CNRM-ALADIN63 |
| CNRM-CERFACS-CNRM-CM5 | GERICS-REMO2015 |
| CNRM-CERFACS-CNRM-CM5 | ICTP-RegCM4-6 |
| CNRM-CERFACS-CNRM-CM5 | MOHC-HadREM3-GA7-05 |
| CNRM-CERFACS-CNRM-CM5 | CLMcom-ETH-COSMO-crCLIM-v1-1 |
| IPSL-IPSL-CM5A-MR | SMHI-RCA4 |
| MOHC-HadGEM2-ES | SMHI-RCA4 |
| MOHC-HadGEM2-ES | CLMcom-ETH-COSMO-crCLIM-v1-1 |
| MOHC-HadGEM2-ES | MOHC-HadREM3-GA7-05 |
| MOHC-HadGEM2-ES | SMHI-RCA4 |
| ICHEC-EC-EARTH | CLMcom-ETH-COSMO-crCLIM-v1-1 |
| ICHEC-EC-EARTH | ICTP-RegCM4-6 |
| ICHEC-EC-EARTH | MOHC-HadREM3-GA7-05 |
| ICHEC-EC-EARTH | SMHI-RCA4 |

### 3.4.2 Flood Frequency curves

For estimating the FFCs, the Spatially Smooth Estimation Method developed by Laio et al. (2011) is used, which is one of the methods operationally used in the area. The results are those described in Section 2.4.1, using the L-moments derived with the purely regional approach:

$$
\begin{aligned}
q_{\text{ind}} &= 0.01239 \cdot A^{0.77905} \cdot k_s^{-0.16514} \cdot a^{2.09555} \cdot n^{1.3146} \\
L_{\text{cv}} &= 0.30465 - 0.00013 \cdot MAP_{\text{mean}} - 0.12571 \cdot MAP_{\text{cv}} - 0.00541 \cdot C2 \\
L_{\text{ca}} &= -0.40728 - 0.2167 \cdot MAP_{\text{cv}} + 2.78896 \cdot L_{ca_{3\text{h}}} - 0.00366 \cdot C2
\end{aligned}
\tag{3.13}
$$

where $A$ is the area of the catchment (km$^2$); $k_s$ is the saturated permeability coefficient (-), calculated as in Claps et al. (2024); $MAP_{\text{mean}}$ is the spatial average of the mean annual precipitation over the basin (mm); $MAP_{\text{cv}}$ is the spatial coefficient of variation of the mean annual precipitation over the basin (-); $L_{ca_{3\text{h}}}$ is the spatial mean of the L-skewness of annual maximum rainfall for the duration of 3 hours (-); $C2$ is the mean value of the C2 coefficient in the Fourier series representation of the monthly rainfall regime (-) as explained in Claps et al. (2024). When data are available for the section of interest, they are integrated into the estimation to make it more robust by using the sample or regional L-moments based on their estimation variability (Laio et al., 2011). For each basin, the flood quantiles are assumed to follow a 3-parameters log-normal distribution, whose CDF is:

$$F_Q(z) = \Phi\left(\frac{\ln(z-\theta_1)-\theta_2}{\theta_3}\right) \tag{3.14}$$

where $\theta_1$, $\theta_2$ and $\theta_3$ are obtained from the L-moments (Hosking and Wallis, 1997) and $\Phi$ is the normal CDF function.

### 3.4.3 Catchment characterization

The basin dataset was first analyzed in terms of catchment response and precipitation distribution parameters variation, identifying 22 basins that required special attention based on the results of the sensitivity analysis. These catchments exhibit characteristics that may result in a percentage error larger than 15% in the estimation of the 100-year flood. Figure 3.7 shows the density probability of the location and scale parameters of the precipitation distribution, as well as their percentage variation between the periods 2071-2100 and 1981-2010. The values of the parameters used in the sensitivity analysis represent a typical small-to-medium Alpine catchment with an area ranging from 50 to 200 km$^2$. These values maximize the representativeness of the catchments analyzed in the case study. In this case study, the shape parameter $\xi$ ranges between 30 mm and 50 mm for more than half of the catchments, with an increase from the present to the future period of less than 30 % for almost the totality of the catchments. The scale parameter $\sigma$ is between 10 mm and 15 mm for almost half of the catchments, with an increase of less than 60% for almost the totality of them. Similarly, the catchments are analyzed in terms of the ratio between the mean annual flood and the mean annual maximum precipitation as a

proxy of the mean value of C (Figure 3.8). The 22 catchments selected as critical were those with a location increase larger than 20% and a value of $\frac{q_{\text{ind}}}{a \cdot d^{\text{n-1}}} < 0.2$. These catchments present characteristics that, according to the sensitivity analysis, may undergo a percentage error PE in the estimation of the 100-year flood larger than 15%. The catchments selected as potentially critical are not necessarily unsuitable for the analysis: the data available for the region does not allow us to gain information on the copula parameter $\theta$, therefore, the worst-case scenario with $\theta = 1$ is assumed, i.e., no correlation between precipitation and runoff coefficient.

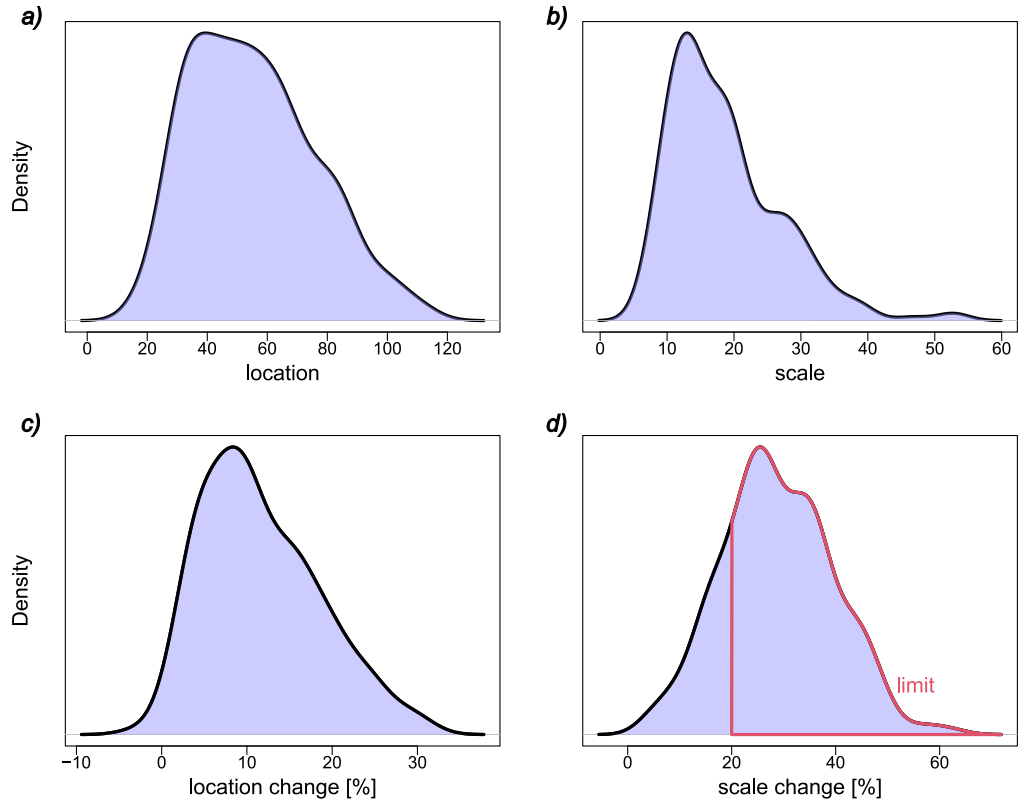


Fig. 3.7 Density probability of the location and scale parameters of the precipitation distribution with duration equal to the time of concentration of the specific catchment (panels a and b). Percentage variation of the parameters when comparing the periods 2071-2100 and 1981-2010 (panels c and d). The range of values considered potentially critical is highlighted in red in panel d.

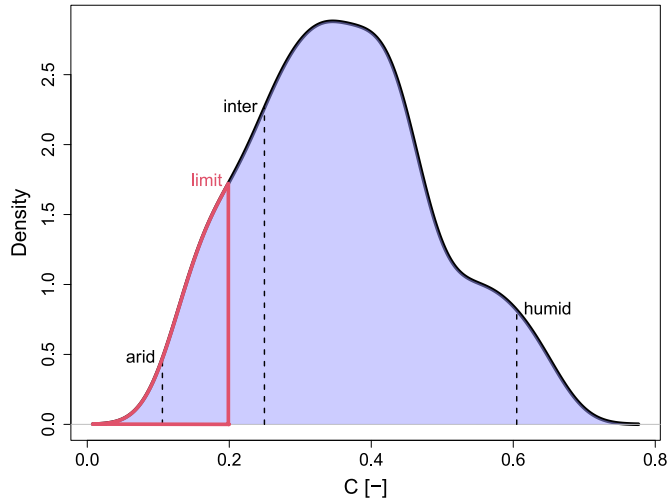


Fig. 3.8 Density probability of the mean value of peak runoff coefficient, estimated as the ratio between index flood and index precipitation. The values corresponding to the arid, intermediate, and humid configurations described in the sensitivity analysis are highlighted, as well as the range of values considered potentially critical.

### 3.4.4 Projected changes in design floods across the Po River Basin

Figure 3.9 (panel c) shows the percentage changes in the 100-year flood for the study area, obtained with the proposed method based on the q-q relationship. The values range between 7% and 90%, but the large majority of the catchments are expected to face an increase of 20-40%. The largest values are mostly found in smaller basins where the precipitation increase is more relevant: the smallest values are instead found in the Valle d'Aosta region in the north-western part of the study area. Most of the critical basins are high-elevation catchments in this area, where floods are often driven by snowmelt. The totality of the catchments included in the case study is expected to undergo an increase in the 100-year flood because, according to the CORDEX models, the precipitation with a return period of 100 years is expected to increase in all the study area. Results for two example catchments are also shown in Results for specific catchments.

The percentage increase of the flood quantiles results from the combination of two distinct factors: the first one is the increase of precipitation quantiles with a duration equal to the concentration time of the catchment, and the second is related to the elasticity of floods to precipitation $E^{qq}$. The percentage changes of Figure 3.9 (panel c) are obtained by the combination of these two factors (panels a and b). Some

spatial patterns are found regarding the elasticity ($E_{100}^{qq}$): the south-western part of the study area is characterized by the largest values with $E_{100}^{qq}$ ranging between 2 and 2.5, while the north-western part has the lowest values with many basins with $E_{100}^{qq}$ smaller than 1. Regarding the precipitation increase, there are some small basins with exceptional increases because they have small concentration times, and short precipitation extremes are projected to increase more than long ones. The clearest and most robust signal is instead found in the Emilia-Romagna region in the Apennine basins (south-western part of the map), where the increase approaches values of 30%. Figure 3.9 (panel d) shows the density function of the predicted variation of $q_{100}$ both for the subset dataset and for the entire one. The exclusion of the 22 basins does not significantly alter the probability density of $q_{100}$ overall.

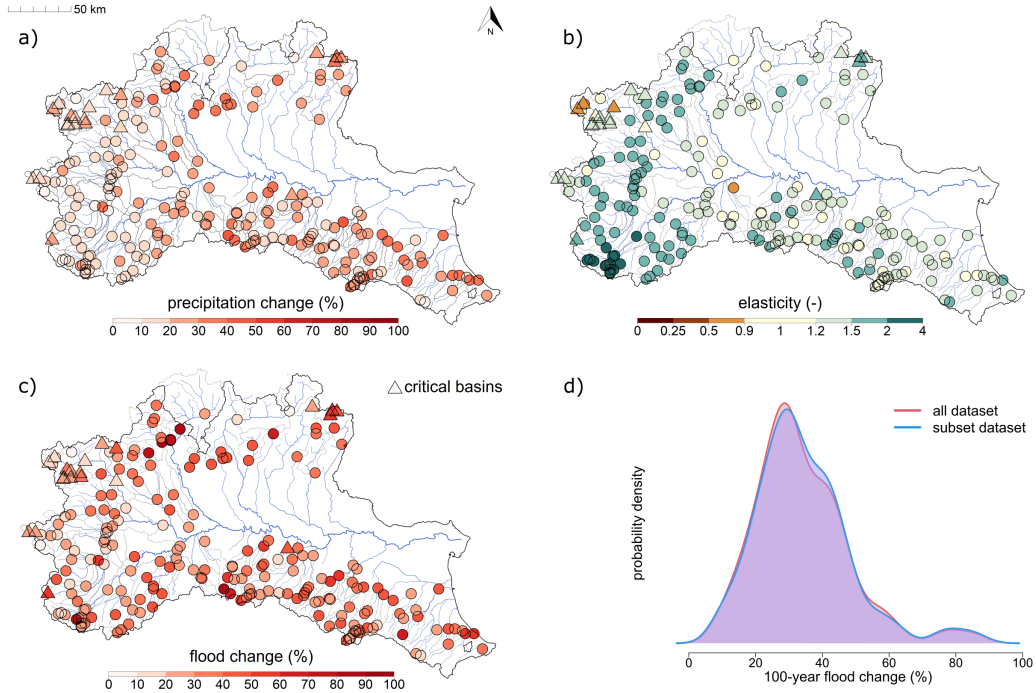


Fig. 3.9 Percentage change of the 100-year return period flood obtained for the period 2071-2100 vs. 1981-2010 with the RCP8.5 scenario (a). Percentage increase of the 100-year return period precipitation with duration equal to the time of concentration of the catchment considering the ensemble mean of the CORDEX models with the RCP8.5 scenario (b). Elasticity (dimensionless) for the 100-year return period based on the regional models applied for the flood and precipitation frequency curves (c). Probability density function of the predicted variation of $q_{100}$ both for the subset dataset and for the entire one (d).

### 3.4.5 Results for specific catchments

The results obtained for two example catchments are also reported. The 'Dora Baltea at Ponte di Mombardone' is among the catchments with the lowest values of elasticity ($E_{100} = 0.8$), while the 'Maira at San Damiano Macra' is among the most elastic catchments ($E_{100} = 2.3$). Forcing the quantile-quantile relationship to be stationary in time, it is possible to obtain in Figures 3.10 and 3.11 the expected variation of FFCs caused by a variation of the IDF curves. As found in Section 3.3, the hypothesis of stationarity of the q-q relationship is credible for large return periods (100 y). In the second catchment, floods are more sensitive to an increase in precipitation intensity, and the percentage increase of $Q_{100}$ is more than double the percentage increase of $P_{100}$.

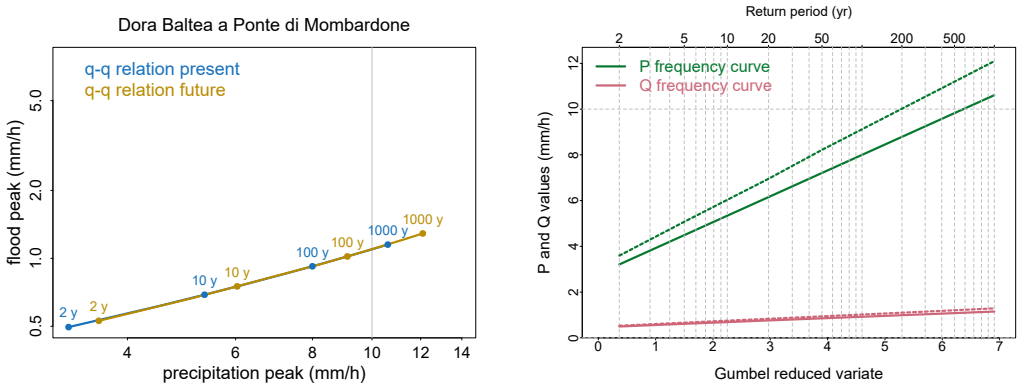


Fig. 3.10 q-q relationship obtained for the catchment 'Dora Baltea at Ponte di Mombardone' (a). The q-q relationships for the present and future periods are forced to coincide following the methodology described, so that it is possible to obtain the future flood frequency curve considering the variation of the precipitation frequency curve. This catchment is characterized by a particularly small value of elasticity. In panel b, the frequency curves of precipitation and flood are shown for the 1981-2010 (solid line) and the 2071-2100 periods (dashed line). Regarding the future frequency curves, the precipitation one is obtained through the ensemble mean of CORDEX models, while the flood one is obtained by forcing the quantile-quantile relationship to be stationary in time. The percentage variation of $q_{100}$ is smaller than the percentage variation of $P_{100}$.

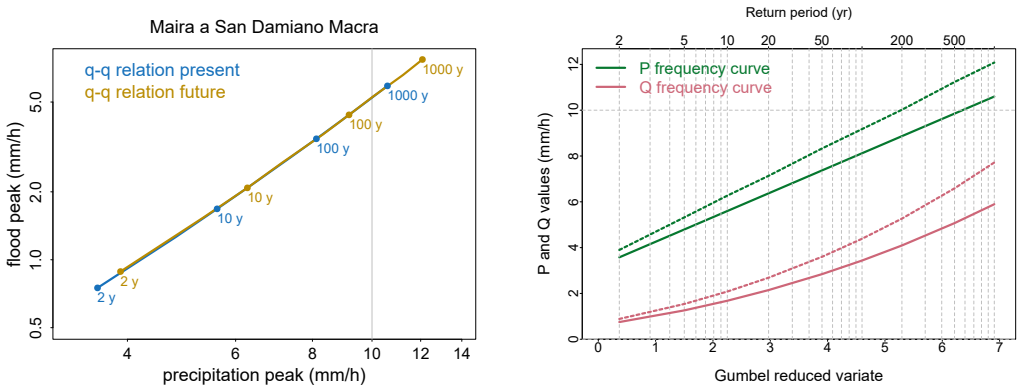


Fig. 3.11 q-q relationship obtained for the catchment 'Maira at San Damiano Macra' (a). The q-q relationships for the present and future periods are forced to coincide following the methodology described, so that it is possible to obtain the future flood frequency curve considering the variation of the precipitation frequency curve. This catchment is characterized by a particularly large value of elasticity. In panel b, the frequency curves of precipitation and flood are shown for the 1981-2010 (solid line) and the 2071-2100 periods (dashed line). Regarding the future frequency curves, the precipitation one is obtained through the ensemble mean of CORDEX models, while the flood one is obtained by forcing the quantile-quantile relationship to be stationary in time. The percentage variation of $q_{100}$ is larger than the percentage variation of $P_{100}$.

## 3.5 Interpretation, applicability, and limitations of the q–q approach

In this work, a method to include the expected variation of extreme precipitation into flood frequency analysis is proposed, based on the assumption that the quantile-quantile relationship between precipitation and flood distributions is stationary. Three questions were posed regarding the proposed methodology: 1) Which conditions allow the usage of the proposed methodology? 2) Is this methodology suitable for all the percentiles across the full distribution of floods? 3) What are the expected flood changes for projected precipitation changes in Northern Italy?

Regarding the first question, a range of cases in which this methodology can be applied is identified. The target catchment for applying this methodology shows a medium to strong correlation between the annual maxima of rainfall and floods, indicating that extreme rainfall is the main flood generation mechanism. One approach to characterize a catchment in this context is to analyze the seasonality of floods and rainfall; if these differ, this may indicate that the q-q methodology has a limitation.

When data are available, continuous series of precipitation and discharge should also be analyzed, isolating some events following, for example, Tarasova et al. (2018) or Giani et al. (2022), and examining the correlation between precipitation and runoff coefficient at the event scale. Moreover, the response type of the catchment in terms of rainfall-runoff transformation was found to be a fundamental aspect to consider. Errors are larger in catchments with generally low values of the peak runoff coefficient of the annual flood, i.e., arid catchments or high-infiltration catchments. These types of catchments are indeed characterized by heavier tails of flood distribution, resulting in steeper flood frequency curves, and consequently large values of elasticity (Metzger et al., 2020). Another factor to consider before employing this methodology is the variation of rainfall distribution. When the distribution is expected to change more in terms of the variance rather than the mean, larger errors may occur in the estimation of future flood quantiles. While each of these aspects has to be considered, the methodology should be discarded only when the catchment presents criticalities in all of them, as PE larger than 15% occurred only in such cases.

Concerning the second question, the q-q approach is recommended for large values of return periods ($T > 100$ years), for which the results show that the percentage error of future flood quantiles remains small. Note that the estimation of precipitation and flood quantiles, as well as their variations, are subject to larger uncertainty for high return periods, but the proposed methodology is more reliable. For this reason, it is preferable to use FFCs and IDF curves obtained through regional methods, which are more robust in capturing the tail behaviour of the distributions than methods applied locally on data belonging to single sites. Additionally, for large return periods, the q-q curve is less influenced by changes in the runoff coefficient parameters, which in this validation analysis were kept constant, given that the focus is solely on the effect of the variation of rainfall. This is because the effect of a change in the runoff generation processes is more likely to have an influence on the lower part of the q-q relationship, describing ordinary floods that can be produced by large rainfall and moderate runoff coefficient or the other way around, while for larger return periods, when initial conditions of the catchment become less relevant under the assumption that big floods are always caused by large rainfall and runoff coefficient, the q-q relationship is less sensitive to changes in their distribution. This interpretation is consistent with Macdonald et al. (2024), who analyzed the tail behaviour of flood and precipitation distributions. They found that beyond a certain return period,

the influence of catchment processes decreases, and the tail of rainfall distribution modulates the tail of flood peak distribution. The threshold value of the return period depends on the ratio between catchment storage and mean annual rainfall. Most of the catchments they analyzed have a threshold return period between 100 and 500 years. Brunner et al. (2021) related the threshold return period with mean catchment elevation instead, finding that for high-elevation catchments this value drops below 10 years. This implies that the return periods for which the methodology may be considered more accurate vary depending on the catchment of interest.

Focusing on the third research question, we now analyze the expected changes in flood peaks in the Po River basin in northern Italy (see Figure 3.9). Analyzing the results of the case study, two distinct factors causing changes in flood quantiles are found. The first one is the percentage increase of the corresponding precipitation quantiles, while the second one is the elasticity of floods to precipitation changes. Large values of elasticity are found in catchments with particularly steep FFCs compared to the IDF curves. In these catchments, even a small increase in precipitation quantiles can produce a large increase in flood quantiles (e.g., a catchment with $E = 2$ will face a 40% increase in flood quantile as a result of a 20% increase of the precipitation quantile). Note that an elasticity of 2 has been found by Haslinger et al. (2025) between heavy hourly rainfall and flood peak increase in small basins in Austria, which is consistent with the range of elasticities estimated through the qq relationship in Northern Italy. Here, some spatial patterns can be identified: the south-western part of the study area, which is characterized by steep FFC (i.e. large values of L-skewness), has the largest values. The lowest values are instead found in north-western part of the study area, where snow processes are dominant given the very high elevations. Regarding the first one, a possible interpretation is given by the role of geology. In this region, springs are fed by aquifers hosted in highly fractured carbonate successions. The carbonate rock mass is bordered by the impermeable metamorphic bedrock, which in general constitutes important permeability sills. This area is also characterized by a fractured and karstic aquifer with an extensive saturated zone, or karst carbonate aquifer covered by a thick layer of glacial deposits that heavily control the infiltration processes (Vigna and Banzato, 2015). These characteristics result in large infiltration during small events, while the karst system has a relevant contribution during major events. With reference to the rational method, this results in particularly low values of $C$ and, consequently, in large values of elasticity. Regarding the north-western part of the study area, floods

often result from snowmelt, leading to less variable mechanisms that produce a flatter FFC and lower elasticity values ($E_{100} < 1$). Breinl et al. (2021) similarly observed inelastic relationships in the glaciated regions of the highest summits of Austria. Most of the basins in question are among those identified as potentially critical in the analysis described in Catchment characterization. When analyzing snow-dominated catchments, a more rigorous approach would involve removing the base flow and isolating floods generated by large precipitation events before applying the proposed methodology.

The results of the increase of the 100-year floods obtained with this methodology agree with those obtained in other studies that used different methodologies. For example, Rojas et al. (2012) assessed future flood hazard in view of climate change at a pan-European scale using a large ensemble of climate projections. They used hydrological models forced by bias-corrected climate data from an ensemble of 12 climate experiments conducted within the ENSEMBLES project, obtaining spatial patterns of variation of the 100-year flood in Europe. In particular, northern Italy shows a robust increase (about 40% when comparing the period 2071-2100 and 1961-1990), mainly due to a pronounced increase in extreme rainfall. A similar approach was used by Roudier et al. (2016) who presented an assessment of the impacts of a +2°C global warming on extreme floods, obtaining an increase of $q_{100}$ in northern Italy between 30% and 40%. Similar values of $q_{100}$ increase in Northern Italy were also found by Kundzewicz et al. (2010), who reviewed projections of flood hazard in Europe based on climatic and hydrological models, to illustrate possible changes of recurrence of a 100-year flood in Europe. Signals of increase in magnitude of the 100-year floods in Northern Italy were also found by Di Sante et al. (2021), who simulated climate change effects on the occurrence of river floods over Europe. They used a distributed hydrological model (CHyM) forced with 44 EURO-CORDEX, 13 CMIP5, and 7 CMIP6 simulations, finding a robust signal of flood magnitude increase due to the increase of extreme precipitation events. Compared to these approaches, the advantage of the q-q methodology is that complex rainfall-runoff modeling is avoided.

This work presents an approach for flood frequency analysis that accounts for the predicted changes in precipitation extremes, applicable also to ungauged basins. The method is based on a combination of a data-based approach to obtain the q-q relationships for each catchment and a model-based approach to obtain the expected variation of the IDF curves. It allows for modifying regional FFC accounting for the

expected variation of regional IDF curves according to climate models.
The methodology constitutes a simple but effective tool for decision-makers, which can be used over many catchments in a wide area, such as the one investigated in this work (coincident with the largest Italian water district). The results obtained in the case study presented here are comparable with those found in other studies that used more complex approaches to evaluate the percentage change of the 100-year flood. This methodology should be applied when the expected flood change is dominated by changes in rainfall extremes rather than in the runoff generation processes of the catchment. In addition, it is expected to provide more reliable results for large return periods and for catchments characterized by a medium-to-large correlation between flood and rainfall annual maxima (see sensitivity analysis in Figure 3.5).
This study can be considered as an example of "flood frequency hydrology", in a broader sense of what is discussed in Merz and Blöschl (2008a,b) and Viglione et al. (2013), i.e., a way of expanding information on how climate change may affect floods by using different techniques and data in a different way that is usually done in studies of non-stationarity on floods. Future research should further test and refine this approach, but these findings suggest that the q-q relationship, and particularly its elasticity, can serve as a practical tool for incorporating extreme precipitation variations into flood frequency analysis, ultimately allowing flood risk assessment under climate change.

# Chapter 4

# Climate-Sensitive Derived Flood Frequency Analysis

The previous chapter deliberately adopted a pragmatic perspective, with limited emphasis on the explicit representation of hydrological processes. Its primary objective was to develop a methodological framework that allows practitioners to incorporate the effects of climate change into the estimation of flood frequency curves, which are a fundamental input for the design and safety assessment of hydraulic infrastructure. Accordingly, the focus was on robustness, transparency, and ease of implementation, rather than on attributing observed or projected flood changes to specific physical mechanisms.

In contrast, the present chapter shifts toward a more process-based perspective. Instead of proposing a direct operational procedure for impact assessment, it aims to investigate how changes in flood frequency emerge from the interaction of different flood drivers under non-stationary hydroclimatic conditions. By explicitly representing the seasonal dependence of rainfall–runoff processes within a Bayesian framework, this chapter seeks to explore the roles of precipitation intensity, soil moisture dynamics, and temperature-driven processes, thereby embracing the inherent complexity of flood generation in a changing climate.

The proposed approach links an event-based rainfall–runoff model with probabilistic representations of storms, antecedent soil moisture, and catchment response, enabling the joint propagation of uncertainty from climate drivers to flood quantiles. Its structure further allows for the attribution of flood changes to individual mechanisms,

such as shifts in the zero-degree isotherm, long-term trends in soil moisture, and variations in precipitation intensity. The case study for this analysis is in Austria, using long-term observations and regional climate projections (EURO-CORDEX). Together, the two chapters provide a coherent and comprehensive perspective on flood non-stationarity.

## 4.1 From statistical flood frequency to process-based derived approaches

Recent attribution studies highlight the importance of changes in precipitation, soil moisture, and snowmelt in shaping flood regime shifts across Europe (Bertola et al., 2021), pointing to the need for a process-based understanding of how different flood generation mechanisms respond to climate forcing. As highlighted in Chapter 1, flood frequencies are the result of the interplay between these flood generation mechanisms. Given these complexities, a wide range of methods has been developed for estimating design floods. These can broadly be classified into statistical, deterministic, and hybrid or derived approaches (Rogger et al., 2012a; Winter et al., 2019). Statistical methods fit probability distributions to observed peak flows and provide robust estimates when long, stationary records exist. Deterministic methods, such as the design storm approach, simulate catchment response to prescribed rainfall events and are more suited to engineering applications but rely on critical assumptions regarding storm duration, shape, and antecedent soil moisture (Camici et al., 2011). Hybrid or derived flood frequency approaches combine both statistical and physical representations. Initially formulated by Eagleson (1972) and further developed in following years (Gioia et al., 2008; Haberlandt and Radtke, 2014; Sivapalan et al., 2005), they link stochastic descriptions of rainfall to rainfall–runoff models to derive the flood frequency curve analytically or through Monte Carlo simulation. These approaches enable a process-based interpretation of flood probabilities, directly connecting storm characteristics, catchment response, and hydrological variability. For example, Viglione and Bloschl (2009) used this approach to examine the effect of event runoff coefficients on the relationship between rainfall and flood return periods. The increasing computational power and availability of stochastic rainfall models have further promoted their application for assessing flood response under

climate and land-use change (Falter et al., 2015; Rogger et al., 2012a; Winter et al., 2019).

The derived flood frequency concept provides an ideal framework for integrating process understanding into flood estimation and for exploring the physical drivers of flood change (Merz and Blöschl, 2003). In particular, event-based formulations (Ball et al., 2016; Ho et al., 2023) allow the explicit consideration of storm properties and rainfall-runoff interactions, which are both sensitive to climatic drivers. The capacity to model these physical processes makes derived approaches particularly valuable for projecting future flood hazard under non-stationary climate conditions. This study builds on this concept to explicitly disentangle the effects of individual flood generation mechanisms (variation of precipitation extremes, soil moisture, and the upward shift of the 0°C isotherm line) to analyse how their relative importance and associated flood frequencies are projected to change under future climatic conditions.

Bayesian inference has emerged as a powerful methodological complement to process-based flood analysis. Bayesian frameworks enable the explicit representation of uncertainty in both parameters and model structure, while coherently integrating diverse data sources and prior hydrological knowledge (Kuczera et al., 2010; Renard et al., 2010; Ribatet et al., 2007; Viglione et al., 2013). Within flood frequency analysis, Bayesian methods provide a natural means to link event-scale processes (e.g., rainfall intensity, duration, runoff coefficient, soil moisture) to flood statistics and to propagate uncertainties from climate drivers through to flood quantiles (Costa and Fernandes, 2017; Meresa et al., 2021). Moreover, they allow for hierarchical modeling of catchment similarity and facilitate the pooling of information across regions, enhancing robustness in data-scarce environments.

Despite significant progress in recent decades, most existing studies treat climatic and hydrological uncertainties independently, which limits their ability to capture the compound effects of changing precipitation and antecedent conditions. Moreover, while several process-based and stochastic models have been proposed for derived flood frequency analysis, few explicitly account for the seasonal dependence of flood generation mechanisms or their sensitivity to climate forcing

Building on these needs, this study presents a Bayesian, event-based framework for derived flood frequency analysis calibrated on event characteristics, that explicitly accounts for the seasonal dependence of rainfall–runoff processes and their climate sensitivity. The approach links probabilistic representations of storm, soil moisture,

and catchment response through a simple event-based rainfall–runoff model, allowing the joint propagation of uncertainty from climate forcing to flood quantiles. The framework is applied to Austrian hydrological hotspots using long-term records and EURO-CORDEX climate projections, providing a transferable methodology to assess climate-sensitive flood hazards in non-stationary environments. Although the present study focuses on climate-driven changes, the same framework can be readily applied to assess the influence of other drivers of non-stationarity, such as land-use modifications or hydraulic interventions (Hall et al., 2014).

The chapter is organized as follows: Section 4.2 describes the study region and data. Section 4.3 outlines the Bayesian stochastic modeling framework and calibration. Section 4.4 presents the results on process variability, uncertainty decomposition, and projected flood frequency changes. Finally, Section 4.5 discusses the implications of the findings and summarizes key conclusions.

## 4.2 Hydroclimatic setting and flood-generating regimes in Austria

The study is conducted in Austria, a hydrologically diverse country with complex interactions among topography, climate, geology, and land use. Elevations range from below 200 m in the eastern lowlands to over 3000 m in the western Alps. This topographic gradient drives substantial spatial variability in precipitation, which ranges from less than 400 mm $yr^{-1}$ in the east to nearly 3000 mm $yr^{-1}$ in the mountainous west. Land cover reflects the altitudinal zones: lowlands are predominantly agricultural, mid-elevation regions are forested, and high alpine areas are characterized by sparse vegetation and exposed bedrock. (Gaál et al., 2012; Merz and Blöschl, 2003).

Flood drivers differ across the country. In the western Alps, streamflow is significantly influenced by snow and glacier melt, and most floods occur in summer as a result of frontal systems and, occasionally, convective storms. Snowmelt can enhance antecedent soil moisture conditions, especially for early summer floods. In the southern and southeastern alpine regions, Mediterranean storm tracks cause large autumn floods, while May floods are often dominated by snowmelt. The northern fringe of the Alps experiences high rainfall due to orographic enhancement of northwesterly

airflows, with summer floods primarily resulting from prolonged frontal precipitation and minimal snowmelt contribution. In the eastern lowlands, annual precipitation is lower, and floods are generally triggered by frontal and convective events in summer, as well as by rain-on-snow processes in winter. The hilly southeast is particularly prone to short-duration, high-intensity convective storms, which often result in flash flooding in small catchments (Gaál et al., 2012).

Geology further modulates flood response. Catchments underlain by flysch formations tend to produce rapid, flashy runoff due to shallow flow paths and limited infiltration capacity. Conversely, catchments composed of phyllite or permeable sediments such as gravel and sand support deeper infiltration and groundwater recharge, resulting in attenuated peaks and delayed hydrographs (Gaál et al., 2012).

To enable a more structured assessment of hydrological response variability, attention was focused on a subset of representative catchment groups, referred to as *hotspots* (Gaál et al., 2012). These are regions in which flood drivers are relatively uniform within the group but differ significantly from other regions. They represent end members along the spectrum of flood process regimes in Austria. Thirteen such hot spots were identified based on hydrological similarity in terms of geology, climate, and runoff behavior. A subset of 10 out of these 13 *hotspots* was considered due to data availability. Each of them contains between two and five catchments, amounting to a total of 38 catchments across all groups. This subdivision enables targeted analysis of dominant processes within distinct hydrological regimes. Details of the *hotspots* selection procedure are provided in Gaál et al. (2012)

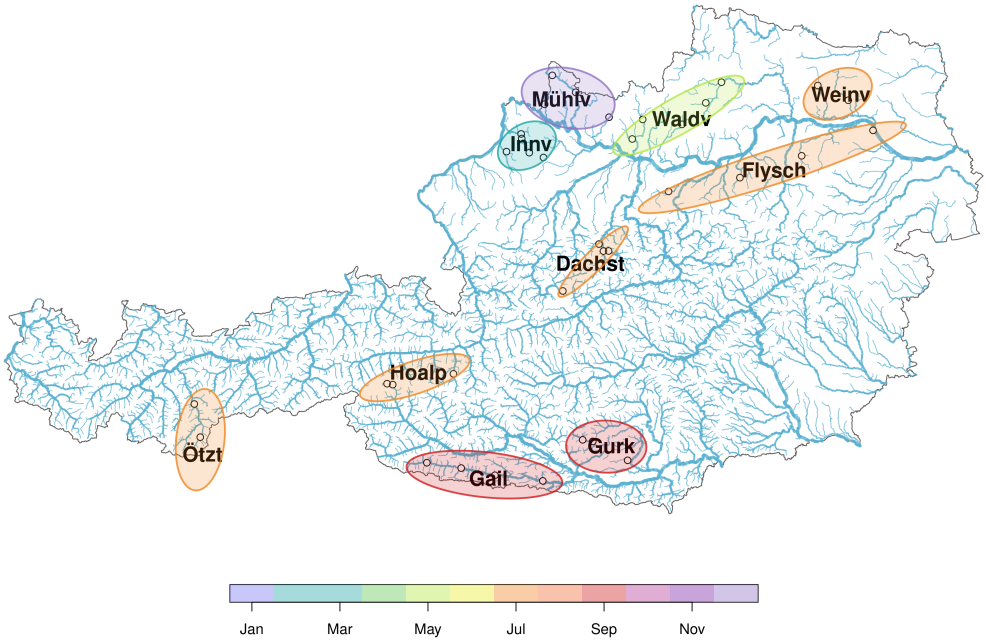


Fig. 4.1 Case study and 10 out of 13 hotspots identified by Gaál et al. (2012) with flood seasonality. The hotspots were identified based on hydrological similarity in terms of geology, climate, and runoff generation processes.

## 4.3 Bayesian event-based framework for derived flood frequency analysis

The framework is organized into three modules. First, flood events are extracted and characterized from the synthetic hydrometeorological series of the *WETRAX* weather generator, deriving event-scale variables such as storm intensity and duration, liquid precipitation ratio, runoff coefficient, and antecedent catchment conditions. Second, these characteristics are used within a Bayesian stochastic framework to calibrate probabilistic distributions for each process variable; a Monte Carlo simulation then propagates their joint uncertainty through a linear reservoir rainfall–runoff model, yielding empirical flood frequency curves for the present period. Third, parameter changes derived from an ensemble of EURO-CORDEX regional climate

projections are introduced to generate future flood frequency curves, and an ANOVA decomposition attributes total uncertainty to model calibration, parameter response, and climate forcing spread.

### 4.3.1 Event separation

A robust population of flood events is obtained from the *WETRAX model*, a multi-site stochastic weather generator that generates synthetic meteorological series, producing spatially and temporally consistent hourly precipitation and air temperature series for a high-density monitoring network in Austria, Germany, and the Czech Republic. These meteorological inputs are then transformed by a distributed rainfall-runoff model into synthetic streamflow series for selected profiles in the Austrian Danube and Drava catchments. The rainfall-runoff model is specifically calibrated to capture extreme flood events, enabling robust flood frequency analyses and the estimation of discharges with very large return periods.

The R package `HydroEvents` (Wasko and Guo, 2025) is employed to identify and characterize hydrologically consistent flood events through a sequence of signal-processing procedures. The method starts with the separation of the discharge time series into slow (baseflow) and fast response components, under the assumption that flood events are primarily associated with the latter. Baseflow is removed using the `baseflowA` recursive digital filter, which applies a filter controlled by a recession parameter ($\alpha = 0.999$). The filter is applied iteratively to stabilize the separation and to reduce edge effects, yielding the fast response component of the catchment. Flood events are identified on the fast response component using the `eventMaxima` function, which detects local discharge peaks and evaluates their hydrological relevance based on both magnitude and temporal separation. A Peak-Over-Threshold criterion is adopted, with a seasonal threshold set to the 90th percentile of the fast-flow series, ensuring that only significant runoff responses are retained, and that a sufficient number of events is identified in each season. In addition, a minimum inter-event time of 72 hours is imposed to enforce statistical independence between successive events and to avoid splitting single hydrological responses into multiple artificial events. For each detected peak, the start and end of the runoff event are delineated using custom procedures based on changes in the discharge trend and relative threshold criteria, allowing the extraction of the complete event hydrograph associated with each flood peak. Rainfall events are identified independently using a Peak-Over-Threshold

approach implemented through the `eventMaxima` function. The threshold is defined as the 90th percentile of non-zero precipitation values. Finally, rainfall and runoff events are paired using the `pairEvents` function, which matches events occurring within a physically plausible time window. Event pairing is performed by searching for rainfall events that temporally precede the runoff response, subject to a maximum admissible lag. This lag is defined based on cross-correlation analysis between precipitation and discharge (see Wasko and Guo (2022) for additional details on the R functions).

The selection of thresholds and parameters involved in event separation and matching was guided by extensive sensitivity testing. Several alternative configurations were explored, varying percentile thresholds, minimum event separation times, and baseflow filter parameters. The final setup was chosen as a compromise that ensured the identification of hydrologically plausible flood events, a consistent temporal correspondence between rainfall and runoff responses, and a sufficient number of events for robust calibration.

For each matched event, a set of key hydrological and meteorological metrics is computed, including event duration, total rainfall, the liquid fraction of precipitation, mean rainfall intensity, runoff volume, fast-response peak flow, peak baseflow, mean event temperature, mean temperature over the 100 days preceding the event, and cumulative precipitation over the 100 days preceding the event. The runoff coefficient was also computed as an explicit parameter within a simple rainfall-runoff model based on a linear reservoir with a storage parameter, following the approach of Merz and Blöschl (2009b). The model parameters were calibrated by minimizing the root mean square difference between the observed and simulated direct runoff hydrographs. This procedure ensures that the estimation is less sensitive to the precise identification of event start and end points (Figure 4.2).

Once the event characteristics are obtained, the *WETRAX* model is simplified to a linear reservoir rainfall-runoff model, which allows the distinct flood drivers to be isolated and their individual contributions to flood peak magnitude to be quantified. The model represents the catchment response as a standard linear reservoir with response time $t_c$, through which the rainfall time series is convoluted. For a single storm, the transformation of rainfall to runoff can be expressed by the convolution integral of the exponential unit hydrograph (UH). Assuming rainfall intensity to be constant over the event duration, the peak flood response is:

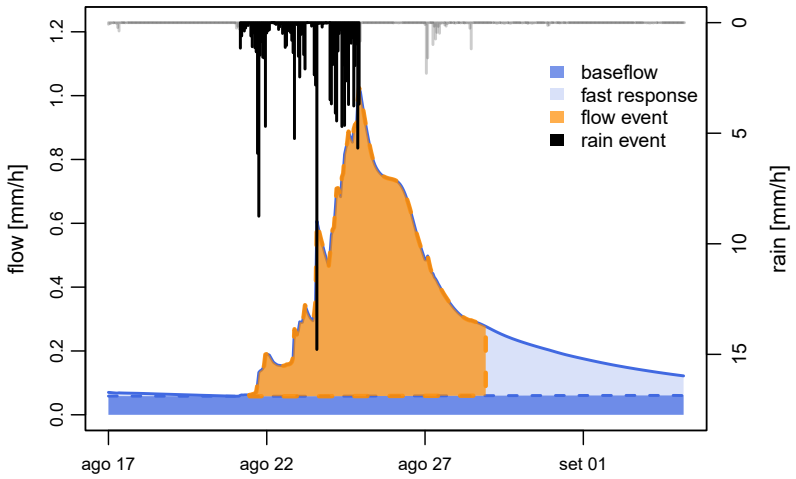


Fig. 4.2 Example of an event identified by the algorithm in an alpine catchment of hotspot 4 (Hochalp)

$$q_p = \Pi_Q(i, t_r, r_c, l_r) = r_c \cdot l_r \cdot i_m \cdot \left[1 - exp\left(-\frac{t_r}{t_c}\right)\right] + q_b \tag{4.1}$$

where $r_c$ is the event runoff coefficient, $l_r$ the percentage of liquid precipitation, $i_m$ the mean intensity of rainfall, and $t_r$ the event duration.

Figure 4.3 shows a comparison of flood peaks obtained from the *WETRAX model* and those derived from the simplified linear reservoir model. The latter are obtained by feeding the event characteristics extracted directly into equation (4.1), thereby reconstructing the flood peak for each identified event. Despite a tendency to overestimate flood peaks in the Weinviertel (Weinv) and Hochalpen (Hoalp) hotspots, the two models show consistently high correlations across all hotspots, suggesting that the linear reservoir captures the relevant flood-generating dynamics. This is essential as the model is not used to reproduce flood magnitudes, but to isolate the response of flood quantiles to changes in individual climatic drivers.

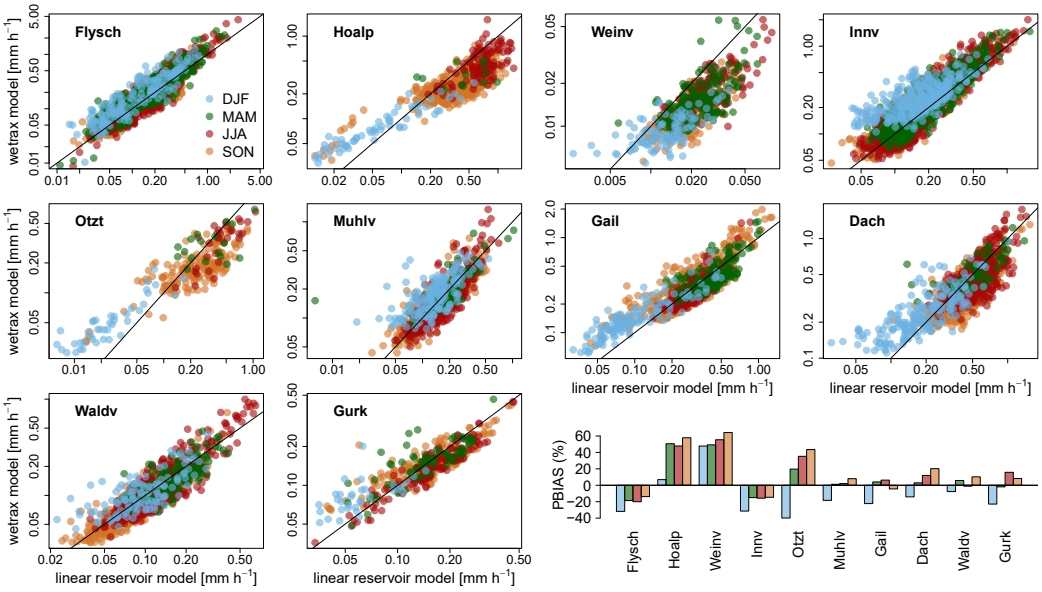


Fig. 4.3 Comparison between flood peaks obtained from the *WETRAX model* and those obtained from the linear reservoir rainfall-runoff model.

### 4.3.2 Stochastic model for flood peaks

The methodology builds upon a stochastic representation of event-scale processes, where uncertainty is propagated from climatic inputs (temperature, precipitation) to flood response through probabilistic models.

The derived flood frequency approach is used to estimate "seasonal" flood frequency curves (Sivapalan et al., 2005). Essentially, the model consists of discrete rainfall events whose durations, average rainfall intensity, and liquid ratio are all random, governed by specified distributions. A large ensemble of synthetic storm events, reflecting the probabilistic behavior of hydro-meteorological processes, is simulated using a Monte Carlo approach. The non-exceedence probability of annual flood is estimated by generating a large number of synthetic events, where event runoff coefficient, liquid ratio, storm duration, storm intensity and baseflow are all random and governed by specified distributions, calibrated on the flood event characteristics identified.

#### Storm duration

The event duration $t_r$ is sampled from a 2-parameter Weibull distribution with parameters $\gamma_r$ (scale) and $\beta_r$ (shape).

$$f_{T_r}(t_r) = \frac{\beta_r}{\gamma_r}\left(\frac{t_r}{\gamma_r}\right)^{\beta_r - 1} exp\left(-\frac{t_r}{\gamma_r}\right)^{\beta_r} \tag{4.2}$$

**Storm intensity**

The mean rainfall intensity $i_m$ is sampled as a Gamma distribution, whose shape and rate parameters depend on the event duration $t_r$. The conditional probability density function is defined as:

$$f_{I_m|t_r,}(i_m|t_r) = \frac{\lambda(t_r)}{\Gamma(k(t_r))}\left[\lambda(t_r)\cdot i_m\right]^{k(t_r)-1}\exp\left[-\lambda(t_r)\cdot i_m\right] \tag{4.3}$$

The shape $k$ and rate $\lambda$ of the Gamma distribution are derived as:

$$\begin{aligned} k(t_r) &= \frac{t_r^{-b_2}}{a_2} \\ \lambda(t_r) &= \frac{t_r^{-b_1-b_2}}{a_1 \cdot a_2} \end{aligned} \tag{4.4}$$

The conditional moments are:

$$\begin{aligned} \mathbb{E}[i_m \mid t_r] &= a_1 \cdot t_r^{b_1} \\ CV^2[i_m \mid t_r] &= a_2 \cdot t_r^{b_2} \end{aligned} \tag{4.5}$$

Here, $CV^2$ denotes the squared coefficient of variation, which quantifies the relative dispersion with respect to the mean.

**Liquid ratio**

The liquid precipitation ratio $l_r$ accounts for the proportion of total precipitation that occurs in liquid form during a flood-triggering event, excluding the part that falls as snow and thus does not contribute to immediate runoff generation. This factor is sampled using a zero-one inflated Beta distribution, conditional on the event temperature. Specifically, the probability of having fully liquid precipitation ($l_r = 1$) is described by a logistic function of the temperature $T$:

$$\Pr(l_r = 1 \mid T) = p_1 = \frac{1}{1 + e^{-(\gamma_l \cdot T + \delta_l)}} \tag{4.6}$$

For events where $0 < l_r < 1$, the variable is assumed to follow a Beta distribution with parameters depending on temperature:

$$l_r \sim \text{Beta}(\alpha_{lr}, \beta_{lr}) \tag{4.7}$$

The mean of the Beta distribution $\mu_{lr}$ is modeled as a logistic function of temperature:

$$\mu_{lr} = \frac{1}{1 + e^{-(\mu_a \cdot T + \mu_b)}} \tag{4.8}$$

The precision parameter $\phi_{lr}$, which controls the concentration of the distribution around its mean, is modeled exponentially as:

$$\phi_{lr} = \exp(\phi_a \cdot T + \phi_b) \tag{4.9}$$

The shape parameters of the Beta distribution are then given by:

$$\alpha_{lr} = \mu_{lr} \cdot \phi_{lr}, \qquad \beta_{lr} = (1 - \mu_{lr}) \cdot \phi_{lr} \tag{4.10}$$

This formulation allows the model to account for the spatial variability of precipitation phase across the basin: at higher elevations, solid precipitation is more likely, while at lower elevations, precipitation is predominantly liquid. At lower temperatures, the parameter $p_1$ is small and solid precipitation is likely in a larger portion of the catchment, while at higher temperatures, the likelihood of fully liquid precipitation increases. For partially solid events (i.e., events with both liquid and solid precipitation within the basin), the flexible Beta distribution accommodates the continuous variability in the liquid fraction. The event temperature $T$ is modeled as normally distributed random variables (mean $\mu_T$ and standard deviation $\sigma_T$). The event temperature $T$ plays a central role in the stochastic model, as it controls the precipitation phase through its influence on the liquid ratio.

### Runoff coefficient

The event runoff coefficient $r_c$ is treated as a random variable and modeled using the Beta distribution (Gottschalk and Weingartner, 1998). Runoff coefficient depends on volume of rainfall event and initial conditions of the catchment, the more it

rains the more the soil is saturated and a soil which was already saturated before the event is more likely to produce larger runoff. For this reason the mean of the runoff coefficient distribution $\mu_c$ is modeled considering a dependence on the volume of precipitation, and the wetness index $W_{100d}$, calculated as the ratio between the cumulated precipitation over the previous 100 days $P_{100}$ and the potential evapotranspiration over the 100 days before the beginning of the flood event. The latter is computed using a modified version of the Blaney–Criddle equation. The logistic formulation ensures $\mu_c \in (0,1)$:

$$\mu_c = \frac{1}{1+\exp(-\eta \cdot (t_r \cdot i_m) - \zeta \cdot W_{100d} + \lambda)} \tag{4.11}$$

where the parameters $\eta$, $\zeta$, and $\lambda$ capture the sensitivity of the runoff coefficient to event precipitation, initial catchment conditions, and a baseline offset, respectively. The runoff coefficient is modeled to explicitly account for both the precipitation volume of the ongoing event and the antecedent hydrological state of the catchment represented by $W_{100d}$. This choice is motivated by evidence showing that runoff coefficients correlate more strongly with indicators of deep soil water storage than with short-term antecedent precipitation indices (Massari et al., 2023). The antecedent temperature $T_{100}$ is modeled as normally distributed random variables (mean $\mu_{T_{100}}$ and standard deviation $\sigma_{T_{100}}$). The cumulative precipitation over the 100 days preceding the event, $P_{100}$, is modeled as a lognormal random variable, with mean $\mu_{P100}$ and standard deviation $\sigma_{P100}$, reflecting the strictly positive and right-skewed nature of accumulated rainfall amounts. High values of $P_{100}$ are associated with wetter and less permeable catchment conditions, which tend to increase the runoff coefficient and amplify the flood response to a given storm.

**Baseflow**

The event-peak baseflow is sampled as a lognormal distribution with mean $\mu_{bs}$ and standard deviation $\sigma_{bs}$. The dependency of $\mu_{bs}$ on precipitation and temperature of the 100 days before the event is given by:

$$\mu_{bs} = \beta_0 + \beta_1 \cdot T_{100d} + \beta_2 \cdot P_{100d} \tag{4.12}$$

**Poisson occurrence of annual events:** For each simulated season, the number of flood-triggering events $N_i$ is drawn from a Poisson distribution with mean $m$, representing the expected number of floods occurring in the season:

$$N_i \sim \text{Poisson}(m)$$

The seasonal maximum peak discharge $q_{\max,i}$ is then recorded as:

$$q_{\max,i} = \max\{q_1, q_2, \ldots, q_{N_i}\}$$

This procedure yields a synthetic time series of $10^6$ seasonal maxima, suitable for frequency analysis, allowing to obtain empirical flood frequency curves.

Although the model involves a relatively large number of parameters, this complexity is offset by a major advantage over traditional calibration approaches. Indeed, the model is calibrated on flood event characteristics rather than directly on the discharge time series. This allows the calibration to target the underlying flood-generation mechanisms, improving the ability of the model to reproduce the processes controlling flood formation.

In this framework, the likelihood function for the Bayesian fitting was specified by linking the observed hydrometeorological variables to the probability distributions described in subsection 4.3.2. Prior distributions were chosen to be weakly informative but consistent with the underlying physical processes, thereby regularizing parameter estimation and avoiding unrealistic values. For instance, Weibull and Gamma parameters were assigned positive priors (e.g., Gamma and truncated Normal distributions), regression coefficients were given Normal priors centered at zero, and precision parameters such as those of the Beta distributions were constrained to positive domains with priors reflecting plausible variability ranges. Regarding the coefficients relating the runoff coefficient to the volume of precipitation event and the wetness ($\eta$, $\zeta$), truncated Normal (mean 0, standard deviation 1) priors were chosen to ensure positivity and prevent implausible negative relationships. In this way, the runoff coefficient increases with larger precipitation amounts and wetter initial conditions. The posterior distribution of all parameters was then obtained by combining these prior specifications with the likelihood contributions from the observed data through Bayes' theorem. Sampling from the posterior was performed using Markov

Chain Monte Carlo methods (Stan Development Team, 2025), enabling the joint estimation of all parameters and quantification of their uncertainty.

Analogously, the parameters of the baseflow model were estimated within a Bayesian framework, which allows explicit integration of uncertainty in both climatic drivers and hydrological response. Observed temperature was modeled as Normally distributed around a mean climatic state, while precipitation was modeled using a Lognormal distribution to capture its positive skewness and variability. These likelihood functions ensured that the observed climatic variables were realistically represented within the model structure. Baseflow observations were then linked to temperature and precipitation through the regression model in equation (4.12), where the expected baseflow $\mu_{bs}$ was expressed as a linear function of observed climate drivers. The stochastic component of baseflow was described using a Lognormal likelihood with mean $\mu_{bs}$ and standard deviation $\sigma_{bs}$, reflecting the strictly positive support and multiplicative variability typical of baseflow processes. Prior distributions were chosen to encode weakly informative beliefs consistent with the physical context. Figure 4.4 shows the density probabilities of the prior distributions described and the posterior distributions obtained after the calibration.

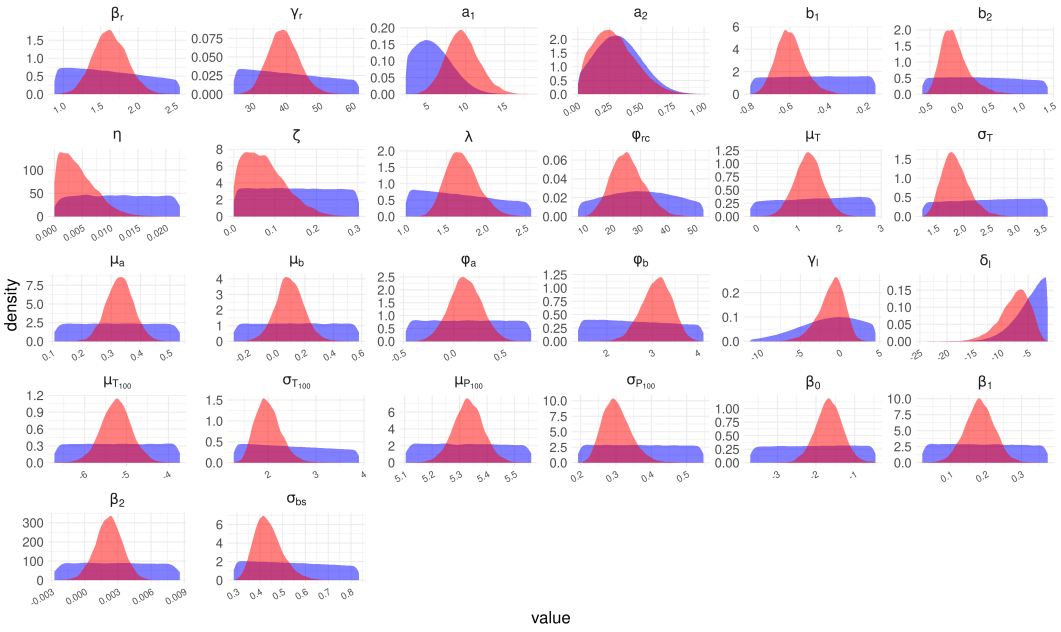


Fig. 4.4 Prior (blue) and posterior (red) distributions of the model parameters for the hotspot Hoalp during the spring season.

Table 4.1 summarizes the choices of likelihoods and priors for each process.

It is worth noting that the event characteristics used for calibration are pooled across all catchments within each hotspot. The primary motivation for this choice is to obtain a substantially larger sample of flood events, which improves the robustness of the Bayesian calibration and reduces parameter uncertainty. The resulting posterior distributions therefore reflect not only the temporal variability of hydrometeorological processes within individual catchments, but also the spatial variability among catchments belonging to the same group. This is consistent with the regionalization rationale underlying the hotspot definition, which assumes sufficient hydrological similarity within each group to justify the pooling of information.

Figure 4.5 shows the fitted probability densities of the hydrometeorological variables entering equation (4.1), obtained by propagating the posterior parameter distributions through the calibrated stochastic model. Each density curve corresponds to a single draw from the posterior, reflecting the parametric uncertainty in the calibration. The fitted densities are compared against the observed event characteristics extracted from the *WETRAX* model, providing a visual diagnostic of the goodness of fit.

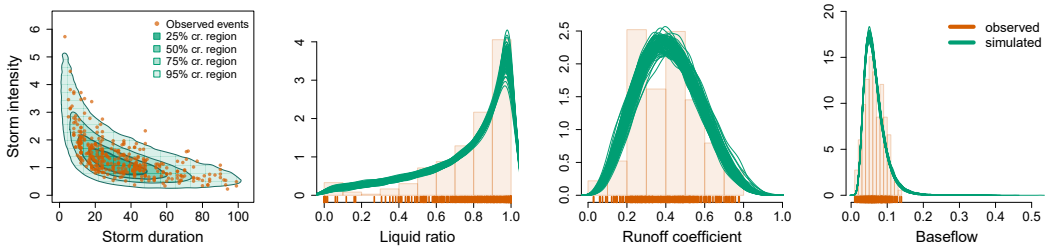


Fig. 4.5 Posterior probability densities of the hydrometeorological variables entering the stochastic flood peak model (equation (4.1)), compared against the empirical distributions of flood event characteristics extracted from the *WETRAX* model. Each curve represents a density estimate obtained from a single draw of the posterior parameter distribution. Results refer to the autumn season at the Hochalp hotspot.

### 4.3.3 Propagation of climate change signals

To assess the impacts of climate change, an ensemble of six CORDEX EUR-11 simulations, based on CMIP5 (Jacob et al., 2014; Taylor et al., 2012), is used, with a spatial resolution of 12.5 km, hourly temporal resolution, and scenario RCP 8.5. Two time windows are considered: a control period (1971–2000) and a future pe-

Table 4.1 Summary of likelihoods and priors for each process in the Bayesian model. Likelihoods are chosen to reflect the physical domain and stochastic behavior of each process variable. Distribution choices were based on Gottschalk and Weingartner (1998); Sivapalan et al. (2005); Viglione et al. (2013); Westra et al. (2014)

| **Process** | **Likelihood** | **Parameters** | **Priors** |
|---|---|---|---|
| Event duration | $t_r \sim \text{Weibull}(\beta_r, \gamma_r)$ | $\beta_r$, $\gamma_r$ | $\beta_r \sim \text{Gamma}(2,1)$; $\log \gamma_r \sim \text{Normal}(4,1)_{>0}$ |
| Event mean intensity | $i_m \sim \text{Gamma}(\kappa = \frac{t_r^{-b_2}}{a_2}, \lambda = \frac{t_r^{-b_1-b_2}}{a_1 \cdot a_2})$ | $a_1, a_2, b_1, b_2$ | $a_1 \sim \text{Normal}(5,3)_{>0}$; $a_2 \sim \text{Normal}(0.3, 0.2)$; $b_1 \sim \text{Normal}(0,2)_{<0}$; $b_2 \sim \text{Normal}(0,2)$ |
| Runoff coefficient | $r_c \sim \text{Beta}(\mu_c = \frac{1}{1+\exp(-\eta \cdot (t_r \cdot i_m) - \zeta \cdot W_{100d} + \lambda)}, \phi_c)$ | $\eta, \zeta, \lambda, \phi_c$ | $\eta, \zeta \sim \text{Normal}(0,1)_{>0}$; $\lambda \sim \text{Normal}(0,2)$; $\phi_c \sim \text{Normal}(30,20)_{>0}$ |
| Liquid ratio | $l_r \sim p_1 \cdot \delta(1) + (1-p_1) \cdot \text{Beta}(\alpha_{lr}, \beta_{lr})$,<br>$p_1 = \text{logistic}(\gamma_l \cdot T + \delta_l)$,<br>$\mu_{lr} = \text{logistic}(\mu_a \cdot T + \mu_b)$,<br>$\phi_{lr} = \exp(\phi_a \cdot T + \phi_b)$ | $\mu_a, \mu_b, \phi_a, \phi_b, \gamma_l, \delta_l$ | All $\sim \text{Normal}(0,5)$ |
| Event temperature | $T \sim \text{Normal}(\mu_T, \sigma_T)$ | $\mu_T, \sigma_T$ | $\mu_T \sim \text{Normal}(0,20)$; $\sigma_T \sim \text{Cauchy}(0,5)_{>0}$ |
| Precipitation 100 days | $P_{100} \sim \text{Lognormal}(\mu_{P_{100}}, \sigma_{P_{100}})$ | $\mu_{P_{100}}, \sigma_{P_{100}}$ | $\mu_{P_{100}} \sim \text{Normal}(0,5)$; $\sigma_{P_{100}} \sim \text{Cauchy}(0,2)_{>0}$ |
| Temperature 100 days | $T_{100} \sim \text{Normal}(\mu_{T_{100}}, \sigma_{T_{100}})$ | $\mu_{T_{100}}, \sigma_{T_{100}}$ | $\mu_{T_{100}} \sim \text{Normal}(0,20)$; $\sigma_{T_{100}} \sim \text{Cauchy}(0,5)_{>0}$ |
| Baseflow | $B \sim \text{Lognormal}(\mu, \sigma_B)$, $\mu = \beta_0 + \beta_1 T_{\text{obs}} + \beta_2 P_{\text{obs}}$ | $\beta_0, \beta_1, \beta_2, \sigma_B$ | $\beta_0 \sim \text{Normal}(0,10)$; $\beta_1, \beta_2 \sim \text{Normal}(0,1)$; $\sigma_B \sim \text{Normal}(0,1)$ |

riod (2071–2100). Precipitation events are extracted from each simulation, and the stochastic model described in Section 4.3.2 is calibrated within a unified Bayesian framework, directly inferring probabilistic parameter changes between the reference and future periods. In this way, the model is constrained to incorporate the climate change signal projected by the climate models. Most parameter changes are expressed in relative terms, and therefore no explicit bias-correction procedure is required. For the parameters describing temperature-related distributions, changes are instead represented as absolute differences.

This framework allows the impacts of climate change to be characterized in terms of altered precipitation event properties, the expected increase in the liquid fraction of precipitation, changes in the baseflow regime, and modified initial catchment conditions, ultimately leading to different runoff coefficients. Figure 4.6 illustrates the most relevant process-level variations induced by climate change forcing. The probability density functions are obtained by evaluating the model using the mean values of the fitted parameters.

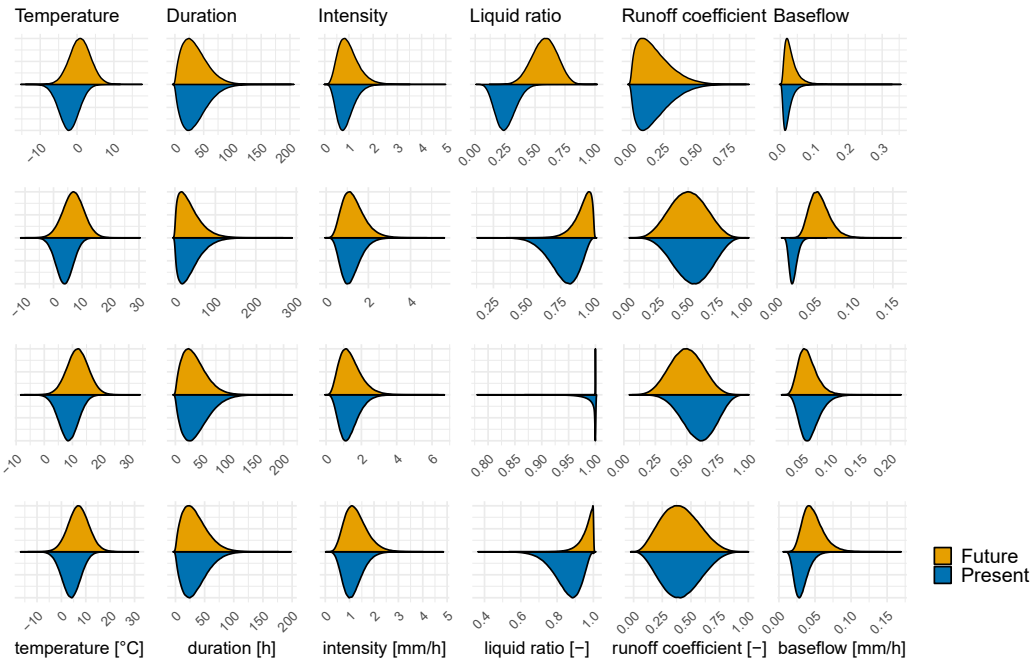


Fig. 4.6 Probability density of the main processes represented in the model and their variation under climate change. The probability density functions are obtained considering the mean values of the fitted parameters. Example shown for the Hochalpen hotspot. The different rows represent different seasons. From top to bottom, winter, spring, summer, and autumn.

### 4.3.4 Uncertainty decomposition and attribution

To quantify the contribution of different sources of uncertainty in flood frequency estimation under changing climatic conditions, an analysis of variance (ANOVA) framework was applied to the simulated flood quantiles. Three distinct sources of uncertainty were considered: (i) *calibration uncertainty* ($\sigma^2{}_{\mathrm{c}}$). This component originates from the variability of the posterior parameter distributions obtained during model calibration. It reflects the epistemic uncertainty in estimating the current values of model parameters given the available observations. Each posterior draw represents a plausible model realization under present-day conditions, and the resulting spread in simulated flood quantiles quantifies the uncertainty that would persist even in the absence of climate change. (ii) *parametric response uncertainty* ($\sigma^2{}_{\mathrm{r}}$). This component captures the uncertainty arising from the propagation of parameter changes under future climatic conditions. While the calibration uncertainty describes the lack of knowledge about current parameters, this term accounts for their expected evolution due to altered hydro-climatic regimes, as well as the variability of such changes within each climate model. (iii) *forcing uncertainty* ($\sigma^2{}_{\mathrm{f}}$). The third component arises from the spread among the different global or regional climate models used as boundary forcing. Each climate model provides distinct climatic trajectories that influence the derived parameter-change distributions. This term thus reflects the structural and scenario uncertainty inherent in external climate projections, encompassing differences in model physics, parameterizations, and climate sensitivity.

Let $q_{p,T}$ denote the simulated peak discharge for a given posterior draw $p$, and return period $T$ for the present period, and $q_{p,m,T}$ for a given posterior draw $p$, model $m$, and return period $T$ for the future period. Flood quantiles were organized into a two-dimensional matrix for the present period and a three-dimensional array for future projections, with indices corresponding to posterior draws, return periods, and climate models (only for the future projections). This configuration allows the total variance of projected flood quantiles to be expressed as the sum of three independent components, assuming that uncertainties arising from model calibration, parameter response, and climatic forcing are mutually uncorrelated:

$$\sigma^2{}_{q_T} = \sigma^2{}_{\mathrm{c}} + \sigma^2{}_{\mathrm{r}} + \sigma^2{}_{\mathrm{f}} \tag{4.13}$$

An ANOVA decomposition on the ensemble of future simulations was used to isolate and normalize each contribution, yielding variance fractions that sum to unity for each return period. Results are shown in Figure 4.19

To quantify the robustness of projected flood changes, a signal-to-noise ratio (S/N) is computed for each hotspot, season, and return period. The ratio expresses the relative magnitude of the expected mean change in flood quantiles between the future and present periods ($\Delta\mu_{q_T}$) against the standard deviation ($\sigma_{q_T}$):

$$\text{S/N} = \frac{|\Delta\mu_{q_T}|}{\sigma_{q_T}} \tag{4.14}$$

Values of S/N $> 1$ indicate that the projected flood signal exceeds uncertainty, implying robust detection of change. Conversely, S/N $< 1$ suggests that uncertainty dominates, and projected changes should be interpreted with caution. This indicator supports the assessment of spatial and seasonal variability in the detectability of flood regime changes across Austria.

## 4.4 Projected flood frequency changes and process attribution

The seasonal non-exceedance probabilities for each hotspot were estimated following the procedure described in subsection 4.3.2 (Figure 4.7). For the present flood frequency curves, the only source of uncertainty considered is the *calibration* component, while for future projections both the *response* and *forcing* components are included. For this reason, the total uncertainty in the future simulations is substantially larger, reflecting the combined contribution of parameter-response variability and the spread among climate models, in addition to the inherent calibration uncertainty.

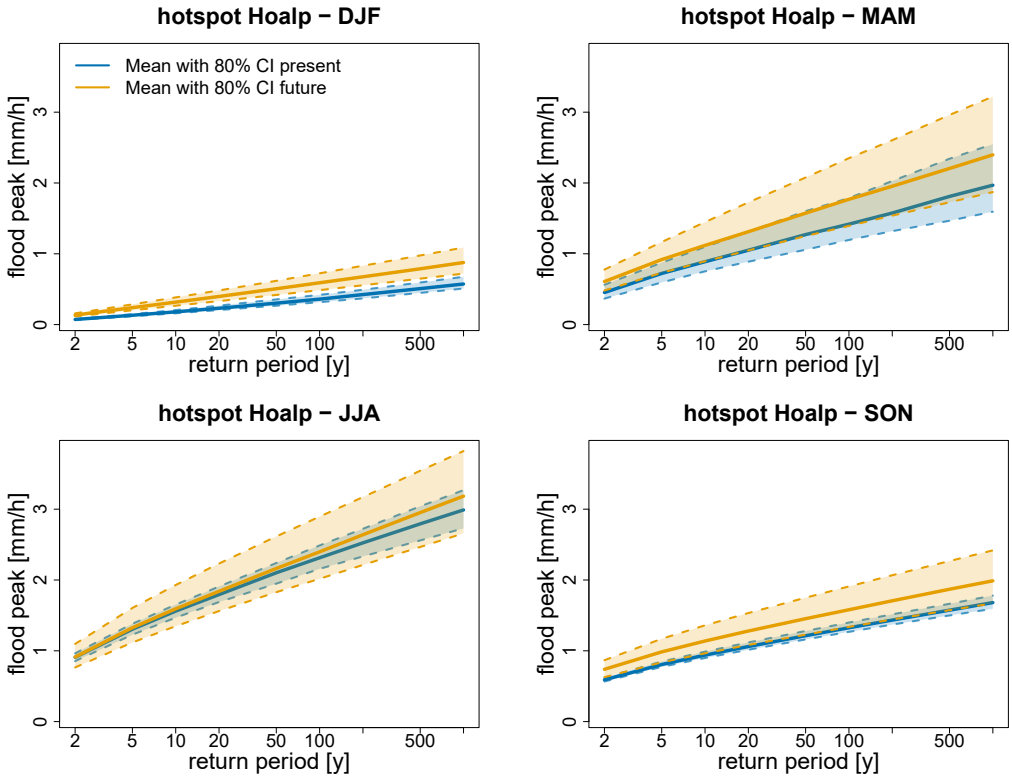


Fig. 4.7 Empirically derived flood frequency curves with 80% confidence intervals for the present and future periods.

The projected shifts in the 2-year and 100-year flood quantiles between the present and future periods are illustrated in Figure 4.8. The key strength of the proposed framework lies in its ability to disentangle the effects of individual flood drivers, thereby isolating distinct physical drivers of change. Three experimental setups were analyzed: one driven by changes in event temperature, representing the 0°C line shift and its influence on the liquid fraction of precipitation; one capturing the role of antecedent catchment conditions; and one focusing on variations in precipitation intensity and duration. The combined influence of all mechanisms is represented by the aggregated scenario (`combined`), which integrates the concurrent effects of the three flood generation mechanisms.

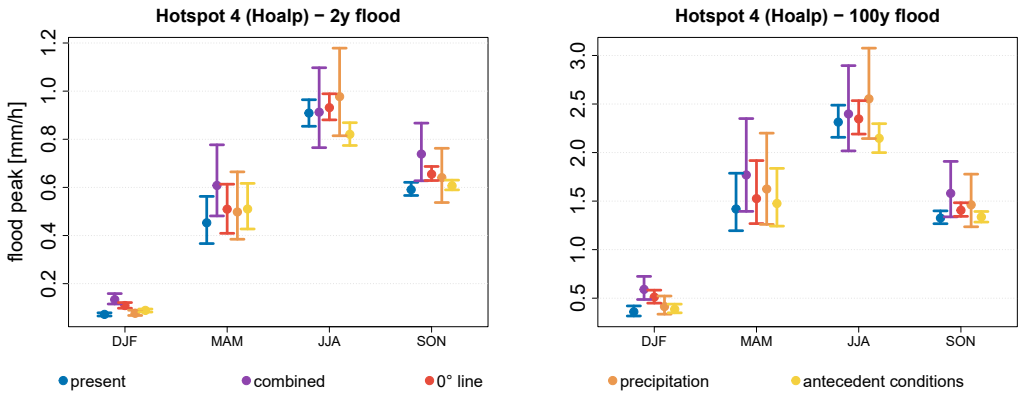


Fig. 4.8 Projected variation of the 2-year (left) and 100-year (right) flood quantile with 80% confidence intervals. Different scenarios are considered to highlight the disentangled effects of distinct flood generation mechanisms. Example for the Hochalpen hotspot.

To provide a spatial overview, Figure 4.9 summarizes the expected direction, magnitude, and confidence of the 2-year flood quantile changes across all hotspots and seasons, while Figure 4.10 summarizes the same results but for the 100-year flood quantile. Triangles indicate whether the change is positive or negative, their size represents the relative magnitude, and their color encodes the robustness of the signal, based on the signal-to-noise ratio (i.e., values $> 1$ denote high confidence in the direction of change).

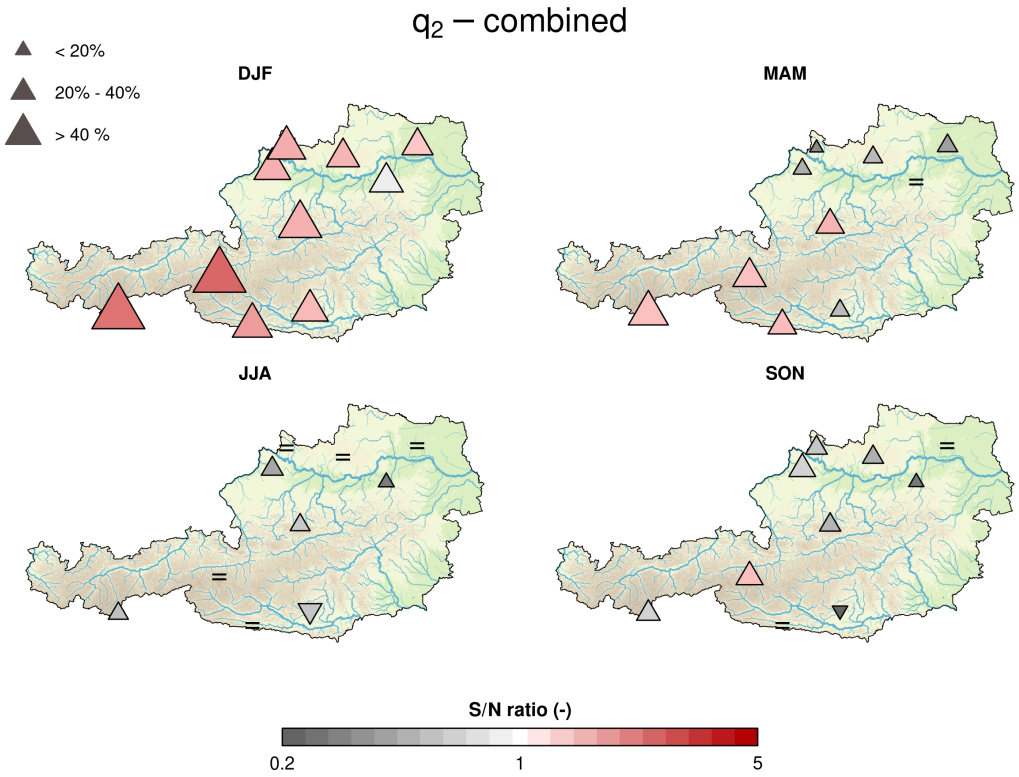


Fig. 4.9 Spatial distribution of projected 2-year flood changes across Austria, shown for each season. Triangles represent the direction (increase/decrease) and magnitude of the change, while colors indicate the robustness of the signal, defined by the signal-to-noise ratio (S/N $>$ 1 indicates high confidence). The '=' symbol denotes locations where the projected change ranges between -5% and +5%.

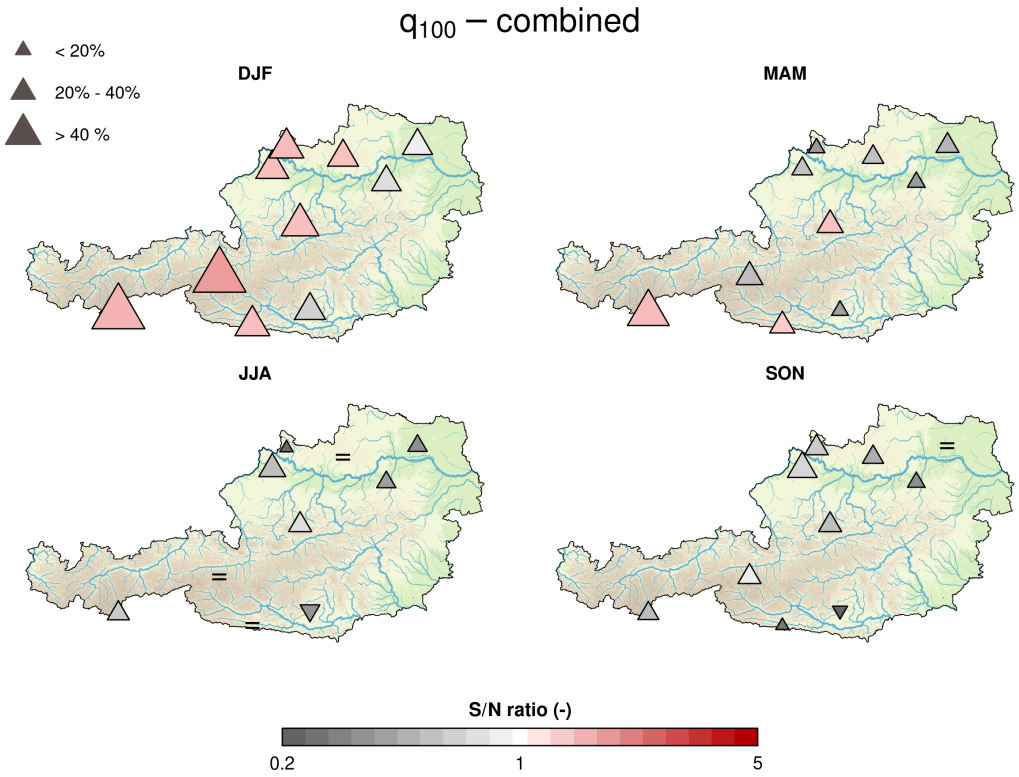


Fig. 4.10 Spatial distribution of projected 100-year flood changes across Austria, shown for each season. Triangles represent the direction (increase/decrease) and magnitude of the change, while colors indicate the robustness of the signal, defined by the signal-to-noise ratio (S/N $>$ 1 indicates high confidence). The '=' symbol denotes locations where the projected change ranges between -5% and +5%.

To further illustrate the contributions of individual flood drivers, separate maps were produced for each mechanism, showing the projected changes in both 2-year (ordinary) and 100-year (extreme) flood quantiles across Austria. Figures 4.11 and 4.12 show the effect of the temperature-driven shift of the 0°C line, which primarily influences the liquid fraction of precipitation. Figures 4.13 and 4.14 highlight the role of antecedent catchment conditions, while Figures 4.15 and 4.16 illustrate the impact of changes in precipitation intensity and duration.

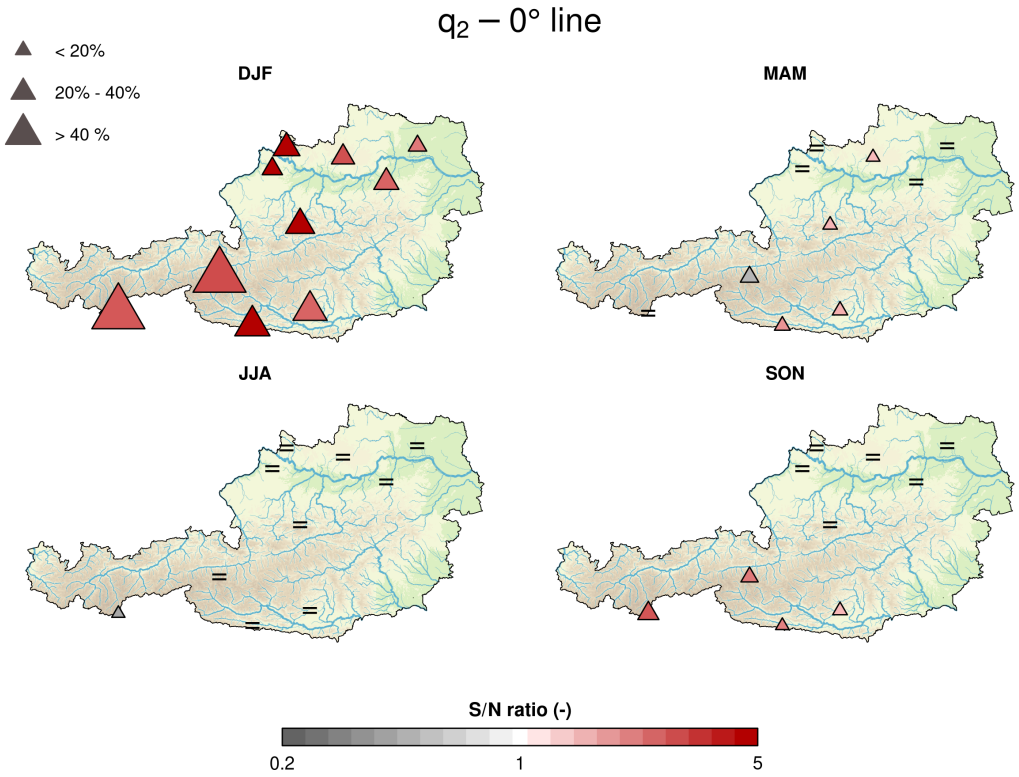


Fig. 4.11 Spatial distribution of projected 2-year changes due to the upward shift of the 0°C line across Austria, shown for each season. Triangles represent the direction (increase/decrease) and magnitude of the change, while colors indicate the robustness of the signal, defined by the signal-to-noise ratio (S/N $>$ 1 indicates high confidence). The '=' symbol denotes locations where the projected change ranges between -5% and +5%.

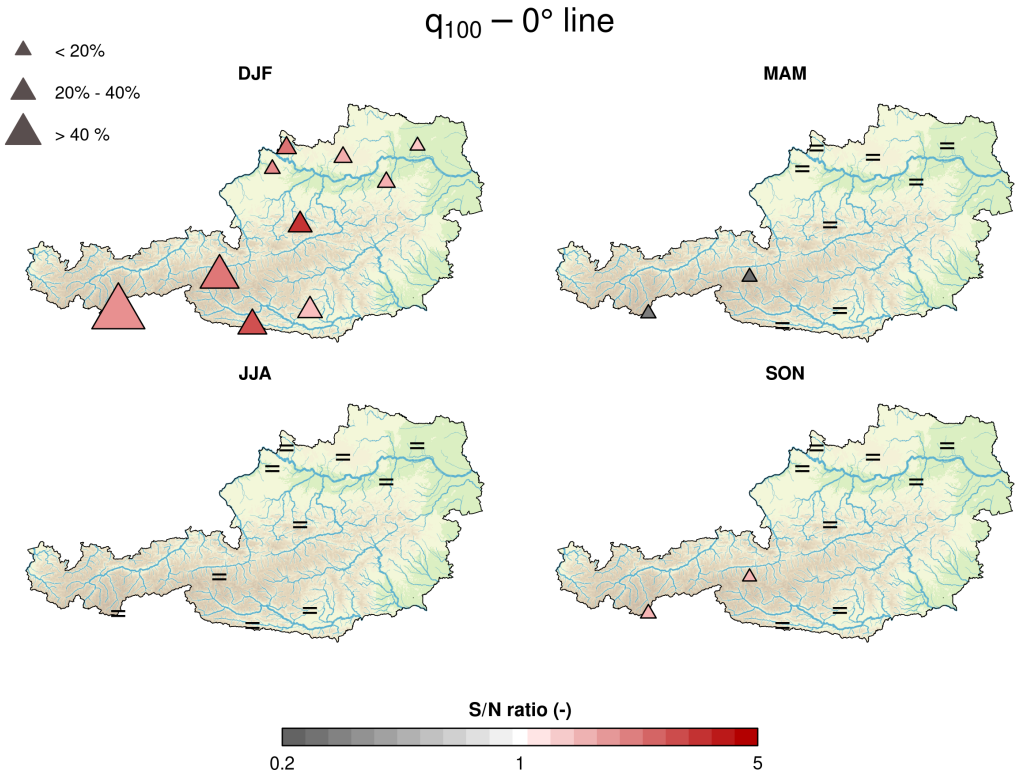


Fig. 4.12 Spatial distribution of projected 100-year flood changes due to the upward shift of the 0°C line across Austria, shown for each season. Triangles represent the direction (increase/decrease) and magnitude of the change, while colors indicate the robustness of the signal, defined by the signal-to-noise ratio (S/N $>$ 1 indicates high confidence). The '=' symbol denotes locations where the projected change ranges between -5% and +5%.

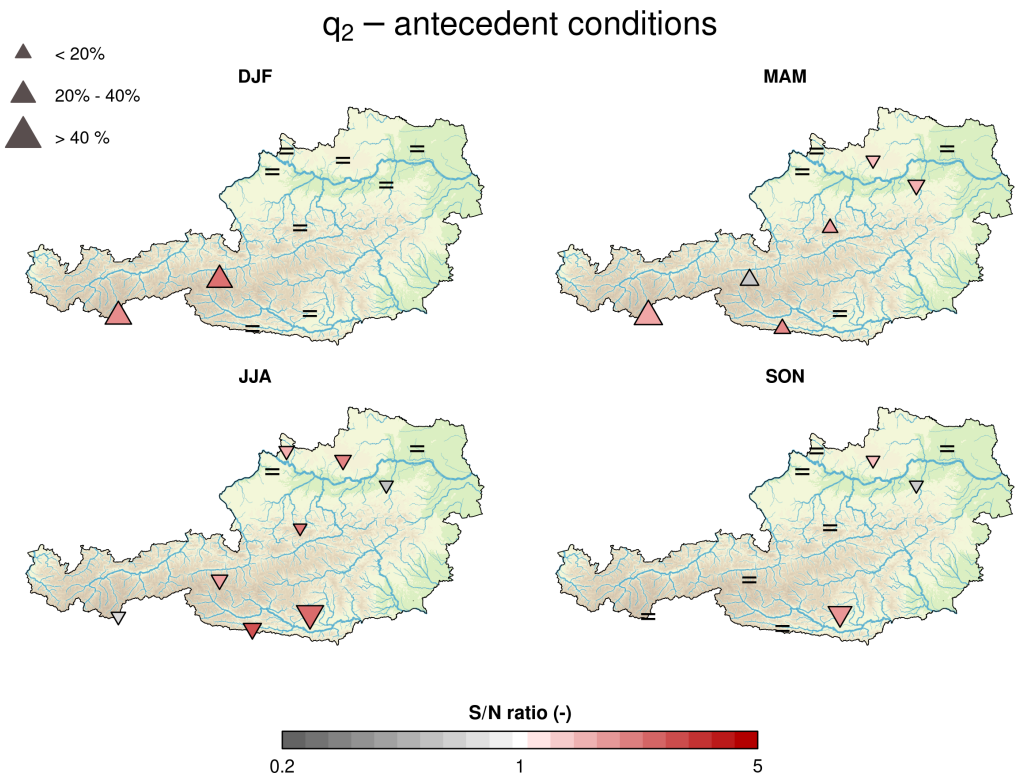


Fig. 4.13 Spatial distribution of projected 2-year flood changes due to the variation of soil moisture across Austria, shown for each season. Triangles represent the direction (increase/decrease) and magnitude of the change, while colors indicate the robustness of the signal, defined by the signal-to-noise ratio (S/N $>$ 1 indicates high confidence). The '=' symbol denotes locations where the projected change ranges between -5% and +5%.

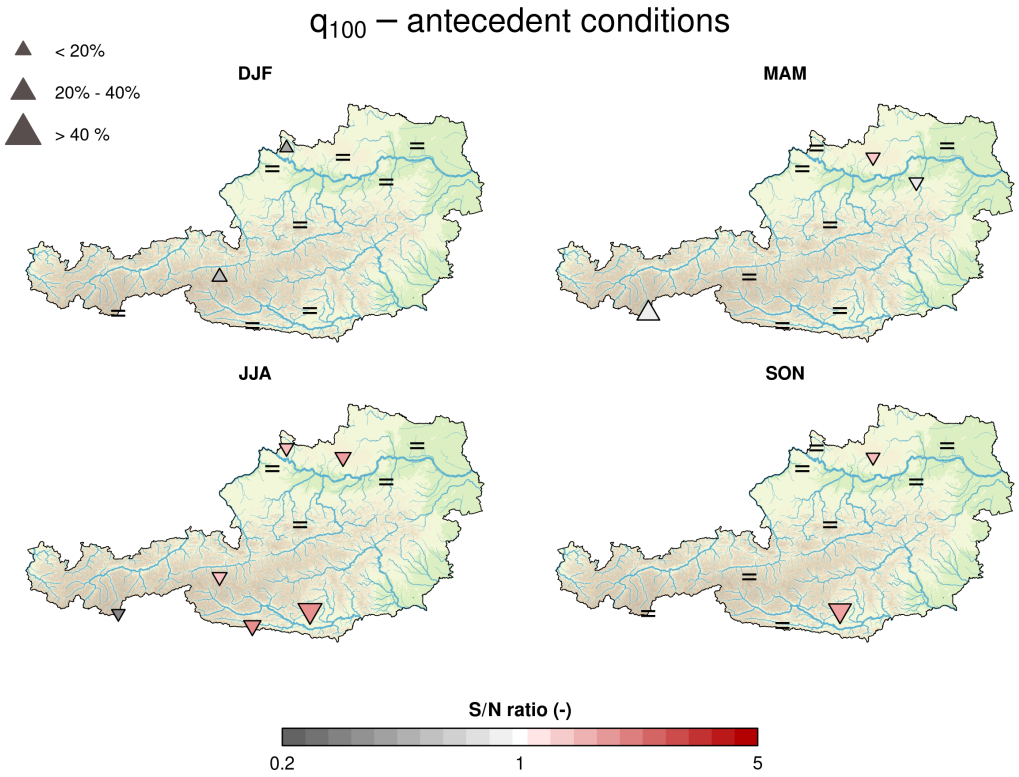


Fig. 4.14 Spatial distribution of projected 100-year flood changes due to the variation of soil moisture across Austria, shown for each season. Triangles represent the direction (increase/decrease) and magnitude of the change, while colors indicate the robustness of the signal, defined by the signal-to-noise ratio (S/N $>$ 1 indicates high confidence). The '=' symbol denotes locations where the projected change ranges between -5% and +5%.

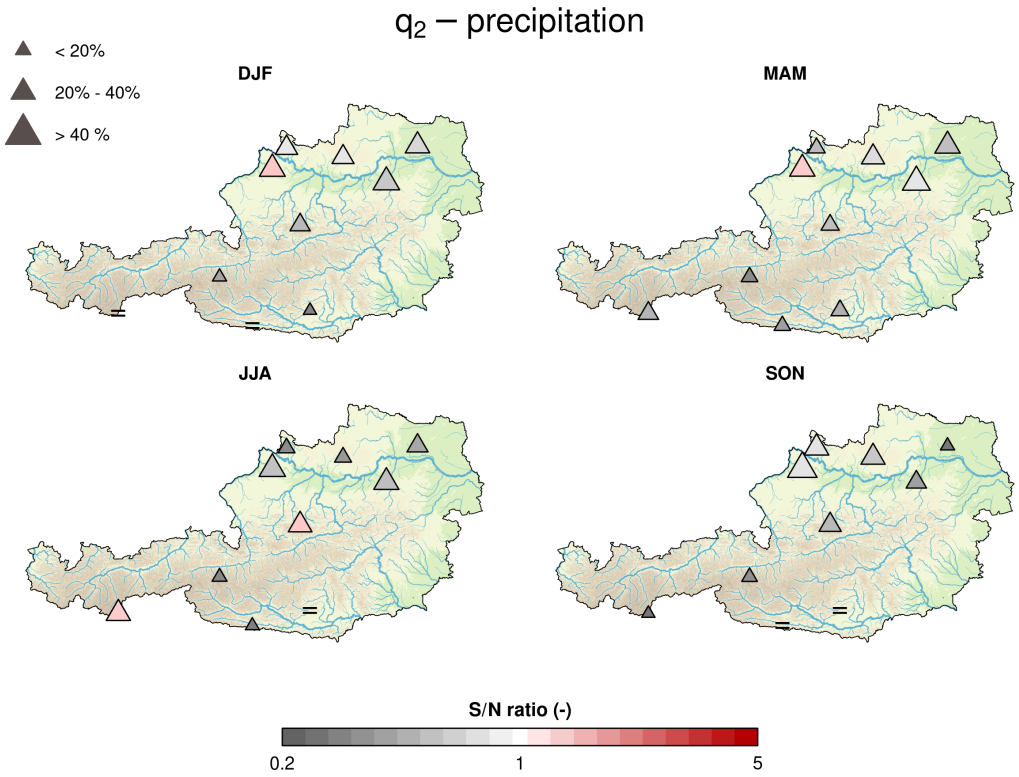


Fig. 4.15 Spatial distribution of projected 2-year flood changes due to precipitation extremes variation across Austria, shown for each season. Triangles represent the direction (increase/decrease) and magnitude of the change, while colors indicate the robustness of the signal, defined by the signal-to-noise ratio (S/N $>$ 1 indicates high confidence). The '=' symbol denotes locations where the projected change ranges between -5% and +5%.

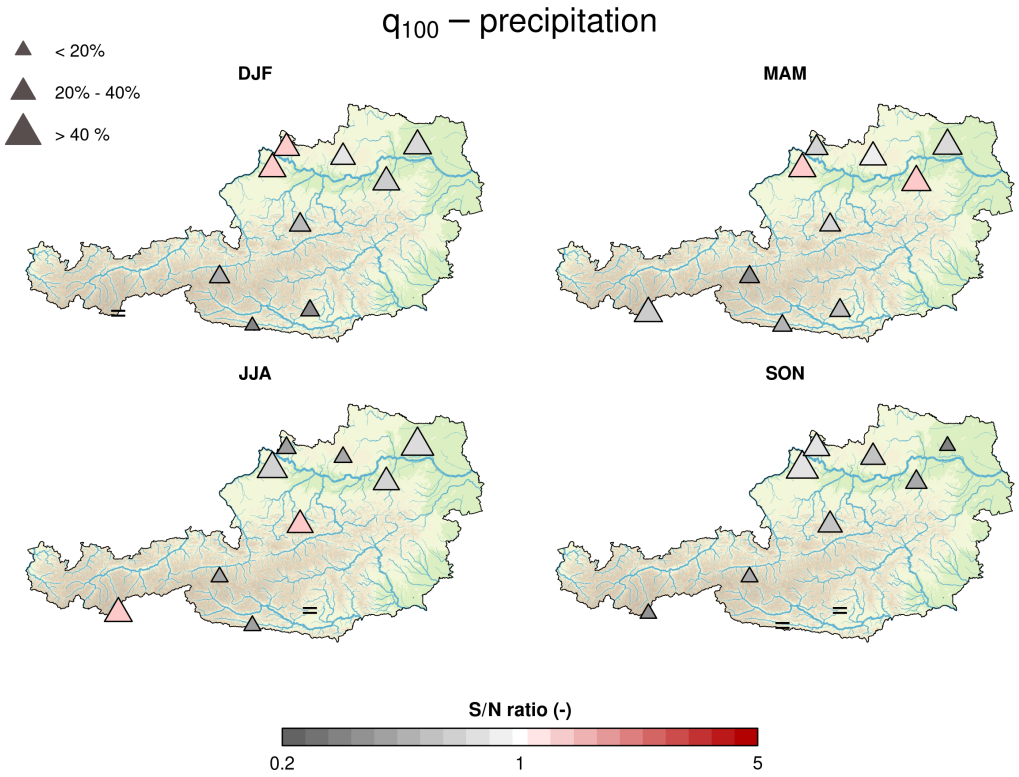


Fig. 4.16 Spatial distribution of projected 100-year flood changes due to precipitation extremes variation across Austria, shown for each season. Triangles represent the direction (increase/decrease) and magnitude of the change, while colors indicate the robustness of the signal, defined by the signal-to-noise ratio (S/N $>$ 1 indicates high confidence). The '=' symbol denotes locations where the projected change ranges between -5% and +5%.

The model is additionally implemented from an annual perspective, complementing the seasonal analysis. In this case as well, the objective is to assess the expected variations in flood quantiles and to disentangle the contributions of different flood drivers to these changes. For each year, the annual maximum flood is derived by comparing the flood events simulated for each season, while explicitly accounting for the expected number of flood events in each season.

The annual perspective is particularly relevant because, in several of the cases discussed in the previous figures, the projected increases in flood quantiles do not necessarily occur in the season associated with the largest floods under current conditions. As a result, changes in seasonal flood behaviour may alter the relative contribution of different seasons to annual flood extremes.

Figures 4.17 and 4.18 illustrate the variations in annual flood quantiles for return periods of 2 and 100 years, highlighting how the combined seasonal responses translate into changes in flood frequency when viewed at the annual scale.

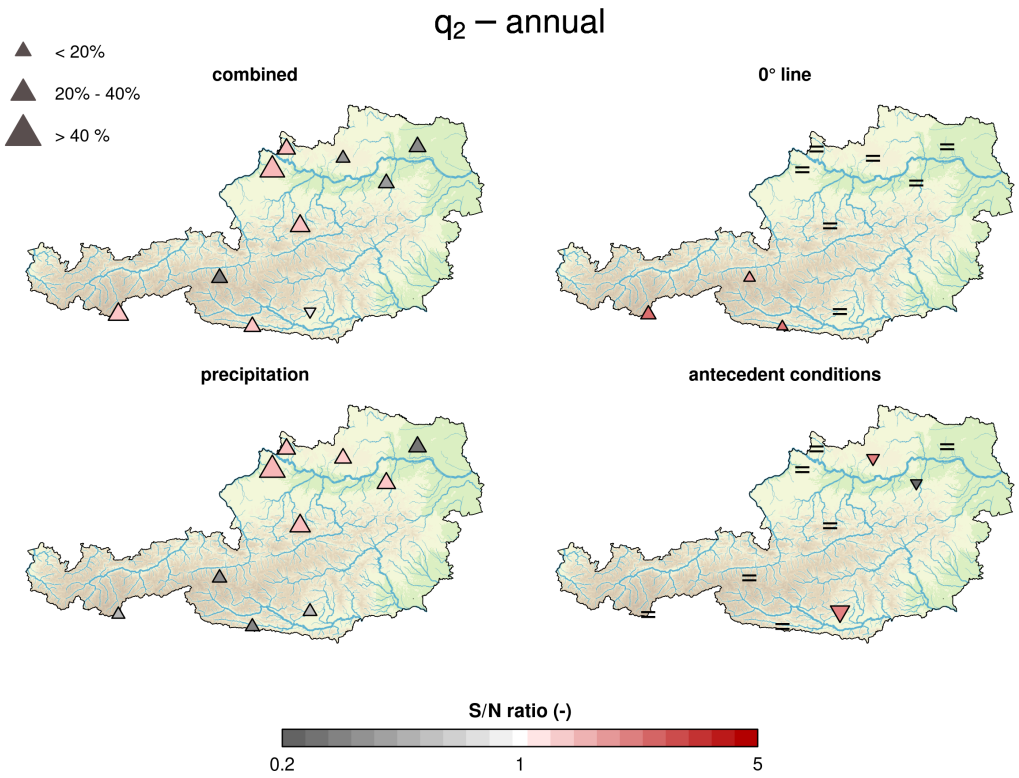


Fig. 4.17 Spatial distribution of projected annual 2-year flood changes caused by different flood generation mechanisms variation across Austria. Triangles represent the direction (increase/decrease) and magnitude of the change, while colors indicate the robustness of the signal, defined by the signal-to-noise ratio (S/N $>$ 1 indicates high confidence). The '=' symbol denotes locations where the projected change ranges between -5% and +5%.

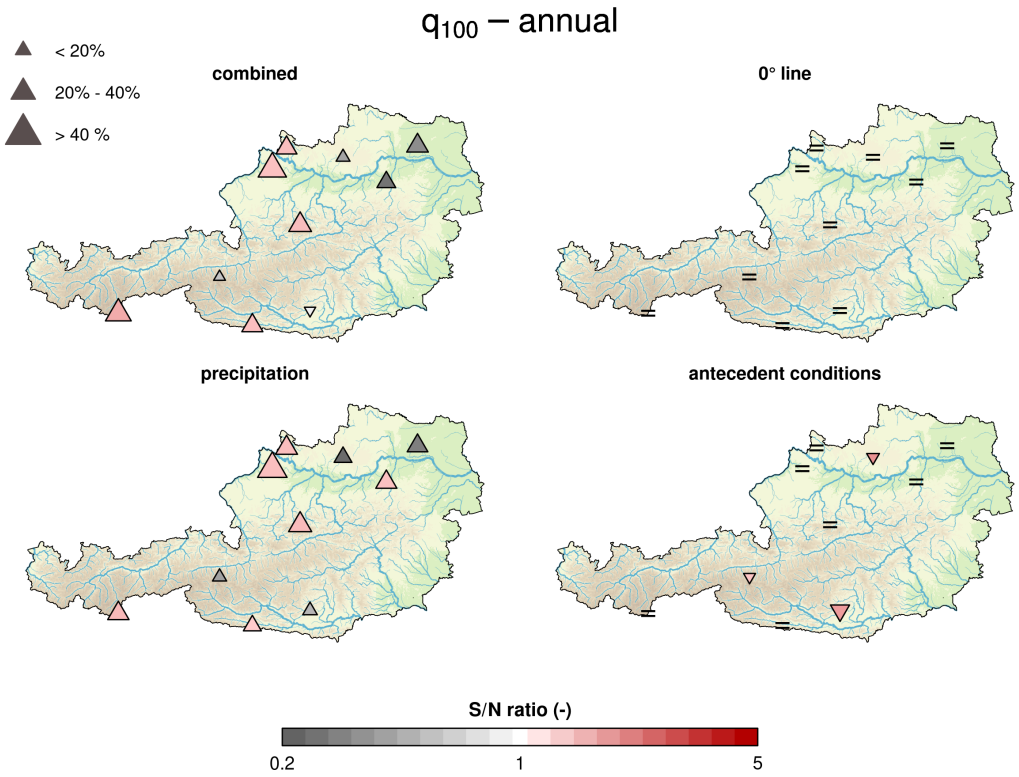


Fig. 4.18 Spatial distribution of projected annual 100-year flood changes caused by different flood generation mechanisms variation across Austria. Triangles represent the direction (increase/decrease) and magnitude of the change, while colors indicate the robustness of the signal, defined by the signal-to-noise ratio (S/N $>$ 1 indicates high confidence). The '=' symbol denotes locations where the projected change ranges between -5% and +5%.

Figure 4.19 illustrates the decomposition of uncertainty sources for the annual configuration of the model, obtained following the methodology described in Section 4.3.4. The results show that calibration uncertainty contributes a relatively small fraction of the total variance (approximately 5–10%) for return periods up to 100 years. However, its contribution increases markedly for larger return periods, highlighting the growing influence of hydrological parameter uncertainty when simulating extreme flood events. This behavior reflects the enhanced sensitivity of model outputs to parameter values under extreme hydrological conditions. The parametric response uncertainty represents the dominant source of variance across all return periods. This finding indicates that the non-linear propagation of parameter perturbations through the hydrological model plays a key role in shaping the uncertainty of projected flood extremes, particularly under altered climatic forcing. Conversely, the contribution of

climate forcing uncertainty decreases with increasing return period. Climate model spread has a stronger influence on the variability of more frequent flood events, while its relative influence diminishes for rare extremes.

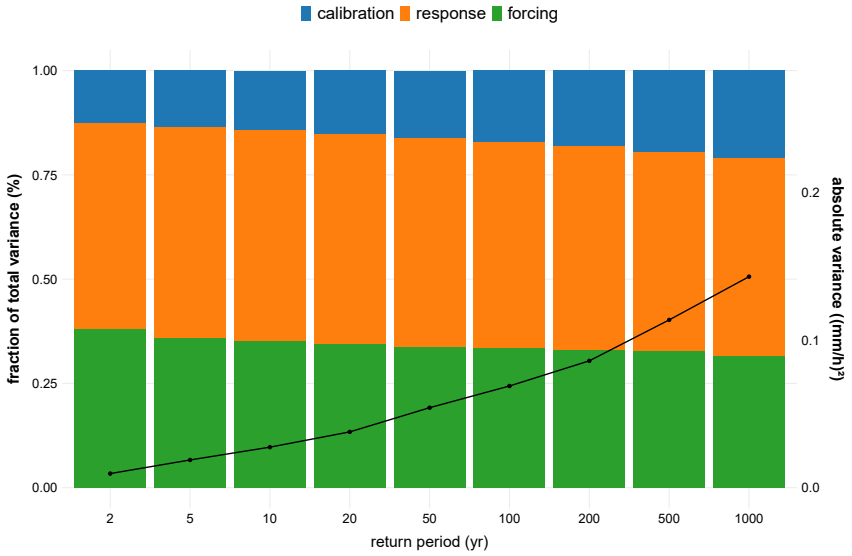


Fig. 4.19 Fractional contribution of each uncertainty source to total flood quantile variance under future climate scenarios. Calibration uncertainty (blue) represents the epistemic uncertainty in estimating current values of model parameters. Response uncertainty (orange) reflects the uncertainty arising from the propagation of parameter changes under future climatic conditions. Forcing uncertainty (green) corresponds to the spread among forcing models. Black lines represent the absolute variance, highlighting the strong increase in uncertainty with larger return periods. These values are obtained by averaging the different uncertainty sources for all the hotspots.

## 4.5 Hydrological interpretation of climate-driven flood changes

Climate and hydrological processes interact in complex ways to shape flood frequency and magnitude, and their relative importance varies considerably across catchment types and seasons. The modeled responses reflect the combined influence of temperature, precipitation, and antecedent catchment conditions, whose contributions need to be disentangled to interpret the regional differences emerging from the results. Understanding which flood drivers dominate under different climatic

regimes is therefore key to assessing future flood hazard and identifying the main sources of uncertainty in the projections.

Overall, the results indicate that changes in precipitation intensity emerge as the primary driver of projected variations in flood frequency and magnitude across the analyzed catchments. At the same time, precipitation projections are characterized by the largest source of uncertainty, reflecting both model spread and the inherent variability of extreme rainfall under climate change. In contrast, temperature-driven processes and antecedent catchment conditions, such as soil moisture and snow dynamics, generally exert a more moderate influence on flood quantile variations at the regional scale. However, their effects tend to be more systematic and therefore easier to anticipate, as they are governed by comparatively robust physical mechanisms and exhibit lower inter-model variability. This highlights a trade-off between impact and predictability: the processes with the strongest influence on future floods are also those characterized by the highest uncertainty, while secondary drivers contribute more modestly but in a more consistent and interpretable manner.

The relative importance of these processes further depends on the type of flood event considered. As suggested by previous studies, antecedent catchment conditions play a particularly relevant role in shaping more frequent, moderate floods, while precipitation extremes increasingly dominate the generation of rare events (Macdonald et al., 2024). Our results strongly confirm this hypothesis: the influence of antecedent conditions is significantly more pronounced for the 2-year flood than for the 100-year flood. Conversely, the relative impact of precipitation intensity on more frequent floods is comparatively smaller than on rare events. Regarding the upward shift of the 0°C isotherm and the resulting change in the partitioning between solid and liquid precipitation, this effect is clearly visible during the winter season across the whole of Austria. Notably, this mechanism affects the 2-year flood much more than the 100-year flood. However, since this increase occurs during a season characterized by minor flood events, the shift in the 0°C line does not significantly influence flood frequency when analyzed on an annual scale. Another widespread pattern concerns the summer season, where a distinct decrease in flood magnitudes is observed when isolating the effect of soil moisture variations, reflecting the impact of increased evapotranspiration and drier initial conditions under a warming climate.

A distinct pattern emerges in Alpine hotspots, characterized by strong seasonal dynamics. First, there is a substantial percentage increase in winter floods; however,

these remain minor in absolute terms when compared to summer floods. This winter trend is almost entirely driven by the upward shift of the 0°C isotherm, which increases the liquid fraction of precipitation. Second, during the spring, all three analyzed mechanisms vary in phase, collectively contributing to a rise in flood magnitudes. This is particularly evident for more frequent floods, where the combined signal is most robust. Third, the summer season is characterized by a clear trade-off between competing drivers: while projected increases in precipitation intensity tend to increase flood magnitudes, this signal is largely uncertain. Conversely, the reduction in available soil moisture decreases flood peaks (especially for more frequent floods). Consequently, ordinary floods are projected to experience a slight, uncertain decrease, while rare floods show a slight, uncertain increase. Fourth, the expected flood variation in autumn is largely dominated by the variation in precipitation intensity, which shows a projected increase. Unlike the summer season, where dry soils act as a significant modulator, the intensification of autumn rainfall translates more directly into increased discharge.

Similar patterns in terms of flood variation were reported by Laaha et al. (2025), who analyzed trends in mean annual flood in Austria for the period 1977–2020. While their study focuses on observed trends in the recent past and the present analysis addresses expected future variations, this comparison provides a consistency check to assess whether projected changes align with recent hydrological behaviour. In particular, they found an increase in winter floods, especially in the southern part of the country. For the spring season, a comparable pattern is observed: flood magnitudes increase in the Alpine region, whereas no clear signal is evident north of the Alps.

The uncertainty analysis reveals that the majority of projected flood variations are accompanied by substantial noise components, reflecting large contributions from both parameter-response and climate-forcing uncertainty, which respectively represent the uncertainty arising from the propagation of parameter changes under future climate conditions, and the one arising from the distinct climate trajectories provided by each member of the ensemble of climate models. On the other hand, calibration uncertainty, reflecting the epistemic uncertainty in estimating the current values of model parameters, remains consistently minor. This indicates that the robustness of flood projections depends primarily on how model parameters respond to climatic perturbations, and on the variability among climate models, rather than model calibration.

Overall, the linear reservoir model performs acceptably in representing the flood peaks of the distributed model, given the trade-off between simplicity and accuracy. However, flood peaks tend to be overestimated in the Weinviertel hotspot and underestimated in the alpine hotspots during winter. Moreover, the number of flood-generating events per season was assumed to remain stationary between historical and future periods. This assumption was required because climate model outputs only provide precipitation, while runoff is not directly simulated. Since flood events were identified from discharge series, potential changes in their frequency cannot be inferred directly from climate model output and are therefore not considered in this analysis. Future work should therefore focus on explicitly representing such changes. It should also be noted that the reported variations in flood frequency refer solely to climatic influences; catchment-related effects and river engineering structures were not considered in the evaluation of future flood frequency changes (Blöschl et al., 2007). Nevertheless, Bertola et al. (2019) analyzed the impacts of these different types of changes in Upper Austria, finding that atmospheric drivers, particularly short-duration extreme precipitation, exert a stronger influence on flood frequency variations than catchment or river-scale modifications.

These results emphasize that reliable projections of flood frequency under climate change depend on the accurate representation of process responsiveness, particularly the nonlinear propagation of precipitation and temperature effects through catchment hydrology. This methodology provides a transparent and flexible tool for attributing and quantifying drivers of change in flood risk under a warming climate, offering valuable insights for adaptation planning and hydrological modeling under uncertainty.

# Chapter 5

# Conclusions

This doctoral thesis addressed the estimation of flood quantiles under conditions of spatial heterogeneity and temporal non-stationarity. Floods arise from the interaction of atmospheric forcing, catchment processes, and river network structure, all of which vary across space and evolve in time. As emphasized by recent syntheses of open problems in hydrology, understanding and predicting hydrological extremes requires frameworks that move beyond purely local, stationary, and data-driven approaches, and that explicitly integrate spatial dependence, temporal variability, and physical process understanding (Blöschl et al., 2019a).

In this context, the main objective of the thesis was to develop a *spatio-temporal framework for flood frequency analysis* that is also suitable for ungauged or poorly gauged basins and takes into account the expected variation of hydroclimatic conditions. This objective was pursued through three complementary research directions, each addressing a distinct but interrelated dimension of the problem: spatial variability through regionalization, temporal variability through non-stationary analysis, and physical consistency through process-based modeling.

## 5.1 Synthesis of main findings

From a *spatial perspective*, the thesis demonstrates how regional flood frequency analysis can be effectively applied to support flood estimation in data-scarce environments. By integrating multiple independent regional models calibrated on a common and rigorously curated dataset, the work demonstrates that a multi-model perspective

enhances robustness and transparency in the estimation of design floods. The application to the Po River basin shows that spatial pooling substantially reduces estimation uncertainty relative to purely at-site analyses, particularly for rare events and short records. Beyond methodological advances, this research has significant practical implications. In close collaboration with the basin authority and other academic partners, the work directly supported the update of design flood estimates across the Po River basin. This process involved extensive dialogue with local stakeholders to examine cases where updated methodologies and newly available data indicated increases in flood quantiles, ensuring that the implications for infrastructure design, floodplain zoning, and risk management were carefully assessed. By providing more accurate estimates of extreme flows, the study contributes to the safe and sustainable planning of hydraulic structures and to floodplain identification, reinforcing the link between scientific research and territorial management. However, the regional models employed in this project inherently assume temporal stability of flood-generating processes, an assumption that is increasingly challenged under climate change and which is subsequently addressed within the scope of this thesis.

From a temporal perspective, the thesis builds on existing evidence indicating that flood frequency curves cannot be treated as stationary across large parts of Europe. Changes in extreme precipitation, soil moisture regimes, and snow-related processes affect not only flood magnitudes but also the shape of flood frequency distributions, with different impacts on frequent and rare events. The third chapter develops an operative and scalable procedure to incorporate projected changes in precipitation extremes into flood frequency analysis. By exploiting quantile-quantile relationships between Intensity-Duration-Frequency curves and Flood Frequency Curves, the method translates projected changes in rainfall extremes into changes in flood quantiles through the concept of flood elasticity. A substantial part of the chapter is devoted to systematically testing the key assumptions underlying this operational approach and to assessing its sensitivity to both climatic and catchment controls. Through controlled numerical experiments and sensitivity analyses, the methodology is evaluated under different hydrological regimes to identify the conditions under which the assumed linkage between precipitation and flood quantiles remains valid. The results show that the approach performs best in catchments where flood changes are predominantly driven by precipitation extremes, while its applicability becomes more limited in arid or highly infiltrating basins, where changes in runoff generation processes play a stronger role. In addition, the analysis highlights that the reliabil-

ity of the method depends on the nature of the projected changes in precipitation extremes: variations affecting the upper tail or the variability of annual maximum precipitation tend to propagate more consistently to rare flood quantiles than changes primarily influencing the mean of the annual maxima. The application to more than 200 catchments in the Po River basin reveals a pronounced spatial heterogeneity in flood response, showing that moderate increases in precipitation extremes can lead to substantially larger increases in rare flood magnitudes, depending on catchment-specific sensitivities. Together, these results delineate a domain of applicability for the proposed operational procedure and clarify its limitations, thereby providing guidance on where and how the method can be robustly applied in practice.

From a *process-based perspective*, the fourth chapter advances flood frequency analysis by explicitly linking climatic drivers to hydrological responses within a Bayesian framework. The proposed model jointly represents storms, antecedent soil moisture, and catchment response, and allows uncertainty to be propagated consistently from climate forcing to flood quantiles. Beyond estimation, the process-based structure enables the attribution of projected flood changes to specific mechanisms, such as increases in precipitation intensity, soil moisture depletion, or shifts in solid-liquid precipitation partitioning dynamics. Applications to Austrian case studies show that precipitation changes dominate the response of rare floods, while temperature-related changes in soil moisture and snow processes act as modulators that shape flood behaviour differently across seasons and return periods.

## 5.2 Complementarity of approaches and generalizability

Considered jointly, the third and fourth chapters outline a broader framework for addressing flood non-stationarity. While both chapters aim to characterize how flood frequency evolves under changing climatic conditions, they rely on different methodological paradigms and are designed to answer different, yet complementary, questions. The approach developed in the third chapter prioritizes operational applicability, offering a parsimonious and computationally efficient tool to translate projected changes in precipitation extremes into modified flood frequency curves. In contrast, the fourth chapter focuses on process attribution and physical understanding,

providing a framework to disentangle the mechanisms driving flood changes and to assess their relative importance across seasons, catchment types, and return periods.

This complementarity reflects the need for multiple approaches to adequately characterize flood behaviour under non-stationary conditions. Importantly, the process-based methodology developed in the fourth chapter offers a natural testbed to further evaluate and refine the assumptions underlying the more operative approach of the third chapter, for instance by assessing under which hydroclimatic and catchment conditions the elasticity-based relationships remain valid, and where deviations may arise due to changes in runoff generation mechanisms. In particular, the results obtained with the process-based framework in Chapter 4 suggest that changes in intense precipitation represent the dominant mechanism driving flood variability in the analyzed hotspots in Austria, supporting the applicability of the more operational approach developed in Chapter 3.

A further key outcome of this work is the recognition that the proposed methodologies are not site-specific. Although demonstrated using European case studies, the frameworks are inherently general and transferable. They rely on broadly available inputs, such as precipitation statistics, climate projections, and conceptual representations of rainfall-runoff processes, and can therefore be applied to other regions and hydroclimatic contexts, provided that the dominant flood-generating mechanisms are adequately represented. This generalizability enhances the relevance of the proposed approaches for flood risk assessment beyond the specific study areas considered in this thesis.

## 5.3 Concluding remarks

A key insight emerging from this work is that flood frequency curves should be interpreted as dynamic representations of evolving hydrological systems. Changes in their slope, curvature, and upper tail reflect shifts in dominant flood-generating processes, which vary across space, time, catchment scale, and flood magnitude.

The results of this thesis have direct implications for flood risk management and hydraulic design. Design floods derived under stationary assumptions may systematically underestimate future risks in regions experiencing intensification of extreme precipitation, particularly for large return periods. Conversely, in regions where

soil moisture depletion or reduced snow storage dominates, changes in frequent floods may differ markedly from changes in rare events. These findings argue against uniform climate change adjustment factors and support the adoption of process-based approaches to flood estimation that take into account the specific characteristics of the catchments.

The methodologies developed in this work provide a flexible toolbox for practitioners, ranging from relatively simple adjustment procedures based on precipitation projections to more comprehensive frameworks suitable for detailed risk assessments. This flexibility allows methods to be selected according to data availability, decision context, and required level of physical detail.

Despite these advances, several limitations remain. The proposed approaches rely on climate model projections that are subject to substantial uncertainty, particularly at the spatial and temporal scales relevant for flood generation. Moreover, while the process-based framework explicitly represents key hydroclimatic drivers, other sources of non-stationarity, such as land-use change, river regulation, and human water management, are only implicitly considered. Future research should aim to integrate these anthropogenic factors more explicitly and to extend the framework to compound and cascading flood hazards. Further challenges include translating non-stationary flood estimates into robust and defensible design criteria and improving the representation of rare, high-impact events that may arise from changing combinations of flood-generating processes.

In conclusion, this thesis demonstrates that reliable flood frequency estimation in a changing climate requires moving beyond stationary, purely statistical paradigms toward spatio-temporal and process-consistent frameworks. By integrating regional analysis, non-stationary methods, and process-based modeling, the work contributes to a more physically grounded, transferable, and adaptable understanding of flood hazards. Such an evolution is essential to ensure that flood risk management and hydraulic design remain effective under the hydroclimatic conditions of the future.

# References


Afrin, N., Rahman, A., Sharafati, A., Ahamed, F., and Haddad, K. (2025). Ensemble machine learning (eml) based regional flood frequency analysis model development and testing for south-east australia. *Journal of Hydrology: Regional Studies*, 59:102320.

Alila, Y. (1999). A hierarchical approach for the regionalization of precipitation annual maxima in canada. *Journal of Geophysical Research: Atmospheres*, 104(D24):31645–31655.

Anzolin, G., Chaffe, P. L. B., Vrugt, J. A., and AghaKouchak, A. (2023). Using climate information as covariates to improve nonstationary flood frequency analysis in brazil. *Hydrological Sciences Journal*, 68(5):645–654.

Archfield, S. A., Hirsch, R. M., Viglione, A., and Blöschl, G. (2016). Fragmented patterns of flood change across the united states. *Geophysical Research Letters*, 43(19):10,232–10,239.

Archfield, S. A., Pugliese, A., Castellarin, A., Skøien, J. O., and Kiang, J. E. (2013). Topological and canonical kriging for design flood prediction in ungauged catchments: an improvement over a traditional regional regression approach? *Hydrology and Earth System Sciences*, 17(4):1575–1588.

Awasthi, C., Archfield, S. A., Ryberg, K. R., Kiang, J. E., and Sankarasubramanian, A. (2022). Projecting flood frequency curves under near-term climate change. *Water Resources Research*, 58(8):e2021WR031246. e2021WR031246 2021WR031246.

Aziz, K., Rahman, A., Fang, G., and Shrestha, S. (2014). Application of artificial neural networks in regional flood frequency analysis: a case study for australia. *Stochastic environmental research and risk assessment*, 28(3):541–554.

Ball, J., Babister, M., Nathan, R., Weinmann, P., Weeks, W., Retallick, M., and Testoni, I. (2016). Australian rainfall and runoff-a guide to flood estimation.

Barbhuiya, S., Ramadas, M., and Biswal, S. S. (2023). *Nonstationary Flood Frequency Analysis: Review of Methods and Models*, pages 271–288. Springer Nature Singapore, Singapore.

Bayliss, A. C. and Reed, D. W. (2001). The use of historical data in flood frequency estimation. Technical report, NERC / Centre for Ecology & Hydrology.

Bennett, B., Leonard, M., Deng, Y., and Westra, S. (2018). An empirical investigation into the effect of antecedent precipitation on flood volume. *Journal of Hydrology*, 567:435–445.

Berends, K. D., Straatsma, M. W., Warmink, J. J., and Hulscher, S. J. M. H. (2019). Uncertainty quantification of flood mitigation predictions and implications for interventions. *Natural Hazards and Earth System Sciences*, 19(8):1737–1753.

Bertola, M., Viglione, A., and Blöschl, G. (2019). Informed attribution of flood changes to decadal variation of atmospheric, catchment and river drivers in upper austria. *Journal of Hydrology*, 577:123919.

Bertola, M., Viglione, A., Lun, D., Hall, J., and Blöschl, G. (2020). Flood trends in europe: are changes in small and big floods different? *Hydrology and Earth System Sciences*, 24(4):1805–1822.

Bertola, M., Viglione, A., Vorogushyn, S., Lun, D., Merz, B., and Blöschl, G. (2021). Do small and large floods have the same drivers of change? a regional attribution analysis in europe. *Hydrology and Earth System Sciences*, 25(3):1347–1364.

Bloetscher, F. (2012). Protecting people, infrastructure, economies, and ecosystem assets: Water management in the face of climate change. *Water*, 4(2):367–388.

Blöschl, G., Buttinger-Kreuzhuber, A., Cornel, D., Eisl, J., Hofer, M., Hollaus, M., Horváth, Z., Komma, J., Konev, A., Parajka, J., Pfeifer, N., Reithofer, A., Salinas, J., Valent, P., Výleta, R., Waser, J., Wimmer, M. H., and Stiefelmeyer, H. (2024). Hyper-resolution flood hazard mapping at the national scale. *Natural Hazards and Earth System Sciences*, 24(6):2071–2091.

Blöschl, G., Sivapalan, M., Wagener, T., Viglione, A., and Savenije, H. H. (2023). *Runoff Prediction in Ungauged Basins: Synthesis across Processes, Places and Scales*. Cambridge University Press.

Blöschl, G., Ardoin-Bardin, S., Bonell, M., Dorninger, M., Goodrich, D., Gutknecht, D., Matamoros, D., Merz, B., Shand, P., and Szolgay, J. (2007). At what scales do climate variability and land cover change impact on flooding and low flows? *Hydrological Processes*, 21(9):1241–1247.

Blöschl, G., Bierkens, M., Chambel, A., Cudennec, C., Destouni, G., Fiori, A., Kirchner, J., McDonnell, J., Savenije, H., Sivapalan, M., Stumpp, C., Toth, E., Volpi, E., Carr, G., Lupton, C., Salinas, L., Széles, B., Viglione, A., Aksoy, H., and Zhang, Y. (2019a). Twenty-three unsolved problems in hydrology (uph) – a community perspective. *Hydrological Sciences Journal/Journal des Sciences Hydrologiques*, 64:1141–1158.

Blöschl, G., Hall, J., Viglione, A., Parajka, H. S., Merz, M. B., Sivapalan, S., Smith, R. A., and Bates, P. A. (2019b). Changing climate both increases and decreases european river floods. *Nature*, 573:108–111.

Bobee, B., Mathier, L., Perron, H., Trudel, P., Rasmussen, P., Cavadias, G., Bernier, J., Nguyen, V., Pandey, G., Ashkar, F., et al. (1996). Inter-comparison of regional flood frequency procedures for canadian rivers. *Journal of hydrology*, 186(1-4):85–103.

Brath, A., Castellarin, A., Franchini, M., and Galeati, G. (2001). Estimating the index flood using indirect methods. *Hydrological Sciences Journal*, 46:399–418.

Breinl, K., Lun, D., Müller-Thomy, H., and Blöschl, G. (2021). Understanding the relationship between rainfall and flood probabilities through combined intensity-duration-frequency analysis. *Journal of Hydrology*, 602:126759.

Brunner, M. I., Swain, D. L., Wood, R. R., Willkofer, F., Done, J. M., Gilleland, E., and Ludwig, R. (2021). An extremeness threshold determines the regional response of floods to changes in rainfall extremes. *Communications Earth and Environment*, 2(1):173.

Burn, D. H. (1990). Evaluation of regional flood frequency analysis with a region of influence approach. *Water Resources Research*, 26(10):2257–2265.

Cafiero, L., Bertola, M., Mazzoglio, P., Blöschl, G., Laio, F., and Viglione, A. (2025). How changes in future precipitation impact flood frequencies: A quantile-quantile mapping approach. *Water Resources Research*, 61(7):e2024WR038471. e2024WR038471 2024WR038471.

Camici, S., Tarpanelli, A., Brocca, L., Melone, F., and Moramarco, T. (2011). Design soil moisture estimation by comparing continuous and storm-based rainfall-runoff modeling. *Water Resources Research*, 47(5).

Castellarin, A. (2007). Probabilistic envelope curves for design flood estimation at ungauged sites. *Water Resources Research*, 43(4).

Castellarin, A., Burn, D., and Brath, A. (2000). Assessing the effectiveness of hydrological similarity measures for flood frequency analysis. *Journal of Hydrology*, 241:270–285.

Castellarin, A., Burn, D., and Brath, A. (2001). Assessing the effectiveness of hydrological similarity measures for flood frequency analysis. *Journal of Hydrology*, 241(3-4):270–285.

Castellarin, A., Camorani, G., and Brath, A. (2007). Predicting annual and long-term flow-duration curves in ungauged basins. *Advances in Water Resources*, 30(4):937–953.

Chokmani, K. and Ouarda, T. B. (2004). Physiographical space-based kriging for regional flood frequency estimation at ungauged sites. *Water Resources Research*, 40(12).

Chong, S. F. and Choo, R. (2011). Introduction to bootstrap. *Proceedings of Singapore Healthcare*, 20(3):236–240.

Claps, P. (2020). *Catalogo delle piene dei corsi d'acqua italiani*. CINID.

Claps, P., Evangelista, G., Ganora, D., Mazzoglio, P., and Monforte, I. (2024). Foca: a new quality-controlled database of floods and catchment descriptors in italy. *Earth System Science Data*, 16:1503–1522.

Cohn, T. A., Lane, W. L., and Baier, W. G. (1997). An algorithm for computing moments-based flood quantile estimates when historical flood information is available. *Water Resources Research*, 33(9):2089–2096.

Coles, S. (2001). *An Introduction to Statistical Modeling of Extreme Values*. Springer.

Collins, M. J., Hodgkins, G. A., Archfield, S. A., and Hirsch, R. M. (2022). The occurrence of large floods in the united states in the modern hydroclimate regime: Seasonality, trends, and large-scale climate associations. *Water Resources Research*, 58(2):e2021WR030480. e2021WR030480 2021WR030480.

Costa, V. and Fernandes, W. (2017). Bayesian estimation of extreme flood quantiles using a rainfall-runoff model and a stochastic daily rainfall generator. *Journal of Hydrology*, 554:137–154.

Cremonini, L., Randi, P., Fazzini, M., Nardino, M., Rossi, F., and Georgiadis, T. (2024). Causes and impacts of flood events in emilia-romagna (italy) in may 2023. *Land*, 13(11).

Cunderlik, J. M. and Burn, D. H. (2003). Non-stationary pooled flood frequency analysis. *Journal of Hydrology*, 276(1):210–223.

Dalrymple, T. (1960). *Flood-frequency analyses*. U.S. Government Printing Office.

De Michele, C. and Rosso, R. (2001). Rapporto sulla valutazione delle piene nell'italia nord-occidentale. In *Progetto VAPI: Valutazione delle Piene in Italia*. CNR-GNDCI, Roma. Pubblicazione del CNR-GNDCI.

Di Baldassarre, G., Brath, A., and Montanari, A. (2006a). Reliability of different depth-duration-frequency equations for estimating short-duration design storms. *Water resources research*, 42(12).

Di Baldassarre, G., Castellarin, A., and Brath, A. (2006b). Relationships between statistics of rainfall extremes and mean annual precipitation: an application for design-storm estimation in northern central italy. *Hydrology and Earth System Sciences*, 10(4):589–601.

Di Sante, F., Coppola, E., and Giorgi, F. (2021). Projections of river floods in europe using euro-cordex, cmip5 and cmip6 simulations. *International Journal of Climatology*, 41(5):3203–3221.

Dittes, B., Špačková, O., Schoppa, L., and Straub, D. (2018). Managing uncertainty in flood protection planning with climate projections. *Hydrology and Earth System Sciences*, 22(4):2511–2526.

Dong, X., Jiang, L., Zeng, S., Guo, R., and Zeng, Y. (2020). Vulnerability of urban water infrastructures to climate change at city level. *Resources, Conservation and Recycling*, 161:104918.

Eagleson, P. S. (1972). Dynamics of flood frequency. *Water Resources Research*, 8(4):878–898.

Eaton, B., Church, M., and Ham, D. (2002). Scaling and regionalization of flood flows in british columbia, canada. *Hydrological Processes*, 16(16):3245–3263.

Elamir, E. A. and Seheult, A. H. (2004). Exact variance structure of sample l-moments. *Journal of statistical planning and inference*, 124(2):337–359.

Estilow, T. W., Young, A. H., and Robinson, D. A. (2015). A long-term northern hemisphere snow cover extent data record for climate studies and monitoring. *Earth System Science Data*, 7(1):137–142.

European Commission, D.-G. f. E. (2021). *Impact of climate change on floods – Survey findings and possible next steps to close the knowledge and implementation gap – Final a survey based study*. Publications Office.

European Union (2007). Directive 2007/60/ec of the european parliament and of the council on the assessment and management of flood risks. Official Journal of the European Union, L288/27.

Evangelista, G., Woods, R., and Claps, P. (2023). Dimensional analysis of literature formulas to estimate the characteristic flood response time in ungauged basins: A velocity-based approach. *Journal of Hydrology*, 627:130409.

Falter, D., Schröter, K., Dung, N. V., Vorogushyn, S., Kreibich, H., Hundecha, Y., Apel, H., and Merz, B. (2015). Spatially coherent flood risk assessment based on long-term continuous simulation with a coupled model chain. *Journal of Hydrology*, 524:182–193.

Farquharson, F., Meigh, J., and Sutcliffe, J. (1992). Regional flood frequency analysis in arid and semi-arid areas. *Journal of Hydrology*, 138(3):487–501.

Ferro, V. (2006). Riqualificazione ambientale dei corsi d'acqua. quaderni di idronomia montana. *Quaderni di Idronomia Montana*, 25(1-20).

Fiorentino, M., Manfreda, S., and Iacobellis, V. (2007). Peak runoff contributing area as hydrological signature of the probability distribution of floods. *Advances in Water Resources*, 30(10):2123–2134. Recent Developments in Hydrologic Analysis.

Fiseha, B., Setegn, S., Melesse, A., Volpi, E., and Fiori, A. (2014). Impact of Climate Change on the Hydrology of Upper Tiber River Basin Using Bias Corrected Regional Climate Model. *Water Resources Management: An International Journal, Published for the European Water Resources Association (EWRA)*, 28(5):1327–1343.

Foufoula-Georgiou, E. (1989). A probabilistic storm transposition approach for estimating exceedance probabilities of extreme precipitation depths. *Water Resources Research*, 25(5):799–815.

Franchini, M., Helmlinger, K., Foufoula-Georgiou, E., and Todini, E. (1996). Stochastic storm transposition coupled with rainfall—runoff modeling for estimation of exceedance probabilities of design floods. *Journal of Hydrology*, 175(1):511–532.

Franks, S. W., White, C. J., and Gensen, M. (2015). Estimating extreme flood events – assumptions, uncertainty and error. *Proceedings of the International Association of Hydrological Sciences*, 369:31–36.

Gabriele, S. and Arnell, N. (1991). A hierarchical approach to regional flood frequency analysis. *Water Resources Research*, 27(6):1281–1289.

Gaál, L., Szolgay, J., Kohnová, S., Parajka, J., Merz, R., Viglione, A., and Blöschl, G. (2012). Flood timescales: Understanding the interplay of climate and catchment processes through comparative hydrology. *Water Resources Research*, 48(4).

Genest, C. and Zidek, J. V. (1986). Combining probability distributions: A critique and an annotated bibliography. *Statistical Science*, 1(1):114–148.

Giani, G., Tarasova, L., Woods, R. A., and Rico-Ramirez, M. A. (2022). An objective time-series-analysis method for rainfall-runoff event identification. *Water Resources Research*, 58(2):e2021WR031283. e2021WR031283 2021WR031283.

Gioia, A., Iacobellis, V., Manfreda, S., and Fiorentino, M. (2008). Runoff thresholds in derived flood frequency distributions. *Hydrology and Earth System Sciences*, 12(6):1295–1307.

Gobiet, A., Kotlarski, S., Beniston, M., Heinrich, G., Rajczak, J., and Stoffel, M. (2014). 21st century climate change in the european alps—a review. *Science of The Total Environment*, 493:1138–1151.

Gottschalk, L. and Weingartner, R. (1998). Distribution of peak flow derived from a distribution of rainfall volume and runoff coefficient, and a unit hydrograph. *Journal of hydrology*, 208(3-4):148–162.

Griffis, V. and Stedinger, J. (2007). The use of gls regression in regional hydrologic analyses. *Journal of Hydrology*, 344(1):82–95.

Grimaldi, S., Kao, S.-C., Castellarin, A., Papalexiou, S.-M., Viglione, A., Laio, F., Aksoy, H., and Gedikli, A. (2011a). 2.18 - statistical hydrology. In Wilderer, P., editor, *Treatise on Water Science*, pages 479–517. Elsevier, Oxford.

Grimaldi, S., Petroselli, A., Arcangeletti, E., and Nardi, F. (2013). Flood mapping in ungauged basins using fully continuous hydrologic–hydraulic modeling. *Journal of Hydrology*, 487:39–47.

Grimaldi, S., Serinaldi, F., Benedetto, F., and Koutsoyiannis, D. (2011b). Statistical properties of three-parameter lognormal distribution in flood frequency analysis. *Hydrological Sciences Journal*, 56(5).

Guo, S., Xiong, L., Chen, J., Guo, S., Xia, J., Zeng, L., and Xu, C.-Y. (2022). Nonstationary regional flood frequency analysis based on the bayesian method. *Water Resources Management*, 37:1–23.

Gupta, H. et al. (2021). Global flood database: A new resource for flood risk analysis and mapping. *Nature Communications*, 12(1):1254.

Haberlandt, U. and Radtke, I. (2014). Hydrological model calibration for derived flood frequency analysis using stochastic rainfall and probability distributions of peak flows. *Hydrology and Earth System Sciences*, 18(1):353–365.

Habersack, H., Moser, A., and Schober, B. (2016). Vienna and the danube: Managing flood risk through integrated river engineering. *Water Science and Technology*, 74(5):1125–1133.

Hall, J., Arheimer, B., Borga, M., Brázdil, R., Claps, P., Kiss, A., Kjeldsen, T. R., Kriaučiūnienė, J., Kundzewicz, Z. W., Lang, M., Llasat, M. C., Macdonald, N., McIntyre, N., Mediero, L., Merz, B., Merz, R., Molnar, P., Montanari, A., Neuhold, C., Parajka, J., Perdigão, R. A. P., Plavcová, L., Rogger, M., Salinas, J. L., Sauquet, E., Schär, C., Szolgay, J., Viglione, A., and Blöschl, G. (2014). Understanding flood regime changes in europe: a state-of-the-art assessment. *Hydrology and Earth System Sciences*, 18(7):2735–2772.

Haslinger, K., Breinl, K., Pavlin, L., Pistotnik, G., Bertola, M., Olefs, M., Greilinger, M., Schöner, W., and Blöschl, G. (2025). Increasing hourly heavy rainfall in austria reflected in flood changes. *Nature*, 639(8055):667–672.

Hauer, C., Paster, M., Pulg, U., Ofenböck, T., and Habersack, H. (2025). Critical flows at the wien river during the 1000-years event in september 2024 – causes, consequences and possible management options for urban river flood management. *Natural Hazards*, 121(9):11173–11185.

Hauer, C., Unfer, G., and Habersack, H. (2019). Danube river regulation: Historical development and modern perspectives. *River Research and Applications*, 35(6):565–579.

Hebson, C. (1987). Assessment of use of at-site and regional flood data for flood frequency estimation. In Singh, V. P., editor, *Hydrologic Frequency Modeling*. Springer, Dordrecht.

Hirsch, R. M. and Archfield, S. A. (2015). Not higher but more often. *Nature Climate Change*, 5(3):198–199.

Hirsch, R. M., Archfield, S. A., and De Cicco, L. A. (2015). A bootstrap method for estimating uncertainty of water quality trends. *Environmental Modelling & Software*, 73:148–166.

Hirsch, R. M. and Stedinger, J. R. (1987). Plotting positions for historical floods and their precision. *Water Resources Research*, 23(4):715–727.

Ho, M., Wasko, C., O'Shea, D., Nathan, R., Vogel, E., and Sharma, A. (2023). Changes in flood-associated rainfall losses under climate change. *Journal of Hydrology*, 625:129950.

Hosking, J. R. M. and Wallis, J. R. (1993). Some statistics useful in regional frequency analysis. *Water Resources Research*, 29(2):271–281.

Hosking, J. R. M. and Wallis, J. R. (1997). *L-moments*, page 14–43. Cambridge University Press.

Hotelling, H. (1933). Analysis of a complex of statistical variables into principal components. *Journal of Educational Psychology*, 24:417–441.

Hu, L., Nikolopoulos, E. I., Marra, F., and Anagnostou, E. N. (2020). Sensitivity of flood frequency analysis to data record, statistical model, and parameter estimation methods: An evaluation over the contiguous united states. *Journal of Flood Risk Management*, 13(1):e12580.

Jacob, D., Petersen, J., Eggert, B., Alias, A., Christensen, O., Bouwer, L., Braun, A., Colette, A., Déqué, M., Georgievski, G., Georgopoulou, E., Gobiet, A., Menut, L., Nikulin, G., Haensler, A., Hempelmann, N., Jones, C., Keuler, K., Kovats, S., and Yiou, P. (2014). Euro-cordex: New high-resolution climate change projections for european impact research. *Regional Environmental Change*, 14.

Katz, R. (2013). Statistical methods for nonstationary extremes. *Advances in Water Resources*, 55:1–6.

Kemter, M., Merz, B., Marwan, N., Vorogushyn, S., and Blöschl, G. (2020). Joint trends in flood magnitudes and spatial extents across europe. *Geophysical Research Letters*, 47(7):e2020GL087464. e2020GL087464 2020GL087464.

Komma, J., Valent, P., Bertola, M., Parajka, J., Haslinger, K., Bica, B., Pistotnik, G., Breinl, K., Müller, G., Pavlin, L., Kahl, B., Naderer, A., and Blöschl, G. (2025). The september 2024 danube flood compared to the 1899, 2002, and 2013 events: A hydrometeorological analysis in a changing climate. *EGUsphere*, 2025:1–32.

Koutsoyiannis, D. and Montanari, A. (2015). Negligent killing of scientific concepts: the stationarity case. *Hydrological Sciences Journal*, 60(7-8):1174–1183.

Kuczera, G. (1999). Comprehensive at-site flood frequency analysis using monte carlo bayesian inference. *Water Resources Research*, 35(5):1551–1557.

Kuczera, G., Renard, B., Thyer, M., and Kavetski, D. (2010). There are no hydrological monsters, just models and observations with large uncertainties! *Hydrological Sciences Journal*, 55(6):980–991.

Kundzewicz, Z., Lugeri, N., Dankers, R., Hirabayashi, Y., Döll, P., Pińskwar, I., Dysarz, T., Hochrainer, S., and Matczak, P. (2010). Assessing river flood risk and adaptation in europe—review of projections for the future. *Climate Change*, 15.

Kundzewicz, Z. W., editor (2012). *Changes in Flood Risk in Europe*. CRC Press, Boca Raton, FL, 1st edition.

Kundzewicz, Z. W., Krysanova, V., Dankers, R., Hirabayashi, Y., Kanae, S., Hattermann, F. F., Huang, S., Milly, P. C. D., Stoffel, M., Driessen, P. P. J., Matczak, P., Quevauviller, P., and Schellnhuber, H.-J. (2017). Differences in flood hazard projections in europe – their causes and consequences for decision making. *Hydrological Sciences Journal*, 62(1):1–14.

Laaha, G., Laimighofer, J., Parajka, J., Bertola, M., and Blöschl, G. (2025). Abflusstrends in österreichs fließgewässern 1977–2020. *Österreichische Wasser- und Abfallwirtschaft*, 77(5):338–346.

Laio, F., Ganora, D., Claps, P., and Galeati, G. (2011). Spatially smooth regional estimation of the flood frequency curve (with uncertainty). *Journal of Hydrology*, 408(1):67–77.

Leclerc, M. and Ouarda, T. B. (2007). Non-stationary regional flood frequency analysis at ungauged sites. *Journal of Hydrology*, 343(3):254–265.

Leopold, L. B. (1994). *A View of the River*. Harvard University Press.

Libertino, A., Allamano, P., Laio, F., and Claps, P. (2018). Regional-scale analysis of extreme precipitation from short and fragmented records. *Advances in Water Resources*, 112:147–159.

Macdonald, E., Merz, B., Guse, B., Nguyen, V. D., Guan, X., and Vorogushyn, S. (2024). What controls the tail behaviour of flood series: rainfall or runoff generation? *Hydrology and Earth System Sciences*, 28(4):833–850.

Madsen, H., Lawrence, D., Lang, M., Martinkova, M., and Kjeldsen, T. (2014a). Review of trend analysis and climate change projections of extreme precipitation and floods in europe. *Journal of Hydrology*, 519:3634–3650.

Madsen, H., Lawrence, D., Lang, M., Martinkova, M., and Kjeldsen, T. R. (2014b). Nonstationarity in extreme rainfall and flooding—review and recommendations. *Hydrological Sciences Journal*, 59(2):573–591.

Madsen, H., Rasmussen, P. F., and Rosbjerg, D. (1997). Comparison of annual maximum series and partial duration series methods for modeling extreme hydrologic events: 1. at-site modeling. *Water Resources Research*, 33(4):747–757.

Mangini, W., Viglione, A., Hall, J., Hundecha, Y., Ceola, S., Montanari, A., Rogger, M., Salinas, J. L., Borzì, I., and Parajka, J. (2018). Detection of trends in magnitude and frequency of flood peaks across europe. *Hydrological Sciences Journal*, 63(4):493–512.

Marchi, L., Borga, M., Preciso, E., and Gaume, E. (2010). Characterisation of selected extreme flash floods in europe and implications for flood risk management. *Journal of Hydrology*, 394(1-2):118–133.

Massari, C., Pellet, V., Tramblay, Y., Crow, W. T., Gründemann, G. J., Hascoetf, T., Penna, D., Modanesi, S., Brocca, L., Camici, S., and Marra, F. (2023). On the relation between antecedent basin conditions and runoff coefficient for european floods. *Journal of Hydrology*, 625:130012.

Mazzoglio, P., Butera, I., Alvioli, M., and Claps, P. (2022). The role of morphology in the spatial distribution of short-duration rainfall extremes in italy. *Hydrology and Earth System Sciences*, 26(6):1659–1672.

Mazzoglio, P., Butera, I., and Claps, P. (2020). I2-red: A massive update and quality control of the italian annual extreme rainfall dataset. *Water*, 12(12).

Meresa, H., Murphy, C., Fealy, R., and Golian, S. (2021). Uncertainties and their interaction in flood hazard assessment with climate change. *Hydrology and Earth System Sciences*, 25(9):5237–5257.

Merz, B., Basso, S., Fischer, S., Lun, D., Blöschl, G., Merz, R., Guse, B., Viglione, A., Vorogushyn, S., Macdonald, E., Wietzke, L., and Schumann, A. (2022). Understanding heavy tails of flood peak distributions. *Water Resources Research*, 58(6):e2021WR030506. e2021WR030506 2021WR030506.

Merz, R., Blöschl, G., and Parajka, J. (2006). Spatio-temporal variability of event runoff coefficients. *Journal of Hydrology*, 331(3-4):591–604.

Merz, R. and Blöschl, G. (2003). A process typology of regional floods. *Water Resources Research*, 39(12).

Merz, R. and Blöschl, G. (2004). Regionalisation of catchment model parameters. *Journal of Hydrology*, 287(1):95–123.

Merz, R. and Blöschl, G. (2008a). Flood frequency hydrology: 1. temporal, spatial, and causal expansion of information. *Water Resources Research*, 44(8).

Merz, R. and Blöschl, G. (2008b). Flood frequency hydrology: 2. combining data evidence. *Water Resources Research*, 44(8).

Merz, R. and Blöschl, G. (2009a). Process controls on the statistical flood moments - a data based analysis. *Hydrological Processes*, 23(5):675–696.

Merz, R. and Blöschl, G. (2009b). A regional analysis of event runoff coefficients with respect to climate and catchment characteristics in austria. *Water Resources Research*, 45(1).

Metzger, A., Marra, F., Smith, J. A., and Morin, E. (2020). Flood frequency estimation and uncertainty in arid/semi-arid regions. *Journal of Hydrology*, 590:125254.

Micevski, T. and Kuczera, G. (2009). Combining site and regional flood information using a bayesian monte carlo approach. *Water Resources Research*, 45(4).

Mishra, B. K. and Herath, S. (2015). Assessment of future floods in the bagmati river basin of nepal using bias-corrected daily gcm precipitation data. *Journal of Hydrologic Engineering*, 20(8):05014027.

Mohr, S., Ehret, U., Kunz, M., Ludwig, P., Caldas-Alvarez, A., Daniell, J. E., Ehmele, F., Feldmann, H., Franca, M. J., Gattke, C., Hundhausen, M., Knippertz, P., Küpfer, K., Mühr, B., Pinto, J. G., Quinting, J., Schäfer, A. M., Scheibel, M., Seidel, F., and Wisotzky, C. (2023). A multi-disciplinary analysis of the exceptional flood event of july 2021 in central europe – part 1: Event description and analysis. *Natural Hazards and Earth System Sciences*, 23(2):525–551.

Montgomery, D. R. (2007). *Dirt: The Erosion of Civilizations*. University of California Press.

Mulvaney, T. (1850). On the use of self-registering rain and flood gauges. *Proceedings-Institution of Civil Engineers*, 4:1–8.

Nourani, V. and Moradkhani, H. (2017). Application of machine learning methods in simulation of groundwater level fluctuations. *Water Resources Management*, 31(9):2849–2868.

Okoli, K., Breinl, K., Brandimarte, L., Botto, A., Volpi, E., and Baldassarre, G. D. (2018). Model averaging versus model selection: estimating design floods with uncertain river flow data. *Hydrological Sciences Journal*, 63(13-14):1913–1926.

Ouarda, T. B., Girard, C., Cavadias, G. S., and Bobée, B. (2001). Regional flood frequency estimation with canonical correlation analysis. *Journal of hydrology*, 254(1-4):157–173.

Paola Mazzoglio, I. B. and Claps, P. (2023). A local regression approach to analyze the orographic effect on the spatial variability of sub-daily rainfall annual maxima. *Geomatics, Natural Hazards and Risk*, 14(1):2205000.

Parajka, J., Kohnová, S., Bálint, G., Barbuc, M., Borga, M., Claps, P., Cheval, S., Dumitrescu, A., Gaume, E., Hlavčová, K., Merz, R., Pfaundler, M., Stancalie, G., Szolgay, J., and Blöschl, G. (2010). Seasonal characteristics of flood regimes across the alpine–carpathian range. *Journal of Hydrology*, 394(1):78–89. Flash Floods: Observations and Analysis of Hydrometeorological Controls.

Pearson, K. (1901). Liii. on lines and planes of closest fit to systems of points in space. *The London, Edinburgh, and Dublin Philosophical Magazine and Journal of Science*, 2(11):559–572.

Peel, M. C., Wang, Q., Vogel, R. M., and McMahon, T. A. (2001). The utility of l-moment ratio diagrams for selecting a regional probability distribution; [utilité des diagrammes de rapports de l-moments pour le choix d'une distribution régionale de probabilité]. *Hydrological Sciences Journal*, 46(1):147 – 155. Cited by: 122; All Open Access, Bronze Open Access.

Petrow, T., Merz, B., Lindenschmidt, K.-E., and Thieken, A. H. (2007). Aspects of seasonality and flood generating circulation patterns in a mountainous catchment in south-eastern germany. *Hydrology and Earth System Sciences*, 11(4):1455–1468.

Petts, G. and Calow, P. (1996). Rivers and their catchments: The changing landscape. *The Rivers Handbook*, 1:1–20.

Pianosi, F., Beven, K., Freer, J., Hall, J. W., Rougier, J., Stephenson, D. B., and Wagener, T. (2016). Sensitivity analysis of environmental models: A systematic review with practical workflow. *Environmental Modelling & Software*, 79:214–232.

Ravazzani, G., Boscarello, L., Cislaghi, A., and Mancini, M. (2019). Review of time-of-concentration equations and a new proposal in italy. *Journal of Hydrologic Engineering*, 24(10):04019039.

Renard, B. (2011). A bayesian hierarchical approach to regional frequency analysis. *Water Resources Research*, 47(11).

Renard, B., Kavetski, D., Kuczera, G., Thyer, M., and Franks, S. W. (2010). Understanding predictive uncertainty in hydrologic modeling: The challenge of identifying input and structural errors. *Water Resources Research*, 46(5).

Ribatet, M., Sauquet, E., Gresillon, J. M., and Ouarda, T. B. M. J. (2007). A regional bayesian pot model for flood frequency analysis. *Stochastic Environmental Research and Risk Assessment*, 21:327–339.

Robson, A. and Reed, D. (1999). *Flood estimation handbook: statistical procedures for flood frequency estimation*. Institute of Hydrology.

Rogger, M., Kohl, B., Pirkl, H., Viglione, A., Komma, J., Kirnbauer, R., Merz, R., and Blöschl, G. (2012a). Runoff models and flood frequency statistics for design flood estimation in austria – do they tell a consistent story? *Journal of Hydrology*, 456-457:30–43.

Rogger, M., Pirkl, H., Viglione, A., Komma, J., Kohl, B., Kirnbauer, R., Merz, R., and Blöschl, G. (2012b). Step changes in the flood frequency curve: Process controls. *Water Resources Research*, 48(5).

Rojas, R., Feyen, L., Bianchi, A., and Dosio, A. (2012). Assessment of future flood hazard in europe using a large ensemble of bias-corrected regional climate simulations. *Journal of Geophysical Research: Atmospheres*, 117(D17).

Roudier, P., Andersson, J. Donnelly, C., Feyen, L., Greuell, W., and Ludwig, F. (2016). Projections of future floods and hydrological droughts in europe under a +2°c global warming. *Climate Change*, 135.

Saltelli, A. (2002). Sensitivity analysis for importance assessment. *Risk Analysis*, 22(3):579–590.

Shao, J. and Tu, D. (2012). *The jackknife and bootstrap*. Springer Science & Business Media.

Shu, C. and Burn, D. H. (2004). Artificial neural network ensembles and their application in pooled flood frequency analysis. *Water Resources Research*, 40(9).

Shu, C. and Ouarda, T. B. (2008). Regional flood frequency analysis at ungauged sites using the adaptive neuro-fuzzy inference system. *Journal of Hydrology*, 349(1-2):31–43.

Sivapalan, M., Blöschl, G., Merz, R., and Gutknecht, D. (2005). Linking flood frequency to long-term water balance: Incorporating effects of seasonality. *Water Resources Research*, 41(6).

Sivapalan, M., Savenije, H. H. G., and Blöschl, G. (2012). Socio-hydrology: A new science of people and water. *Hydrological Processes*, 26(8):1270–1276.

Skøien, J. O., Merz, R., and Blöschl, G. (2006). Top-kriging - geostatistics on stream networks. *Hydrology and Earth System Sciences*, 10(2):277–287.

Slater, L., Villarini, G., Archfield, S., Faulkner, D., Lamb, R., Khouakhi, A., and Yin, J. (2021). Global changes in 20-year, 50-year, and 100-year river floods. *Geophysical Research Letters*, 48(6):e2020GL091824. e2020GL091824 2020GL091824.

Stan Development Team (2025). RStan: the R interface to Stan. R package version 2.32.7.

Stedinger, J. and Lu, L.-H. (1995). Appraisal of regional and index flood quantile estimators. *Stochastic hydrology and hydraulics*, 9(1):49–75.

Stedinger, J. R. (1993). Frequency analysis of extreme events. *Handbook of hydrology*.

Steirou, E., Gerlitz, L., Apel, H., Sun, X., and Merz, B. (2019). Climate influences on flood probabilities across europe. *Hydrology and Earth System Sciences*, 23(3):1305–1322.

Tarasova, L., Basso, S., Zink, M., and Merz, R. (2018). Exploring controls on rainfall-runoff events: 1. time series-based event separation and temporal dynamics of event runoff response in germany. *Water Resources Research*, 54(10):7711–7732.

Tarasova, L., Lun, D., Merz, R., Blöschl, G., Basso, S., Bertola, M., Miniussi, A., Rakovec, O., Samaniego, L., Thober, S., and Kumar, R. (2023). Shifts in flood generation processes exacerbate regional flood anomalies in europe. *Communications Earth & Environment*, 4(1):49.

Tasker, G. D. and Stedinger, J. R. (1989). An operational gls model for hydrologic regression. *Journal of Hydrology*, 111(1):361–375.

Taylor, K. E., Stouffer, R. J., and Meehl, G. A. (2012). An overview of cmip5 and the experiment design. *Bulletin of the American Meteorological Society*, 93(4):485 – 498.

Thober, S., Kumar, R., Wanders, N., Marx, A., Pan, M., Rakovec, O., Samaniego, L., Sheffield, J., Wood, E. F., and Zink, M. (2018). Multi-model ensemble projections of european river floods and high flows at 1.5, 2, and 3 degrees global warming. *Environmental Research Letters*, 13(1):014003.

Thomas, D., Benson, M., (U.S.), G. S., and of the Interior, U. S. D. (1970). *Generalization of Streamflow Characteristics from Drainage-basin Characteristics*. Number No. 1975 in Generalization of Streamflow Characteristics from Drainage-basin Characteristics. U.S. Government Printing Office.

Vafakhah, M., Nourani, V., and Rahman, A. (2012). Regional flood frequency analysis using decision trees and artificial neural networks. *Stochastic Environmental Research and Risk Assessment*, 26(1):1–14.

Valente, M., Del Prete, C., Facci, G., Martino, A., Grilli, G. R., Bravi, F., Reno, C., and Ragazzoni, L. (2025). The 2023 floods in the emilia-romagna region, italy: A retrospective qualitative investigation into response strategies and criticalities. *International Journal of Disaster Risk Reduction*, 116:105089.

Viglione, A. and Bloschl, G. (2009). On the role of storm duration in the mapping of rainfall to flood return periods. *Hydrology and Earth System Sciences*, 13(2):205–216.

Viglione, A., Chirico, G. B., Komma, J., Woods, R., Borga, M., and Blöschl, G. (2010a). Quantifying space-time dynamics of flood event types. *Journal of Hydrology*, 394(1):213–229. Flash Floods: Observations and Analysis of Hydrometeorological Controls.

Viglione, A., Chirico, G. B., Woods, R., and Blöschl, G. (2010b). Generalised synthesis of space–time variability in flood response: An analytical framework. *Journal of Hydrology*, 394(1):198–212. Flash Floods: Observations and Analysis of Hydrometeorological Controls.

Viglione, A., Laio, F., and Claps, P. (2007). A comparison of homogeneity tests for regional frequency analysis. *Water Resources Research*, 43(3).

Viglione, A., Merz, R., and Blöschl, G. (2009). On the role of the runoff coefficient in the mapping of rainfall to flood return periods. *Hydrology and Earth System Sciences*, 13(5):577–593.

Viglione, A., Merz, R., Salinas, J. L., and Blöschl, G. (2013). Flood frequency hydrology: 3. a bayesian analysis. *Water Resources Research*, 49(2):675–692.

Vigna, B. and Banzato, C. (2015). The hydrogeology of high-mountain carbonate areas: an example of some alpine systems in southern piedmont (italy). *Environmental Earth Sciences*, 74.

Villarini, G., Smith, J. A., Serinaldi, F., and Ntelekos, A. A. (2011). Analyses of seasonal and annual maximum daily discharge records for central europe. *Journal of Hydrology*, 399(3):299–312.

Vogel, R. M. and Fennessey, N. M. (1993). L moment diagrams should replace product moment diagrams. *Water resources research*, 29(6):1745–1752.

Vogel, R. M. and Wilson, I. (1996). Probability distribution of annual maximum, mean, and minimum streamflows in the united states. *Journal of hydrologic Engineering*, 1(2):69–76.

Vogel, R. M., Yaindl, C., and Walter, M. (2011). Nonstationarity: Flood magnification and recurrence reduction factors in the united states1. *JAWRA Journal of the American Water Resources Association*, 47(3):464–474.

Wang, Q. (1990). Unbiased estimation of probability weighted moments and partial probability weighted moments from systematic and historical flood information and their application to estimating the gev distribution. *Journal of Hydrology*, 120(1):115–124.

Wasko, C. and Guo, D. (2022). Understanding event runoff coefficient variability across australia using the hydroevents r package. *Hydrological Processes*, 36.

Wasko, C. and Guo, D. (2025). *hydroEvents: Extract Event Statistics in Hydrologic Time Series*. R package version 0.12.0.

Wasko, C., Nathan, R., Stein, L., and O'Shea, D. (2021). Evidence of shorter more extreme rainfalls and increased flood variability under climate change. *Journal of Hydrology*, 603:126994.

Westra, S., Alexander, L. V., and Zwiers, F. W. (2013). Global increasing trends in annual maximum daily precipitation. *Journal of Climate*, 26(11):3904 – 3918.

Westra, S., Fowler, H. J., Evans, J. P., Alexander, L. V., Berg, P., Johnson, F., Kendon, E. J., Lenderink, G., and Roberts, N. M. (2014). Future changes to the intensity and frequency of short-duration extreme rainfall. *Reviews of Geophysics*, 52(3):522–555.

Wilhelm, B., Rapuc, W., Amann, B., Anselmetti, F., Arnaud, F., Blanchet, J., Brauer, A., Czymzik, M., Giguet-Covex, C., Gilli, A., Glur, L., Grosjean, M., Irmler, R., Nicolle, M., Sabatier, P., Swierczynski, T., and Wirth, S. (2022). Impact of warmer climate periods on flood hazard in the european alps. *Nature Geoscience*, 15:118–123.

Winter, B., Schneeberger, K., Dung, N., Huttenlau, M., Achleitner, S., Stötter, J., Merz, B., and Vorogushyn, S. (2019). A continuous modelling approach for design flood estimation on sub-daily time scale. *Hydrological Sciences Journal*, 64(5):539–554.

Wittenberg, H. (1999). Some aspects of regional flood frequency analysis using neural networks. *Hydrological Sciences Journal*, 44(4):563–575.

WMO (2021). Atlas of mortality and economic losses from weather, climate and water extremes (1970–2019). *World Meteorological Organization*. WMO-No. 1267.

Wright, D. B., Yu, G., and England, J. F. (2020). Six decades of rainfall and flood frequency analysis using stochastic storm transposition: Review, progress, and prospects. *Journal of Hydrology*, 585:124816.

Zalnezhad, A., Rahman, A., Nasiri, N., Haddad, K., Rahman, M. M., Vafakhah, M., Samali, B., and Ahamed, F. (2022). Artificial intelligence-based regional flood frequency analysis methods: A scoping review. *Water*, 14(17).

Zrinji, Z. and Burn, D. H. (1996). Regional flood frequency with hierarchical region of influence. *Journal of Water Resources Planning and Management*, 122(4):245–252.

Šraj, M., Viglione, A., Parajka, J., and Blöschl, G. (2016). The influence of non-stationarity in extreme hydrological events on flood frequency estimation. *Journal of Hydrology and Hydromechanics*, 64(4):426–437.

# Appendix A

# Catchments of the Po River basin

Table A.1 Hydrometric stations database (codes and names)

| Code | Name (EN) |
|---|---|
| A001 | Adda at Tirano |
| A002 | Adda at Fuentes |
| A007 | Agogna at Novara |
| A008 | Arda at Mignano (reservoir dam) |
| A009 | Artanavaz (Dora Baltea) at St Oyen |
| A010 | Aveto (Trebbia) at Cabanne |
| A011 | Ayasse (Dora Baltea) at Champorcher |
| A012 | Banna at Santena |
| A013 | Belbo at Castelnuovo Belbo |
| A014 | Bevera at Colombaio |
| A015 | Borbera (Scrivia) at Baracche |
| A016 | Borbore at San Damiano d'Asti |
| A017 | Bormida at Cassine (Caranzano) |
| A018 | Bormida at Alessandria |
| A019 | Bormida di Mallare at Ferrania |
| A020 | Bormida di Millesimo at Cessole |
| A021 | Bormida di Millesimo at Murialdo |
| A022 | Bormida di Spigno at Mombaldone |
| A023 | Bormida di Spigno at Valla |
| A024 | Bousset at Tetti Porcera |

| Code | Name |
|---|---|
| A025 | Brembo at Ponte Briolo |
| A026 | Breuil at Alpette |
| A027 | Bucera at Ponte Rovine |
| A029 | Cannobino at Traffiume |
| A030 | Cervo (Sesia) at Passobreve |
| A031 | Cervo at Vigliano Biellese |
| A032 | Cervo at Quinto Vercellese |
| A033 | Chiavanne at Alpette |
| A034 | Chiese at Malga Bissina |
| A035 | Chiese at Malga Boazzo (interbasin) |
| A037 | Chiese at Gavardo |
| A038 | Chisone at Soucheres Basses |
| A039 | Chisone at Fenestrelle |
| A040 | Chisone at San Martino |
| A041 | Chiusella at Gurzia |
| A043 | Corsaglia (Tanaro) at Molline intake |
| A044 | Dolo (Secchia) at Fontanaluccia (reservoir dam) |
| A047 | Dora Baltea at Ponte di Mombardone |
| A048 | Dora Baltea at Aosta |
| A049 | Dora Baltea at Tavagnasco |
| A051 | Dora Baltea at Mazzè |
| A052 | Dora di Bardonecchia at Beaulard |
| A053 | Dora di Courmayeur at San Desiderio Terme |
| A054 | Dora di Rhemes at Palaud |
| A055 | Dora di Rhemes at Notre Dame |
| A056 | Dora di Rhemes at Saint Georges |
| A057 | Dora Riparia at Oulx |
| A061 | Dora Riparia at Turin – Washington Bridge |
| A063 | Enza at Sorbolo |
| A064 | Erro (Bormida) at Sassello |
| A065 | Evancon at Champoluc |
| A068 | Gesso della Barra at San Giacomo |
| A069 | Gesso della Valletta (Stura di Demonte) |
| A071 | Gesso di Entracque (Stura di Demonte) |

| Code | Name |
|---|---|
| A072 | Gesso di Monte Colombo at San Giacomo |
| A073 | Grana at Monterosso |
| A074 | Grand'Eyvia at Cretaz |
| A075 | Isorno at Pontetto |
| A077 | Lys at d'Ejola |
| A078 | Lys (Dora Baltea) at Gressoney-Saint-Jean |
| A079 | Lys at Guillemore |
| A080 | Maira at Saretto |
| A081 | Maira at San Damiano Macra |
| A082 | Maira at Racconigi |
| A083 | Malone at Brandizzo |
| A084 | Malone at Front |
| A085 | Marmore at Perreres |
| A086 | Mastallone (Sesia) at Ponte Folle |
| A087 | Melezet at Melezet |
| A088 | Meris at Sant'Anna Valdieri |
| A092 | Nontey at Valnontey |
| A093 | Oglio at Temù |
| A098 | Orba at Casal Cermelli |
| A099 | Orco at Pont Canavese |
| A100 | Orco at San Benigno Canavese |
| A101 | Panaro at Bomporto |
| A103 | Parma at Barganzola |
| A104 | Pellice at Luserna San Giovanni |
| A105 | Pellice at Villafranca Piemonte |
| A106 | Po at Crissolo |
| A107 | Po at Carignano |
| A108 | Po at Moncalieri (Meirano) |
| A109 | Po at Turin – Murazzi |
| A110 | Po at San Mauro Torinese |
| A111 | Po at Casale Monferrato |
| A122 | Rio Bagni (Stura di Demonte) at Bagni di Vinadio |
| A124 | Rio Freddo at Rio Freddo |
| A125 | Ripa at Bousson |

| Code | Name |
|---|---|
| A128 | Rutor (Dora Baltea) at Promise |
| A130 | San Bernardino at Trobaso |
| A131 | San Giovanni at Possaccio |
| A132 | Sarca at Ponte Plaza |
| A133 | Sarca at Saone |
| A134 | Sarca at Nago |
| A135 | Sarca di Nambron at Pian di Nambron |
| A137 | Sarca di Val Genova (intake) |
| A138 | Savara at Eau Rousse |
| A139 | Savara at Fenille |
| A140 | Scrivia at Isola del Cantone |
| A141 | Scrivia at Serravalle |
| A142 | Secchia at Ponte Cavola |
| A143 | Secchia at Ponte Bacchello |
| A145 | Sermenza at Rimasco |
| A146 | Sesia at Campertogno |
| A147 | Sesia at Ponte Aranco |
| A149 | Sesia at Palestro |
| A150 | Strona di Omegna at Gravellona Toce |
| A151 | Stura di Demonte at Pianche |
| A152 | Stura di Demonte at Gaiola |
| A153 | Stura di Demonte at Roccasparvera |
| A154 | Stura di Demonte at Fossano |
| A155 | Stura di Lanzo at Lanzo |
| A156 | Stura di Lanzo at Turin |
| A158 | Stura di Viù at Malciaussia |
| A159 | Stura di Viù at Usseglio |
| A160 | Tanaro at Ponte di Nava |
| A161 | Tanaro at Ormea |
| A162 | Tanaro at Garessio |
| A163 | Tanaro at Nucetto |
| A164 | Tanaro at Piantorre |
| A166 | Tanaro at Farigliano |
| A167 | Tanaro at Alba |

| Code | Name |
|---|---|
| A171 | Tanaro at Montecastello |
| A172 | Taro at Santa Maria |
| A173 | Taro at Piane di Carniglia |
| A174 | Taro at Pradella |
| A175 | Taro at Ostia |
| A176 | Taro at San Quirico |
| A177 | Ticino at Bellinzona |
| A187 | Toce at Cadarese |
| A188 | Toce at Domodossola |
| A189 | Toce at Candoglia |
| A190 | Trebbia at Due Ponti |
| A191 | Trebbia at Valsigiara |
| A192 | Trebbia at San Salvatore |
| A194 | Varaita at Castello |
| A195 | Varaita at Rore |
| A196 | Varaita at Rossana |
| A198 | Vobbia at Vobbietta |
| A199 | Bormida di Millesimo at Camerana |
| A200 | Chisola at La Loggia |
| A201 | Germanasca at Perrero |
| A202 | Orba at Basaluzzo |
| A203 | Vermenagna at Robilante |
| A206 | Agogna at Lomello |
| A207 | Arno at Cavaria |
| A208 | Bevera at Molteno |
| A209 | Brembo at Camerata Cornello |
| A211 | Lambro at Caslino |
| A218 | Mella at Bovegno |
| A223 | Olona at Ponte Vedano |
| A224 | Serio at Grabiasca |
| A226 | Seveso at Cantù Asnago |
| A228 | Staffora at Voghera |
| A229 | Terdoppio at Gambolò |
| A230 | Dora Riparia at Susa |

| Code | Name |
|---|---|
| A231 | Varaita at Polonghera |
| B001 | Bidente di Corniolo at Campigna |
| B002 | Bidente di Ridracoli at Ridracoli (reservoir dam) |
| B003 | Brasimone (Setta) at Santa Maria (reservoir dam) |
| B007 | Lamone at Sarna |
| B008 | Lamone at Grattacoppa |
| B009 | Limentra di Riola (Reno) at Stagno |
| B010 | Limentra di Sambuca (Reno) at Pavana (reservoir dam) |
| B011 | Limentra di Treppio (Reno) at Suviana (reservoir dam) |
| B012 | Orsigna (Reno) at Setteponti |
| B013 | Quaderna (Reno) at Palesio |
| B014 | Reno at Pracchia |
| B015 | Reno at Molino di Pallone |
| B016 | Reno at Ponte della Venturina |
| B017 | Reno at Calvenzano |
| B018 | Reno at Casalecchio |
| B021 | Rio Faldo (Reno) at Setteponti |
| B022 | Ronco (Fiumi Uniti) at Meldola Casa Luzia |
| B023 | Samoggia (Reno) at Calcara |
| B024 | Savena (Reno) at Castel dell'Alpi |
| B025 | Savena (Reno) at San Ruffillo |
| B026 | Savio at Mercato Saraceno |
| B027 | Savio at San Vittore |
| B028 | Senio (Reno) at Castel Bolognese |
| B029 | Silla (Reno) at Silla |
| B031 | Baganza at Berceto |
| B032 | Trebbia at Bobbio |
| B034 | Santerno at Borgo Tossignano |
| B035 | Tresinaro at Ca' de' Caroli |
| B037 | Pisciatello at Calisese |
| B038 | Scodogna at Casella Nuova |
| B039 | Arda at Case Bonini |
| B040 | Senio at Casola Valsenio |
| B041 | Stirone at Castellina Soragna |

| Code | Name |
|---|---|
| B045 | Tassobbio at Compiano |
| B046 | Parma at Corniglio |
| B048 | Enza at Currada |
| B049 | Leo at Fanano |
| B050 | Nure at Farini |
| B051 | Nure at Ferriere |
| B054 | Acquicciola at Fiumalbo |
| B056 | Secchia at Gatta |
| B060 | Lonza at Vetto |
| B061 | Secchia at Lugo |
| B062 | Lamone at Marradi |
| B064 | Riglio at Montanaro |
| B065 | Conca at Morciano |
| B067 | Recchio at Noceto |
| B073 | Ceno at Ponte Ceno |
| B074 | Ceno at Ponte Lamberti |
| B077 | Panaro at Ponte Samone |
| B078 | Sissola (Taro) at Pontestrambo |
| B079 | Scoltenna at Ponte Val Sasso |
| B082 | Crostolo at Puianello |
| B084 | Marecchia at Rimini SS16 |
| B085 | Rio Cella at Querceto |
| B087 | Trebbia at Rivergaro |
| B088 | Rossenna at Prignano sulla Secchia |
| B090 | Secchia at Rubiera SS9 |
| B091 | Chiavenna at Saliceto |
| B092 | Ghiara at Salsomaggiore |
| B093 | Aveto at Salsominore |
| B094 | Rubicone at Savignano |
| B095 | Cedra at Selvanizza |
| B098 | Sesto Imolese |
| B099 | Uso at Santarcangelo |
| B101 | Tiepido at San Donnino |
| B103 | Panaro at Spilamberto |

| Code | Name |
|---|---|
| B106 | Taro at Tornolo |
| B107 | Reno at Vergato |
| B108 | Enza at Vetto |